Decoding protein phosphorylation during oocyte meiotic divisions using phosphoproteomics

Leonid Peshkin[1#]✉, Enrico Maria Daldello[2#], Elizabeth Van Itallie[1], Matthew Sonnett[1], Johannes Kreuzer[1], Wilhelm Haas[1], Marc W Kirschner[1] and Catherine Jessus[2]

[1] Systems Biology Department, Harvard Medical School, Boston, MA, 02115, USA

[2] Sorbonne Université, CNRS, Laboratoire de Biologie du Développement - Institut de Biologie Paris Seine, LBD - IBPS, F-75005 Paris, France

[#] Equal contribution

✉ Corresponding author: Leonid_Peshkin@hms.harvard.edu

Running title: Protein phosphorylation during oocyte meiotic divisions

ABSTRACT

Oocyte meiotic divisions represent a critical process in sexual reproduction, as a diploid non-dividing oocyte is transformed into a haploid fertilizable egg, as a prelude for the subsequent embryonic divisions and differentiation. Although cell differentiation and proliferation are governed by transcription, oocyte maturation and early embryonic divisions depend entirely on changes in protein abundance and post-translational modifications. Here, we analyze the abundance and phosphorylation of proteins during *Xenopus* oocyte meiotic maturation. We reveal significant shifts in protein stability, related to spindle assembly, DNA replication and RNA-binding. Our analysis pinpoints broad changes in phosphorylation correlating with key cytological meiotic milestones, noteworthy changes in membrane trafficking, nuclear envelope disassembly and modifications in microtubule dynamics. Additionally, specific phosphorylation events target regulators of protein translation, Cdk1 and the Mos/MAPK pathway, thereby providing insight into the dynamics of Cdk1 activity, as related to the meiotic cell cycle. This study sheds light on the orchestration of protein dynamics and phosphorylation events during oocyte meiotic divisions, providing a rich resource for understanding the molecular pathways orchestrating meiotic progression in the frog, and most likely applicable to other vertebrate species.

Key Words: Meiotic divisions/Protein phosphorylation/Phosphoproteome/*Xenopus* oocyte

INTRODUCTION

In mature females, the oocyte undergoes a long period of growth, during which meiosis is arrested at prophase I. In the *Xenopus* oocyte, transcription is switched off when the oocyte reaches the end of its growth phase (Dumont, 1972). The full-grown oocyte is transcriptionally silent and equipped with a stock of mRNAs and proteins that will support without transcription three critical embryonic processes: first, two meiotic divisions that transform the oocyte into a fertilizable haploid egg; second, the process of fertilization; and third, 12 embryonic divisions, after which transcription is initiated.

The transformation of a fully-grown oocyte arrested in prophase into a fertilizable cell, arrested in metaphase of the second meiotic division is a process called meiotic maturation. Meiotic maturation is triggered by progesterone, secreted by the follicle cells surrounding the oocyte. The secretion of progesterone is stimulated by Luteinizing Hormone produced by the pituitary. Progesterone initiates a molecular signaling cascade that lasts 3 to 4 hours and occurs with little change in oocyte morphology. Notably, this cascade leads to the activation of the Cdk1-Cyclin B kinase, the universal inducer of cell division in eukaryotes. Cdk1 phosphorylates many substrates that promote meiotic nuclear events: nuclear envelope breakdown (NEBD), the formation of the first meiotic spindle marking the metaphase I (MI), the completion of the first meiotic division with expulsion of a polar body, and formation of the second meiotic spindle (Figure 1). As in all vertebrates, the frog oocyte arrests a second time in metaphase II (MII), until fertilization stimulates the completion of the second meiotic division. The entire process of oocyte maturation occurs in the absence of transcription. The regulation of the two meiotic divisions and the 13 embryonic divisions that follow are thought to be largely regulated by changes in protein abundance and phosphorylation/dephosphorylation.

The prophase-arrested oocyte contains a store of Cdk1-Cyclin B complexes that are kept inhibited by Cdk1 phosphorylation at Y15 and T14, which are substrates of the kinase, Myt1 (Mueller *et al*, 1995). In all vertebrates, the prophase arrest is maintained by high levels of cAMP and PKA (cAMP-activated protein kinase) activity (Figure 1). The release of this prophase block is triggered by a drop in the levels of cAMP and the consequent inhibition of PKA, which occurs within 60 min after progesterone stimulation. The identity of the critical PKA substrates whose dephosphorylation is thought to induce the pathway leading to Cdk1 activation is still unknown, with the exception of Arpp19 whose mechanism of action is not completely understood (Dupré *et al*, 2014; Santoni *et al*, 2024). Nevertheless, a drop in PKA activity leads to the synthesis of new proteins from cytoplasmic stockpiles of mRNAs as well as increases in protein level through regulation of the ubiquitination machinery (Santoni *et al*, 2024). Among the accumulated proteins are Cyclin B1, the best-known activator of Cdk1 in mitotic cells, RINGO/Speedy (Ferby *et al*, 1999;

Lenormand, 1999) and Mos, a kinase specific to the oocytes (Figure 1). The newly synthesized B1-Cyclins bind to monomeric Cdk1 to form a small pool of active complexes that evade the inhibition of Myt1 (Hochegger *et al*, 2001; Gaffré *et al*, 2011). Subsequently, this small amount of active Cdk1 initiates a complex network of feedback loops, involving many kinases and phosphatases, thereby creating an auto-amplification loop (Jessus, 2010) (Figure 1). Within this loop, the activation of the Cdc25 phosphatase that dephosphorylates Cdk1 and the inhibition of the PP2A phosphatase that counteracts Cdk1, lead to a rapid and full activation of Cdk1-Cyclin B (Jessus, 2010; Lemonnier *et al*, 2020). Another important player in this positive feedback loop is Mos, whose translation is induced by progesterone and which accumulates at the time of Cdk1 activation (Sagata *et al*, 1988, 1989a; Frank-Vaillant *et al*, 1999). Mos activates Erk1/2 (also known as MAPK) indirectly, which modulates the core regulators of Cdk1 (Haccard & Jessus, 2006) (Figure 1). Cdk1 and the kinases activated under its control (Mos/MAPK, Aurora-A, Plk1, etc.) trigger a second wave of protein translation and accumulation, as well as mediating the structural changes of cell division: NEBD, chromosome condensation and formation of the Meiosis I spindle (Jessus, 2010; Santoni *et al*, 2024). They also activate the anaphase-promoting complex (APC), an E3 ubiquitin ligase, leading to the degradation of both Cyclin B and securin, thus enabling entry into anaphase I, chromosome separation and the expulsion of the 1st polar body (Figure 1). The decrease in Cdk1 activity is rapidly followed by the inhibition of APC, which then allows the accumulation of B-Cyclins and increase of Cdk1 activity (Figure 1). These events trigger the entry into metaphase II and the formation of the MII spindle. In all vertebrates, oocytes arrest in the middle of the meiotic division as a result of the stabilization of cyclin B, resulting from APC inhibition by the Emi2/Erp1 (Jessus, 2010) (Figure 1).

The burst of phosphorylation, which occurs at NEBD when Cdk1 is activated, targets proteins belonging to three categories (Maller *et al*, 1977): first, regulators of translation and/or degradation of proteins that are essential for the progression of meiotic divisions; second, proteins directly involved in the intracellular reorganization of the oocyte, such as the components of meiotic spindles, the nuclear envelope or other cytoskeletal elements; third, proteins that do not have a role in meiotic divisions but regulate fertilization and early embryonic development. Notably, the sperm does not contribute any proteins or RNA except for its genome and its two centrioles. With fertilization there is extrusion of the 2nd polar body, the fusion of the male and female pronuclei. Within a few minutes after fertilization, the first S-phase starts, followed by the first 12 embryonic division cycles, all occurring in the absence of transcription (Blitz & Cho, 2021). Thus, these events depend exclusively on maternal proteins and mRNA. Phosphoregulation is a central and conserved mechanism that enables remodeling of the oocyte proteome and supports cell division. It prepares the oocyte to transform into the egg and undertake development. In the absence transcription

our knowledge of the dynamic patterns of phosphorylation of thousands of oocyte phosphosites represents an essential tool for study of oogenesis, embryogenesis, especially the unique meiotic and mitotic processes. Interestingly, two recent studies based on phosphoproteomics have revealed new insights into how phosphorylation dynamics regulate meiotic divisions in yeast (Celebic *et al*, 2024; Koch *et al*, 2024) and mouse (Sun *et al*, 2024). We now extend this analysis to the physiological process of oogenesis specific to non-mammalian metazoans. The study of mitotic processes in somatic cells, which are short in duration, requires exquisite synchronization, which is difficult. Although previous studies of protein phosphorylation during mitosis have revealed the identity of numerous players of cell division, especially those controlling the structural reorganization of the dividing cell and its checkpoints, they have not been able to fully elucidate the epistatic relationships between kinases and phosphatases, which are nonetheless crucial to understanding the temporal sequences regulating the various events of mitosis. This weakness is due to the fact that cell proliferation is a continuous phenomenon, without physiological arrest. Its duration varies from one cell to another within the same population. The necessity of using synchronizing agents induces non-physiological arrests, which activate checkpoints, leading to the resumption of the cell cycle not comparable to that of untreated cells. Moreover, these studies often use transformed cell lines with accumulation of mutations that makes it hard to compare with cells in a physiological cellular context. The exceptional features of oocyte maturation for experimental studies of mitosis and meiosis are: 1) the synchronicity of the process in the oocyte, initiated by a physiological signal, progesterone, 2) the natural oocyte arrests in oocyte maturation at either prophase I (equivalent to a late G2-arrest) or at MII (M-phase arrest), 3) and the large size of the oocyte (1.2 mm in diameter) and its high protein content (30 μg soluble proteins per cell), offering the rare opportunity of single-cell proteomics. In addition, the *Xenopus* model offers great assets. From a technical perspective, in the mouse, the small number of oocytes and their low protein content limit proteomic approaches (30,000 oocytes isolated from 950 mice were required for the phosphoproteomic profiling by (Sun *et al*, 2024)). Furthermore, the resumption of meiotic divisions in mouse obeys a particular regulation: unlike other mammalian models (including the human species) and other vertebrates whose entry into meiosis I depends strictly on protein translation, it does not require the synthesis of new proteins, making it a somewhat marginal model(Meneau *et al*, 2020). For these reasons, we performed time-resolved proteomics and phosphoproteomics in *Xenopus* oocytes from prophase I through the MII arrest of the unfertilized egg.

In this study, we have analyzed the changes in the phosphorylation in relation to three categories of events: specific periods of meiotic maturation, activities of the master regulators of meiosis and

peculiar cellular features of meiosis. Our analysis confirms the high quality of our phosphoproteome by the detection of multiple phosphorylation events with previously-documented functional effects on meiotic divisions or early development. Through the detection of many new regulated phosphosites, it provides a rich pool of candidate proteins for multiple avenues of investigation of previously uncharacterized important players of the oocyte to embryo transition.

RESULTS

The temporal resolution of the events of meiotic divisions

To determine both proteome and phosphoproteome of *Xenopus* oocytes during meiosis resumption, meiotic maturation was triggered by progesterone, and oocytes were collected at regular intervals after progesterone exposure (Movie EV1, Methods): prophase oocytes (PRO) at the time of progesterone addition, then 2 hours after progesterone treatment, with hourly timepoints past that, up to 9 hours post-treatment. Groups of ten or fifty oocytes were collected at each timepoint for protein and phospho-proteomics measurements respectively. After oocyte lysis, digestion into peptides and phospho-peptide enrichment in the case of phosphoproteomics analysis, samples were processed for TMT-MS3 LC/MS (Methods).

To correlate the time-points of this experiment with the cytological events known to occur during meiosis resumption, a set of proteins whose accumulation had been extensively studied during *Xenopus* oocyte meiosis progression were used as markers. One of the first events following progesterone stimulation is the accumulation of Cyclin B1 that begins before and independently of Cdk1 activation (Santoni *et al*, 2024; Frank-Vaillant *et al*, 1999). In our experiments, Cyclin B1 accumulation starts at about 2 hours and increases linearly until MII arrest at 6.5 hours (Figure 2A). It has been reported that Mos translation is stimulated by progesterone concomitant with the accumulation of Cyclin B1; however the Mos protein does not accumulate before NEBD because it turns over rapidly (Santoni *et al*, 2024; Frank-Vaillant *et al*, 1999). Another critical well documented event that occurs downstream to Cdk1 activation is the degradation of CPEB1 (Santoni *et al*, 2024; Mendez *et al*, 2002), an RNA-binding protein whose degradation activates protein translation in MI. Hence, Mos accumulation and the degradation of CPEB1 are well established markers for the timing of NEBD. After NEBD, activation of the anaphase-promoting complex (APC) leads to the ubiquitination and degradation of Cyclin B2, which marks the entry into anaphase I. During the MI-MII transition, multiple additional events take place: Cyclin B3 is degraded (Bouftas *et al*, 2022), Cdc6 (Lemaître *et al*, 2002; Whitmire *et al*, 2002; Daldello *et al*, 2015), Wee2 (Nakajo *et al*, 2000) and Cyclin E (Rempel *et al*, 1995) accumulate, reaching their maximal levels in MII. These four events mark the entry into MII. Based on these markers, the timing of cytological events in our experiment is as follows (Figure 2A): NEBD and MI occur between 3 and 4 hours, the MI-MII transition takes place between 5 and 6 hours, and entry and arrest in MII are at 7 hours. This time course is in agreement with the cytological previously described events (Huchon *et al*, 1981; Gard, 1992). A physiological measure of MII arrest can be ascertained by the ability of the oocytes to be activated by an electric shock, a property that is acquired only in MII (Movie EV2).

Validation of the quantitative proteomic data

The quality of oocytes resuming meiosis is also confirmed by the dynamics of protein accumulation and degradation that occur during meiotic progression (Figure 2B). A set of 34 proteins, whose changes in concentration have been previously studied during meiotic divisions was used to validate the quality of our quantitative proteomics data (Figure 2B-figure supplement 3A). Our proteome correctly classifies 15 out of 18 proteins accumulating during *Xenopus* meiosis resumption (FC(MII/PRO) > 1.5), 11 out of 12 proteins whose concentration is constant (0.75 < FC(MII/PRO) < 1.5), and 4 out of 4 proteins whose accumulation was reported to decrease (FC(MII/PRO) < 0.75) (Figure 2B-figure supplement 3A). The concordance between our dataset (30/34 proteins) with the changes in the protein levels reported in the literature is substantially higher than in a previously published system-wide proteomic dataset from *Xenopus* oocytes where only 7 out of these 34 proteins were correctly measured (Peuchen *et al*, 2017) (Figure 2-figure supplement 3A-B). This also may explain why changes in protein concentration reported in that study poorly correlate with the one measured in our proteomic study (Figure 2-figure supplement 3B). The high quality of the new proteomic data is also confirmed by the strong correlation of the translational pattern of *Xenopus* allo-alleles (Figure 2-figure supplement 3C-D), which were derived by genome endoduplication (Session *et al*, 2016).

Protein homeostasis during meiotic divisions

Absolute concentrations of proteins during meiotic maturation

The absolute concentration of 7974 proteins identified in our proteome dataset was calculated (See Appendix 1). We then performed a qualitative comparison of average oocyte abundance of proteins belonging to distinct functional groups (see Appendix 2). As expected, the less abundant subgroups include signaling molecules and transcription factors. Perhaps of more surprise, E3 enzymes and kinases are not abundant. At the other end of the spectrum are glycolytic and tricarboxylic acid cycle enzymes, as well as proteasome and ribosome components. These observations are expected because the oocyte has a stock of nutrient molecules and all the enzymes linked to their metabolism, which are used in viviparous animals throughout embryonic and larval development. For instance, the glycolytic enzyme GAPDH that catalyzes an important energy-yielding step in carbohydrate metabolism, is a very abundant protein in the oocyte (average concentration of between 8.88 μM and 17.83 μM). The ribogenesis program, which takes place during the oocyte growth from stage III to stage VI, before meiosis resumption, allows the accumulation of very large quantities of ribosomal RNAs and proteins that are used during embryonic

development, until the swimming tadpole stage (Woodland, 1974). Similarly, the components of the DNA replication machinery are quite abundant, probably in anticipation of the post-fertilization cell cycles. All these data are therefore consistent with biological understanding of their roles during embryonic development after post-fertilization (Peshkin *et al*, 2015).

Temporal profiles of protein levels

We clustered the relative data for protein abundance across subsequent hourly timepoints post-progesterone stimulation (see Methods). As illustrated in Appendix 3A, the majority of the 60 expression profiles are flat, demonstrating that most (over 80%) proteins are stable during meiotic maturation. Our proteomic dataset allowed to identify 12% of proteins affected by changes in concentration during meiotic progression by applying the same fold change threshold: 413 proteins that accumulate and 562 proteins whose concentration decreases (Figure 2B-figure supplement 3E; see Appendix 4). Although these changes only concern a minority of proteins, they are critical for the meiotic process. Since transcription is silent during this period, these documented changes must result from the regulation of translation or/and degradation (Meneau *et al*, 2020).

Protein accumulation: the machinery of cell division and DNA replication. Gene ontology analysis was used to characterize the functional significance of the 413 proteins whose level increases during meiosis. Proteins involved in spindle assembly and mitotic division were significantly enriched (Figure 2C). Among these important regulators are the Targeting-protein-for-Xklp2 (Tpx2) and Protein-regulator-of-cytokinesis 1 (Prc1) that also accumulate during meiotic maturation in mouse oocytes (Brunet *et al*, 2008; Li *et al*, 2021). We also find that the centrosomal maturation factor, SSX2IP, a plus-end motor kinesin, Kif11/Eg5, and a minus-end one, Kifc1 (Houliston *et al*, 1994), also accumulate significantly during meiotic maturation. Three of these proteins, Tpx2 and the two kinesins, play an important role in the assembly of both acentrosomal meiotic spindles and centrosomal mitotic spindles (Gruss, 2018; Kufer *et al*, 2002; Ems-McClung *et al*, 2020; Miller *et al*, 2019). Interestingly, the prophase oocyte is equipped with most of the proteins essential for the formation of division spindles. Hence these new results suggest that increases in the relative level of some components is required to support the meiotic and first rapid embryonic divisions.

Another protein category found to increase is the machinery of DNA replication initiation (Figure 2C). Indeed, oocytes accumulate the components of the DNA replication machinery during meiosis resumption to support the 12 rapid rounds of cell cycles occurring during early embryogenesis, all of which occur in the absence of transcription. In *Xenopus*, Cdc6 is a component of the pre-replicative (pre-RC) complex that is not detectable in the prophase-arrested oocyte by western blot (Lemaître *et al*, 2002;

245 Whitmire *et al*, 2002; Daldello *et al*, 2015). Cdc6 accumulation occurs during the MI-MII transition to
246 confer oocytes the competence to replicate DNA (Lemaître *et al*, 2002; Whitmire *et al*, 2002; Daldello *et*
247 *al*, 2015) (Figure 1). Translational and then post-translational mechanisms targeting Cdc6 prevent the pre-
248 RC from functioning between the two meiotic divisions, thus ensuring the production of a haploid gamete.
249 Our proteomic analysis shows that, additional pre-RC proteins, as ORC1, ORC2 and ORC6 accumulate
250 during meiotic maturation, revealing a strong co-regulation of the components of the pre-RC.

251 Another process controlled by highly enriched proteins is vesicle tethering, which includes the
252 family of exocyst proteins (Figure 2C). Interestingly, exocyst proteins are involved in the completion of cell
253 division during the secretory-vesicle-mediated abscission (Gromley *et al*, 2005). The accumulation of
254 these proteins during meiotic maturation could be important to support the extrusion of the polar bodies,
255 as already suggested in *C. elegans* (Kumar *et al*, 2019) and the rapid cell divisions sustaining early
256 embryogenesis.

257 ***Protein degradation: RNA-binding proteins (RBPs).*** Gene ontology analysis of the 562 proteins
258 whose concentration decreases during meiosis reveals that 116 (21 %) are annotated to bind RNA. Among
259 them, a large portion are RNA helicases (Figure 2D). Among these RBPs, another important group are
260 proteins that are involved in ribosome biogenesis. The ribogenesis program takes place during the oocyte
261 growth, allowing the accumulation of ribosomal RNAs and proteins that are used during embryonic
262 development (Woodland, 1974). This process is downregulated during meiotic maturation (Hyman &
263 Wormington, 1988; Chen *et al*, 2011). The decrease in the concentration of proteins involved in rRNA
264 synthesis and processing does not result in a general decrease of ribosomal proteins that are stable during
265 meiotic divisions (Figure 2-figure supplement 4A). Halting ribogenesis may allow the oocyte to re-allocate
266 its energy resources to the production of other cellular components required for meiotic divisions and
267 embryogenesis. Intriguingly, Rpl26 (Ribosomal protein L26) is the only ribosomal protein detected to
268 decrease during meiotic divisions (Figure 2-figure supplement 4A). Since this protein is known to be
269 dispensable for ribosome formation in yeast (Babiano *et al*, 2012; Warner & McIntosh, 2009; Takagi *et al*,
270 2005), the distinct regulation of Rpl26 as compared to the other Rpls suggests that Rpl26 might have extra-
271 ribosomal functions. This hypothesis is reinforced by its specific modification by the ubiquitin-like
272 UFMylation modification (Walczak *et al*, 2019) and its role in the regulation of protein stability (Zhang *et*
273 *al*, 2016). Another subgroup of RBPs that decrease during meiotic divisions is involved in the repression
274 of translation during prophase arrest, such as CPEB1 (Mendez *et al*, 2002; Reverte *et al*, 2001; Piqué *et al*,
275 2008), PATL2 (Nakamura *et al*, 2010; Cao *et al*, 2021; Christou-Kent *et al*, 2018) and Zar1l (Zar2)
276 (Charlesworth *et al*, 2012; Yamamoto *et al*, 2013; Rong *et al*, 2019). Remodeling the repertoire of RBPs in

the oocyte could be a general mechanism to regulate translation during meiotic divisions. Among these RBPs is Serbp1, which in mouse is involved in the stabilization of mRNA involved in meiosis resumption (Chew *et al*, 2013) and in ribosome hibernation (Leesch *et al*, 2023), as well as Caprin2, whose degradation is also observed during meiotic maturation of human oocytes (Virant-Klun *et al*, 2016). Caprin2 is a RBP with unknown function and highly enriched in the oocyte Balbiani body (Boke *et al*, 2016), a non-membrane compartment specific to the early diplotene oocytes, which contains mitochondria, RNAs and endoplasmic reticulum. The functions of this organelle are not clear, although it is strongly correlated in *Xenopus* to the establishment of oocyte polarity and to the localization of maternal determinants (Jamieson-Lucy & Mullins, 2019). In *Xenopus*, it disperses at the onset of vitellogenesis, leaving a wedge-shaped cytoplasmic region rich in mitochondria (Wilk *et al*, 2005) and promotes the formation of RNP condensates in the vegetal cortex of the oocyte (Yang *et al*, 2022). Interestingly, Rbpms2, another regulator of the Balbiani body (Kaufman *et al*, 2018), is strongly degraded during meiotic maturation, highlighting how dynamic during meiosis is the composition of this transient compartment specific to the oocyte.

Interestingly, distinct E3 ubiquitin ligases, mainly APC and SCF (Skp, Cullin, F-box containing complex) have been shown to be active at different time periods of meiosis resumption in *Xenopus* oocytes (Kinterová *et al*, 2022). 186 proteins (37%) identified as decreasing in our proteome include in their sequences one of the APC degrons (Figure 2-figure supplement 4B). This group of proteins includes two known APC targets, Cyclin B2 (Glotzer *et al*, 1991) and Securin (Cohen-Fix *et al*, 1996). Additionally, 30 proteins (6%) whose concentration decreases in the oocytes have one SCF degron in their sequence (Figure 2-figure supplement 4B), including CPEB1 (Reverte *et al*, 2001) and Cdc6 (Daldello *et al*, 2015), two characterized SCF-targets. Interestingly, 253 proteins (57%) of proteins that decrease during meiotic divisions do not bear in their sequence any of the degrons for the ubiquitination systems identified in *Xenopus* oocytes (Figure 2-figure supplement 4B). Further research is therefore required to identify the sequences and the E3 enzymes and deubiquitinating enzymes that control the turnover of this important protein class.

The highly dynamic landscape of phosphorylation during meiotic maturation

We performed phosphoproteomic mass spectrometry analysis in order to measure the overall dynamics of protein phosphorylation taking place during meiotic divisions and to identify which specific proteins and which sites are phosphorylated during this process. We identified 6783 different phosphor-peptides and quantified the dynamics of relative change across all time points (see Appendix 5). These peptides

309 came from 2308 distinct proteins. Our phosphosites dataset contains 80% Ser, 19.9% Thr, and 0.01% Tyr.
310 Phospho-Tyr are slightly less abundant than what has been described in most cells (up to 0.05% (Sharma
311 *et al*, 2014)). The same observation was made regarding the distribution of phosphorylated amino acids
312 in mouse oocytes, where phospho-Tyr abundance is relatively diminished in oocytes compared to mouse
313 organs (Sun *et al*, 2024). When respective protein and un-phosphorylated peptide were also measured,
314 we were able to compute the stoichiometry (see Methods). A list of all 415 phosphosites for which it was
315 possible to calculate the phospho-occupancy is provided (see Appendix 6).
316 We identified the human homologous counterparts of 5901 (87%) among the 6783 sites found to be
317 phosphorylated during meiotic divisions. Interestingly, only 177 (3%) out of 5901 conserved sites were
318 already known to be phosphorylated on phosphosite.org database
319 (https://www.phosphosite.org/homeAction). Thus, our phosphosite dataset identifies a very large
320 number of novel phosphosites, never previously identified and characterized. Such a small number of
321 previously reported phosphorylations among those detected by our phosphoproteome might suggest that
322 a large portion of these phosphorylation events are related to cell division. Dividing cells generally account
323 for a small fraction of tissue mass. This leads to a high dilution of the phosphorylation signature of cell
324 division, as compared to the highly synchronous meiotic divisions of oocyte maturation. Interestingly, 60%
325 of the phosphosites detected in oocytes are dynamically regulated during meiotic maturation, highlighting
326 the importance of this post-translational regulation in controlling this last step of oogenesis and meiosis.
327 Unbiased clustering reveals that changes in protein phosphorylation are pervasive and far more dynamic
328 than changes in protein abundance (see Appendix 3), which was also noted during yeast meiosis (Koch *et*
329 *al*, 2024). Comparing the three stages of meiotic division (PRO, MI and MII) and based on the main cellular
330 events of these stages, we can group phosphor-peptide stoichiometry into 5 classes (Figure 3A; see
331 Appendix 5). Class I includes proteins bearing a phosphosite whose occupancy decreases during the first
332 2 hours following progesterone stimulation. This class includes only 136 phospho-peptides (2%) which
333 might be involved in the early signaling pathway induced by progesterone and PKA downregulation. This
334 small number was expected since there is a low level of phosphorylation detectable in prophase-arrested
335 oocytes (Maller *et al*, 1977). This makes sense since there are presumably only a few substrates of PKA
336 sufficient to initiate meiosis resumption. Class II is larger (39% of the phosphor-peptides) and includes
337 proteins whose phosphorylation increases between NEBD and MI and which remain highly
338 phosphorylated in both MI and MII. The massive amount of Class II phosphosites presumably reflects the
339 catalytic power of Cdk1 as well as its downstream kinases, to generate the thousands of substrates
340 essential for cell division. We used the online server (https://kinase-library.phosphosite.org/kinase-

341 library/score-site) to score the phosphosites in the Class II and predict the kinases likely responsible for
342 their phosphorylation (Johnson *et al*, 2023). Using a percentile score threshold of 90, we identified 303,
343 304, and 267 peptides predicted to be phosphorylated by Cdk1, Erk1/2, and Plk1, respectively (Figure 3—
344 figure supplement 1A). Among these, 166 sites were predicted to be efficiently phosphorylated by either
345 Cdk1 or Erk1/2, consistent with the similarity in their phosphorylation consensus motifs. In contrast, there
346 was minimal overlap between the sites predicted to be phosphorylated by Plk1 and those targeted by
347 Cdk1 or Erk1/2. Consequently, Class II phosphorylations are largely dependent on Cdk1 activity, whether
348 they are directly catalyzed by this kinase or indirectly through kinases under its control, such as Erk1/2
349 and Plk1 (see below). Our measurements that most of the sites, which are phosphorylated in MI, remain
350 stably phosphorylated during MI to MII transition is consistent with the observations made in yeast
351 showing that most of Cdk1 motifs remain phosphorylated at the end of meiosis I (Celebic *et al*, 2024).
352 Class III (5%) consists of proteins whose phosphorylation peaks in MI then decreases while oocytes
353 progress throughout meiotic maturation. This is the most predominant class of phosphosites present
354 during meiotic maturation in starfish (Swartz *et al*, 2021) and follow the peculiar pattern of Cdk1 activity
355 peaking at MI in these oocytes (Okano-Uchida *et al*, 1998; Kishimoto, 2003). Class IV (9%) is composed of
356 proteins whose phosphorylation progressively increases from MI to MII, hence potentially implicated in
357 MII entry. Finally, Class V (5%) comprises proteins whose phosphorylation increases from MII and which
358 could play a role in establishing the MII arrest. The phosphosites that are specific for either MI (Class III)
359 or MII (Classes IV and V) are much less abundant (5%, 9% and 5% respectively, Figure 3A) and might
360 distinguish the biochemical state of the two meiotic divisions. These conclusions were supported by the
361 identification of the kinases whose predicted phosphorylation sites are most enriched within each class,
362 by using the same server (https://kinase-library.phosphosite.org/kinase-library/score-site). Each class was
363 associated with a distinct set of enriched kinases (Figure 3-figure supplement 1B). It confirms that Cdk1
364 and its downstream kinases, Erk1/2 and Plk1 are the master regulators in Class II. The kinases identified
365 in Classes IV and V may represent novel regulators of entry into and arrest at MII.
366

367 **The release of the prophase arrest: receptors and membrane trafficking**

368 ***Receptors.*** Since meiotic maturation signaling begins with the interaction of progesterone with
369 membrane receptors, we first focused our analysis on these proteins (Josefsberg Ben-Yehoshua *et al*,
370 2007; Sadler & Maller, 1985). Progesterone signals through activation of a seven-pass-transmembrane
371 progesterone receptor (mPRβ or PAQR8) that belongs to the progestin and adiponectin receptor family
372 (Josefsberg Ben-Yehoshua *et al*, 2007; Nader *et al*, 2018, 2020) (Figure 1). The release of the prophase

373 block also involves the inactivation of an orphan constitutively active GPCR, GPR185, responsible for
374 maintaining oocyte prophase arrest by ensuring high cAMP levels and PKA activity (Ríos-Cardona *et al*,
375 2008; Deng *et al*, 2008). Progesterone decreases GPR185 signaling either through its cleavage by a
376 metalloproteinase (Deng *et al*, 2008) or through its endocytosis (Nader *et al*, 2014). One limitation of our
377 dataset lies in the loss of some membrane proteins during the fractionation protocol, explaining why our
378 proteomic workflow did not detect mPRβ and GPR185 or its close relative GPR12. Nevertheless, it does
379 detect some proteins that interact with mPR, *i.e.* PGRMC1, VLDLR and APPL1. PGRMC1 is known to form
380 a receptor complex with mPRα and is necessary for mediating progesterone signaling in zebrafish oocytes
381 (Wu *et al*, 2018). Interestingly, our phosphorylation data reveals that PGRMC1 and its close relative
382 PGRMC2 are phosphorylated on two homologous threonine residues during meiotic maturation,
383 suggesting that these proteins may contribute to mPRβ activity in *Xenopus* oocytes. In the prophase-
384 arrested oocyte, VLDLR regulates mPR trafficking from the endoplasmic reticulum through the Golgi to
385 the plasma membrane, preparing the oocyte to be responsive to progesterone (Nader *et al*, 2018). In
386 contrast, progesterone induces clathrin-dependent endocytosis of mPRβ into signaling endosomes, where
387 mPR interacts transiently with APPL1 and Akt2 to induce meiosis (Nader *et al*, 2020). The
388 phosphoproteomic data reveal that both APPL1 and Akt are phosphorylated in response to progesterone
389 but at the time of Cdk1 activation and on residues distinct from those identified by Nader *et al*. (2020).
390 Hence, phosphorylation events may continue to regulate the trafficking and activity of this receptor during
391 meiotic maturation, ensuring that the plasma membrane of the future egg is devoid of any steroid
392 receptor.

393 ***Membrane traffic.*** Vesicular trafficking at the cell membrane appears to be crucial for the
394 maintenance and the release the prophase meiotic arrest, and may also function through early
395 embryogenesis (Figure 1). In the prophase-arrested oocyte, the accumulation of the GPR185 receptor at
396 the plasma membrane maintains high cAMP levels (Nader *et al*, 2014) while the plasma membrane
397 targeting of mPRβ renders the oocyte competent to respond to progesterone (Nader *et al*, 2018).

398 Exocytosis is also crucial for the formation of the fluid-filled blastocoele cavity during
399 embryogenesis (Müller, 2001). Indeed, the apical membrane of the epithelium surrounding the blastula,
400 where the polarized activities of ion channels and transporters generate the blastocoele fluid, is formed
401 from the oocyte cell membrane (Müller, 2001). This requires further remodeling. Progesterone rapidly
402 blocks this exocytosis pathway (Colman *et al*, 1985; Leaf *et al*, 1990), leading to a decrease in membrane
403 surface area, which is revealed by the disappearance of microvilli that are enriched in oocytes but almost
404 absent in eggs (Dumont, 1972; Kado *et al*, 1981; Larabell & Chandler, 1989; Bluemink *et al*, 1983).

405 Importantly, blocking exocytosis induces meiotic maturation, in the absence of hormonal stimulation
406 (Mulner-Lorillon *et al*, 1995; El-Jouni *et al*, 2007). Furthermore, progesterone stimulates endocytosis of
407 membrane proteins, such as GPR185, whose activity is suppressed by its internalization, and mPRβ, whose
408 internalization is required to transduce its effects (Nader *et al*, 2018, 2020, 2014). The stimulation of
409 endocytosis also converts plasma membrane into intracellular vesicles that can provide membrane
410 reserves, necessary to support the rapid cell divisions, and hence the requirement for greater total
411 membrane surface area, during embryogenesis (Angres *et al*, 1991; Gawantka *et al*, 1992). However, it is
412 unknown whether PKA is responsible for the active secretory transport during the prophase arrest and
413 how progesterone blocks exocytosis and stimulates endocytosis (Figure 1).

414 To improve our understanding of vesicular trafficking and membrane organization, we analyzed
415 the proteins involved in these processes whose phosphosites belong to Class I (Figure 3B). Among these
416 proteins, PI4KB deserves special attention. This protein is critical for the maintenance of the Golgi and
417 trans-Golgi phosphatidylinositol-4-phosphate (PI4) pools. PI4KB regulates Golgi
418 disintegration/reorganization during mitosis and is involved in Golgi-to-plasma membrane trafficking (De
419 Matteis *et al*, 2013). The phosphoproteome reveals that PI4KB is dephosphorylated within 2 hours after
420 progesterone stimulation, on a PKA consensus phosphorylation site conserved in vertebrates. The
421 phosphorylation of this site by PKA is known to control the interaction of PI4KB with Armadillo-like helical
422 domain-containing protein 3 (ARMH3), an interaction important for the Golgi membrane integrity
423 (McPhail *et al*, 2020; Isobe *et al*, 2017; Blomen *et al*, 2015). PI4KB is also regulated by its interaction with
424 ACBD3, an AKAP-like scaffold platform in Golgi, which directly binds the R regulatory subunit of PKA and
425 regulates the traffic between Golgi and endoplasmic reticulum in a PKA-depending manner (Jia *et al*, 2023;
426 Klima *et al*, 2016; Sasaki *et al*, 2012). The phosphoproteome reveals that ACBD3 is phosphorylated during
427 meiotic maturation at the time of NEBD (Class II). PI4KB is therefore at the crossroad between PKA and
428 intra-membrane endoplasmic reticulum-Golgi-plasma membrane trafficking. Since these are key events
429 involved in meiosis resumption, PI4KB is a particularly attractive candidate as a PKA substrate for future
430 functional studies of membrane relocalization.

431 Proteins involved in the actin cytoskeleton are also represented in Class I phosphosites (Figure
432 3B). Their early post-translational modifications could regulate the reorganization of the actin
433 cytoskeleton that is known to accompany the modification of the secretory/endocytosis pathways (Gard,
434 1999). Among them, ITPRID2/KRAP tethers IP_3 receptors, which are located in the membrane of the
435 endoplasmic reticulum, to the actin under the plasma membrane, to mediate Ca^{2+} signalling (Thillaiappan
436 *et al*, 2021). During meiotic maturation, the endoplasmic reticulum, which is the major Ca^{2+} store, is

437 enriched in the cortex of the oocyte (Campanella *et al*, 1984; Charbonneau & Grey, 1984; Terasaki *et al*,
438 2001). This remodeling brings the Ca^{2+} source close to its primary targets at fertilization, when Ca^{2+} release
439 from endoplasmic reticulum activates the oocyte and blocks polyspermy. The proteins highlighted above
440 (Figure 3B) could participate to this critical reorganization of the endoplasmic reticulum.
441
442 **Protein translation and accumulation orchestrate meiotic divisions**
443 Two waves of translation take place in the oocytes: the first depends on PKA inactivation. It occurs
444 upstream and independently of Cdk1 activity and is required for Cdk1 activation. The second translation
445 wave takes place downstream Cdk1 activation (Santoni *et al*, 2024). Hence, in contrast to mitosis, a period
446 when protein synthesis is repressed (Ross, 1997), translation is activated during meiotic maturation,
447 indicating the existence of meiosis-specific controls of the process. However, the regulation of the two
448 waves of protein translation and the identity of the newly translated proteins had not been unraveled.
449 Interestingly, protein translation components are extensively regulated at the level of phosphorylation as
450 demonstrated by the enrichment of the proteins regulating these processes among 3 of the 5 phospho-
451 peptide classes (Figure 4A).
452 ***RBPs and translational control.*** Interestingly, several proteins implicated in the control of translation bear
453 phosphosites belonging to Class I, as eIF4ENIF1/4E-T, PATL1 and TACC3/Maskin (Figures 3B and 4B).
454 eIF4ENIF1/4E-T is required for eIF4e1b localization to P-bodies where mRNAs are stored in a dormant
455 state in zebrafish oocytes (Lorenzo-Orts *et al*, 2023). Both 4E-T and eIF4e1b are extensively
456 phosphorylated on multiple residues during meiotic divisions, suggesting a highly dynamic regulation of
457 P-bodies during this process (Figure 4B). Many RBPs known to control translation in oocytes are also
458 regulated at the phosphorylation level, including Pum proteins (Nakahata *et al*, 2003; Ota *et al*, 2011;
459 Padmanabhan, 2006), Zar proteins (Charlesworth *et al*, 2012; Yamamoto *et al*, 2013; Rong *et al*, 2019;
460 Heim *et al*, 2022) and PATL proteins (Christou-Kent *et al*, 2018; Zhang *et al*, 2023; Marnef *et al*, 2010).
461 PATL1 is a RNA-binding protein required for cytoplasmic mRNA P-body assembly in oocytes (Marnef *et al*,
462 2010). PATL1 and PATL2 have mutually exclusive expression patterns in *Xenopus* oocytes: PATL2 is
463 degraded, as confirmed by our proteomic data (Figure 2B,D, Figure 2-figure supplement 3A-B), while
464 PATL1 accumulates during meiotic maturation (Marnef *et al*, 2010) or is stable (Figure 2B, Figure 2-figure
465 supplement 3B). Although the role of PATL2 and the regulation of its stability by phosphorylation have
466 been well documented in the oocyte (Christou-Kent *et al*, 2018; Zhang *et al*, 2023), little is known about
467 the role of PATL1 during meiosis. Both PATL1 and 2 inhibit translation when tethered to mRNA and
468 assemble a complex that includes CPEB1, Xp54/DDX6, Rap55B/LSM14b (Marnef *et al*, 2010) (Figure 4B).

469 The early dephosphorylation of PATL1 detected in the phosphoproteome could modulate this inhibitory
470 complex during early events of meiotic maturation, while the extensive phosphorylation of the other
471 components of the complex could control its activity later during meiotic divisions (Figure 4B). Another
472 component of the repressive complex is TACC3/Maskin. It interacts with CPEB1, although this interaction,
473 and thus its role in regulation of translation, could not be reproduced in other studies (Minshall *et al*,
474 2007; Duran-Arqué *et al*, 2022). Importantly, besides its function in translation (Barnard *et al*, 2005;
475 Groisman *et al*, 2002), TACC3/Maskin also regulates the centrosome-mediated microtubule nucleation
476 through γ-TuRC (Peset *et al*, 2005). TACC3/Maskin is found widely regulated during meiotic divisions in
477 the phosphoproteome (Figure 4B). Eight residues in TACC3/Maskin, of which only two are conserved in
478 human Maskin (214/228 and 298/317 in human/*Xenopus*), exhibit a complex profile of phosphorylation
479 (Figure 4B). Two sites identified in the phosphoproteome, S266 and S298, were previously found to be
480 phosphorylated in egg extracts, regulating the function of TACC3/Maskin in the control of translation
481 (Barnard *et al*, 2005). S626 was also reported to be phosphorylated in prophase oocytes and during oocyte
482 meiotic maturation, although there is some controversy about the kinase (either PKA or Aurora-A) and
483 the role of this phosphorylation in either the control of translation or centrosome attachment (Barnard *et*
484 *al*, 2005; Pascreau *et al*, 2005). Interestingly, in our studies S240 is phosphorylated in the prophase oocyte
485 and dephosphorylated early in response to progesterone (Class I) (Figure 4B). Since the sequence
486 surrounding S240 does not correspond to a PKA consensus motif, it is hard to establish the biological
487 significance; nevertheless, such an early dephosphorylation deserves further attention.

488 ***The control of translation initiation.*** Translation regulation might not only depend on the
489 expression and post-translational regulation of the RBPs but could also involve the regulation of the core
490 translation initiation machinery, since we find that many of its components are phosphorylated (Figure
491 4C). Indeed, eIF4b, an activator of the eIF4a helicase that facilitates ribosome scanning (Jackson *et al*,
492 2010), eIF2b/eIF2s2, a component of the molecular machinery recruitment on the met-tRNA (Jackson *et*
493 *al*, 2010), and eIF4g, involved in the recognition of the mRNA 5'Cap (Jackson *et al*, 2010), are among the
494 proteins bearing sites whose phosphorylation peaks in MII (Figure 4-figure supplement 1). These
495 phosphorylation patterns correlate with the second wave of activation of translation that begins under
496 the control of Cdk1 activity in MI and continues progressively through MII (Meneau *et al*, 2020; Santoni
497 *et al*, 2024).

498 ***The control of ubiquitin ligases***. The levels of specific proteins are also regulated by proteolysis
499 at each step of meiotic maturation. Targeted regulation allows for the accumulation of key proteins
500 independently of any general increase in their translation, such as for Cyclin B1 (Santoni *et al*, 2024), or

501 the well-studied degradation of proteins, such as Cyclin B2, securin or CPEB1 (Taieb *et al*, 2001;
502 Wassmann, 2022; Setoyama *et al*, 2007). Interestingly, proteins controlling polyubiquitination display
503 phosphor-peptides enriched in Class II, strengthening the view that a major regulation of protein turnover
504 takes place at NEBD in order to orchestrate meiotic divisions (Figures 3 and 5A). APC is the key E3 ubiquitin
505 ligase that promotes metaphase-anaphase transition. Although the phosphorylation status of some
506 substrates determines their recognition by APC and influences the precise timing of their degradation,
507 APC activity is also regulated by the phosphorylation of its core subunits (Bansal & Tiwari, 2019) (Figure
508 5B).

509 Another important ubiquitination system that regulates stability of proteins during mitosis and
510 meiosis is the SCF complex (Kinterová *et al*, 2022). SCF is composed of three main components: Cul1, a
511 scaffold protein; Skp1, which interacts with specific F-box proteins that are involved in the substrate
512 recognition; and Rbx1, which interacts with the E2-ubiquitin ligases (Kinterová *et al*, 2022) (Figure 5C). SCF
513 ligases play important roles during oocyte meiotic maturation, especially the $SCF^{\beta TrCP}$ complex. Indeed,
514 $SCF^{\beta TrCP}$ mediates the degradation of multiple cell cycle regulators as Emi1, Emi2/Erp1, CPEB1 and BTG4,
515 whose degradation is required for progression through MI and MII in mouse and *Xenopus* oocytes
516 (Kinterová *et al*, 2022). Similar functions played by such protein degradations occur in mitosis, as Emi1
517 degradation that releases APC inhibition, then inducing Cyclin B destruction and mitotic exit (Reimann *et*
518 *al*, 2001).

519 Many F-Box proteins are also expressed in *Xenopus* oocytes, but they do not display high
520 phosphorylation dynamics. An exception is Lmo7/Fbxo20, which is degraded during meiosis, and is
521 dynamically phosphorylated (Figure 5C). Interestingly, Lmo7 overexpression causes defects at the spindle
522 assembly checkpoint, affecting the progression through mitotic divisions (Tzeng *et al*, 2018).

523 Additionally, many E2 enzymes were identified in our datasets as highly regulated at the
524 translational/accumulation and post-translational levels during meiotic maturation (Figure 5C). This layer
525 of regulation of protein ubiquitination remains understudied. Interestingly, an E2/E3 hybrid ubiquitin-
526 protein ligase, UBE2O, UBE4B (also known as UBOX3 or E4) and FAF2 (or Ubxn3B/UBXD8) display
527 phosphorylation sites belonging to Class I (Figures 3B and 5C). FAF2 is involved in stress granule clearance
528 (Gwon *et al*, 2021). UBE2O is also known to be involved in the drastic proteome remodeling during
529 erythroid differentiation (Nguyen *et al*, 2017), as well as quality control factor for orphans of multiprotein
530 complexes (Yanagitani *et al*, 2017). Ribosomal proteins are known substrates of UBE2O which leads to
531 their degradation (Nguyen *et al*, 2017). Whether UBE2O is involved in the downregulation of ribosome
532 biogenesis that occurs during meiotic maturation (Hyman & Wormington, 1988), and in the decrease of

533 Rpl26 (Figure 2-figure supplement 4A), is an interesting question. The dephosphorylation of UBE2O,
534 UBE4B and FAF2 could also be involved in the accumulation of Cyclin B1, which was recently shown to
535 occur independently of any increase in translation but to result from protein stabilization (Santoni *et al*,
536 2024).

537 Another important regulator of the SCF system, DCUN1D5, is found regulated in our
538 phosphoproteome. DCUN1D5 catalyzes the neddylation of all cullins, which is necessary for the activation
539 of cullin-RING E3 ubiquitin ligases (Keuss *et al*, 2016). DCUN1D5 is dephosphorylated at S9, a PKA
540 consensus site, and phosphorylated starting NEBD at S10 and S12 (Figure 5C). These phosphorylations
541 could control DCUN1D5 ability to activate SCF, especially since the inhibition of neddylation causes a
542 meiotic arrest in MI in mouse oocytes (Yang *et al*, 2019). Altogether, our dataset provides attractive
543 candidates to be involved in the regulation of both translation and protein stability that occur during
544 meiotic maturation.

545

546 **Activation of Cdk1 occurs through an intricate network of phosphorylation of Cdk1 regulators**

547 The activation of Cdk1 during oocyte maturation relies on an intricate network of feedforward and
548 feedback phosphorylation pathways mediated by kinases and phosphatases (Figure 1). Indeed,
549 components of the cell division machinery are highly enriched among Class II, III, IV and V (Figure 6A).
550 Some of the phosphorylation sites implicated in cell division control have been identified previously
551 through detailed studies using site-specific mutagenesis and phospho-specific antibodies. Our
552 phosphoproteomic analysis of oocyte maturation provides new regulatory elements (Figure 6B). An
553 important regulator of the Cdk1 auto-amplification loop is the kinase Plk1 that contributes to the
554 phosphorylation of the two direct Cdk1 regulators, Cdc25 and Myt1. Plk1 is activated by Aurora-A, a kinase
555 itself under the indirect control of Cdk1 in *Xenopus* oocyte (Maton *et al*, 2003), through the
556 phosphorylation of T210 (T201 in *Xenopus*)(Macůrek *et al*, 2008), a residue localized in the activation T-
557 loop of the kinase domain. We show here that Plk1 phosphorylation at T210 increases in MI and is then
558 constant throughout meiotic maturation (Class II) (Figure 6B and EV2A). This is consistent with the
559 function of Plk1, which phosphorylates multiple proteins required for the mechanics of division, and which
560 must logically be kept active throughout both meiotic divisions (Hansen *et al*, 2006; Solc *et al*, 2015).
561 Interestingly, the phosphoproteome also detects additional phosphorylation sites of Plk1, S326 (S335 in
562 human) and S340 (not conserved in human), which were previously found to be upregulated in response
563 to okadaic acid (Wind *et al*, 2002), an inhibitor of PP2A that strongly induces M-phase. These two residues
564 are located between the two functional domains of Plk1, the kinase domain and the Polo-box domain

565 (Cheng, 2003). This suggests that the phosphorylation of other critical residues than T210 of Plk1 could be
566 essential for its catalytic activation. Aurora-A kinase is activated during meiotic maturation downstream
567 Cdk1 (Maton *et al*, 2003; Castro *et al*, 2003; Maton *et al*, 2005). While our phosphoproteome does not
568 detect Aurora-A autophosphorylation at T288 (T295 in *Xenopus*), it registers the extensive
569 phosphorylation of Bora, an activator of Aurora-A involved in Plk1 activation (Thomas *et al*, 2016) (Figure
570 6B-figure supplement 1B). Several phosphorylation sites of Bora have been reported to be important for
571 its function as an Aurora-A activator: S41/38, S112/110, S137/135 and S252/S252 (human/*Xenopus*)
572 (Thomas *et al*, 2016; Vigneron *et al*, 2018; Tavernier *et al*, 2015, 2021). Among these sites, S110
573 phosphorylation of Bora by Cdk1-Cyclin A is critical for mitotic entry in *Xenopus* egg extracts (Vigneron *et*
574 *al*, 2018; Tavernier *et al*, 2015, 2021). Our phosphoproteome reveals that Bora belongs to Class II, being
575 phosphorylated starting NEBD, but surprisingly on distinct sites that were never reported in the literature:
576 S191/189, T294/287, S552/549, S-/521, T12/9 and T15/12 (human/*Xenopus*), with the exception of
577 S278/285. In contrast to the situation in mitosis, Cyclin A is very weakly expressed in the prophase oocyte
578 and accumulates during meiotic maturation (Kobayashi *et al*, 1991). Our proteome dataset reveals that
579 Cyclin A accumulates after MI. Hence, the phosphorylation of Bora at MI cannot be catalyzed by Cdk1-
580 Cyclin A in the *Xenopus* oocyte. Cdk1-Cyclin B is probably involved in these phosphorylations that take
581 place concomitantly with its activity and at Cdk1 phosphorylation consensus sites for 5 of the 7
582 phosphosites (Figure 6B-figure supplement 1B). Thus, this analysis reveals that Bora activation correlates
583 with its phosphorylation at residues not previously identified in earlier studies of the oocyte. We also
584 detect additional phosphorylation events on other players of the Cdk1 amplification loop, as Cdc25 and
585 Gwl/MASTL (Figure 6B-figure supplement 1C-D), whose extensive phosphorylation during M-phase is
586 usually detected by a large electrophoretic shift (Dupré *et al*, 2014).
587
588 **Phosphoregulation of the bimodal activity of Cdk1 during MI-MII transition**
589 In *Xenopus* oocytes, Cdk1 is not fully inactivated at anaphase I and during extrusion of the 1st polar body.
590 Indeed, the low Cdk1 activity that persists during the MI-MII transition is essential to avoid the
591 reformation of a nucleus, chromosome decondensation and DNA replication (Huchon *et al*, 1993; Thibier
592 *et al*, 1997). This short period is followed by a further increase of Cdk1 activity, due to a sustained synthesis
593 of B-cyclins; the increased Cdk1 activity allows the formation of the MII spindle (Gerhart *et al*, 1984)
594 (Figure 1). Although this bimodal subtle regulation of Cdk1 activity is essential for the success of meiosis,
595 *i.e*. linking two successive divisions without intervening DNA replication, it has never been quantified
596 precisely. Cdk1 activity can be measured by looking at the phosphorylation of one of its direct substrates,

597 Cdc27, a core APC component, at S428 (S426 in human)(Patra & Dunphy, 1998). Since PP2A, the
598 phosphatase responsible for dephosphorylating Cdc27, is inactive during the MI-MII transition, the
599 phosphorylation levels of Cdc27 can be directly attributed to Cdk1 activity during this period (Deák *et al*,
600 2003; Torres *et al*, 2010; Lemonnier *et al*, 2021; Labbé *et al*, 2021). Our precise quantification of the
601 phospho-occupancy of this site shows that its phosphorylation is virtually absent in prophase, increases
602 by 40% in MI, decreases during the MI-MII transition to 20%, then increases again in MII by 60% (Figure
603 6-figure supplement 1E). Three other residues of Cdc27, T205/207, S435/437 and S438/440
604 (human/*Xenopus*), also known to be phosphorylated at M-phase (Kraft, 2003), follow the same bimodal
605 pattern than S428. The subsequent increase in Cdk1 activity essential for MII entry requires that the kinase
606 escapes inhibitory phosphorylations by Myt1 and Wee2. Both Myt1 and Wee2 are reported to be inhibited
607 by phosphorylations, although the sites responsible for this inhibition are not precisely defined. In
608 *Xenopus*, Wee2 is not expressed in prophase oocytes and accumulates after NEBD (Nakajo *et al*, 2000;
609 Charlesworth *et al*, 2012) (Figure 1). Our analysis reveals that newly synthesized Wee2 is immediately
610 phosphorylated at 4 sites (Classes II and IV), one of them being not conserved in human, and none of them
611 corresponding to the proposed inhibitory S53 and S123 sites (Figure 6A-B-figure supplement 1F). Hence,
612 these data provide exciting new avenues of research to discover unexpected new regulations of old
613 players in Cdk1 activation.
614
615 **The Mos/MAPK pathway activation**
616 Mos plays a well-known role at the origin of a critical pathway controlling meiotic maturation (Yew *et al*,
617 1992; Furuno *et al*, 1994). It phosphorylates Mek1/2, which in turn phosphorylates Erk1/2 (also known as
618 MAPK) which leads to Rsk1/2 activation (Figure 6B). These play multiple essential roles, such as preventing
619 the reformation of a replicating nucleus between MI and MII (Dupre *et al*, 2002), enabling arrest in MII
620 (Sagata *et al*, 1989b), but also participating in Cdk1 activation (Sagata *et al*, 1989a) and the functioning of
621 meiotic spindles (Araki *et al*, 1996; Choi *et al*, 1996; Bodart *et al*, 2005). The phosphoproteome detects
622 the activation of the Mos-MAPK module, with the phosphorylation of Erk2 on T185 and Y187 (T188 and
623 Y190 in *Xenopus*) by MEK1/2 (Payne *et al*, 1991), an event that begins in MI (Figure 6B-figure supplement
624 2A). Interestingly, additional phosphorylation sites are identified in MEK1 and Rsk1/2, the latter being
625 hyperphosphorylated during meiosis as detected by a large electrophoretic shift (Bhatt & Ferrell, 2000)
626 (Figure 6B-figure supplement 2B-E). Rsk1 auto-phosphorylation at S381 (S380 in human) is required for
627 its activity (Vik & Ryder, 1997). Our phosphoproteome measures a highly-confident phospho-occupancy
628 for this site demonstrating the switch-like activation of the MAPK pathway at NEBD, followed by the

629 maintenance of a constant level of its activity (Figure 6B-figure supplement 2F). The timing of activation
630 of the Mos-MAPK cascade has been controversial, one hypothesis being that it is activated before Cdk1
631 and participates in the activation of this kinase (Sagata *et al*, 1988; Gavin *et al*, 1999), while another is that
632 it is under the control of the starter Cdk1 activity and is only involved in the autoamplification loop
633 (Santoni *et al*, 2024; Dupre *et al*, 2002; Fisher *et al*, 1999). The phosphoproteomic data clearly support the
634 latter.
635
636 **Phosphorylation of key components of the nuclear envelope during breakdown**
637 As a result of the massive activation of kinase activities under the control of Cdk1, hundreds of proteins
638 are phosphorylated and orchestrate the structural events choreographing the mechanics of meiotic
639 divisions. The first of these is the massive vesiculation of the nuclear envelope surrounding the enormous
640 oocyte nucleus. During mitosis, nuclear pore proteins are extensively phosphorylated by Cdk1-Cyclin B,
641 Plk1 and Nek6/7 to promote the breakdown of the nuclear envelope (Kutay *et al*, 2021). The *Xenopus*
642 oocyte has the unusual feature of having an enormous nucleus (475 μm in diameter), and therefore a
643 considerable surface area of the nuclear envelope (0.96 mm^2), as well as large stocks of annulate lamellae
644 in the cytoplasm. Annulate lamellae are cytoplasmic stack cisternae of nuclear envelope perforated with
645 nuclear pores, 10 times more abundant than in the nucleus in the *Xenopus* oocyte, but devoid of lamins
646 (Bement & Capco, 1990; Miller & Forbes, 2000; Cordes *et al*, 1995). Their surface area also far exceeds
647 that of the nuclear envelope surrounding the nucleus (Cordes *et al*, 1995). This correlates with the high
648 protein concentrations of the nuclear pore proteins (0.1 to 0.7 μM) that we have measured (Figure 7A).
649 Annulate lamellae play a critical role as a reservoir for the formation of the 4000 of nuclei that form during
650 the embryonic cell divisions leading up to the mid-blastula transition and the onset of transcription (Kessel
651 *et al*, 1986; De Magistris & Antonin, 2018; Feldherr, 1974). During meiotic maturation, NEBD and
652 vesiculation of annulate lamellae occur at the same time, in a progressive spatial manner, starting from
653 the vegetal pole. Importantly, the nucleus and annulate lamellae do not re-form between the two meiotic
654 divisions, reducing the risk that an S-phase can take place between MI and MII (Bement & Capco, 1990).
655 A gene ontology analysis of our phosphoproteome highlights that the phosphorylation of nuclear pore
656 components is enriched in Classes II, III and IV, displaying the highest level of enrichment in Class III, hence
657 characteristic of MI (Figure 7B). The nucleoporin Nup53 (also called Nup35) is a component of the soluble
658 core region of the nuclear pore complex that is extensively phosphorylated in mitosis by Cdk1 and Plk1
659 (Linder *et al*, 2017). Phosphomimetic mutations of all Cdk1 and Plk1 sites in Nup53 slow down the
660 reformation of nuclear pores in interphase and mutation to phospho-null amino acids impairs the nuclear

661 breakdown during meiosis (Linder *et al*, 2017). Our phosphoproteome reveals that Nup53
662 phosphorylation is more dynamic than previously believed (Figure 7C). Indeed, 6 phospho-peptides are
663 found to peak in MI (Class III), 9 phospho-peptides are phosphorylated both in MI and MII (Class II), and 2
664 phospho-peptides continuously increase in phosphorylation during meiotic maturation (Class IV) (Figure
665 7C). We were able to calculate the phospho-occupancy of the S59 (S66 in human), showing that it
666 increases from 30% in prophase to 90% in MI oocytes and stays constant until MII (Class II) (Figure 7D).
667 Several other transmembrane nucleoporins, notably NDC1 and POM121C, undergo dramatic increase of
668 phosphorylation at transition to MI. Altogether, these observations indicate that dissociation of the
669 nuclear envelope and the annulate lamellae occurring in MI might require either a specific set of
670 phosphorylations and/or a general level of phosphorylation that is higher than the level of
671 phosphorylation required to maintain the nucleus and the annulate lamellae dissociated during the MI-
672 MII transition through MII.
673
674 **The regulation of centrosomal proteins during oocyte maturation**
675 An intriguing feature of oocytes in most, if not all, metazoan species is the elimination of their centrioles.
676 This allows the sperm to contribute its centriole and thereby initiates the division cycle and the cell cycle.
677 There is longstanding literature that proves that the oocyte or egg has retained its ability to generate
678 centrioles. However, in nature, the female centrioles are lost and the sperm centriole is the main
679 contributor. In *Xenopus*, oocytes entering prophase I contain a typical centrosome, including a pair of
680 centrioles and pericentriolar material (PCM) containing γ-tubulin and pericentrin. Centrioles disappear at
681 the end of the pachytene stage of prophase I and PCM disperses in multiple foci in the cytoplasm that are
682 no longer functional as microtubule nucleation sites (Gard *et al*, 1995). At fertilization, the male gamete
683 delivers two centrioles but does not provide the PCM (Delattre & Gönczy, 2004). Therefore, in most
684 species (with the exception of rodents), the complete centrosome of the one-cell stage embryo is a bi-
685 parental inheritance, reconstituted from paternal centrioles and maternal PCM (Delattre & Gönczy, 2004).
686 In *Xenopus*, oocytes store enough quiescent centrosomal building blocks for duplicating and assembling
687 1000 to 2000 centrosomes (Gard *et al*, 1990). This implies that oocytes should comprise an enormous
688 reserve of centrosomal proteins, *i.e.* centriolar and PCM proteins, that sustain the reconstitution of a
689 functional centrosome at fertilization and its subsequent rounds of duplication in the early embryo.
690 ***Centriolar proteins.*** The centriole is formed by a polarized cylinder of microtubule triplets,
691 decorated along the proximal to distal axis with several appendages that define the three main regions of
692 the organelle: the proximal part, the central core, and the distal region (LeGuennec *et al*, 2021). In

693 agreement with a published RNA-seq and proteome of *Xenopus* eggs (Session *et al*, 2016; Wühr *et al*,
694 2014), our proteome reveals that most of the centriolar proteins are expressed in the oocyte (Table 1).
695 The components of the proximal part, as SAS-6 and CPAP/CENPJ, and of the central core, as POC1B, POC5
696 and Centrin 1, are either constant or accumulate during meiotic maturation (Table 1). In contrast, proteins
697 of distal and subdistal appendages are present at lower concentration, either constant or decreasing
698 during meiotic maturation (Table 1). Indeed, the appendages are critical for the docking of mature
699 centrioles at the plasma membrane and ciliogenesis (Tanos *et al*, 2013), a process that is not functional in
700 the oocyte and during the early embryonic divisions (Drysdale & Elinson, 1992).

701 Besides the basic building blocks forming the centriole, the oocyte is expected to provide the
702 machinery for its duplication, the first cycle occurring immediately after fertilization. The key regulators
703 of centriole duplication, including Plk4, SAS-6 and STIL, are generally expressed at very low levels (Bauer
704 *et al*, 2016). While Plk4 is expressed at the mRNA level in oocytes but escaped our proteomic detection,
705 SAS-6 and STIL are expressed at a constant level during meiotic maturation (Table 1). The estimated
706 concentrations of both proteins are in agreement with the previous predictions, that cartwheels comprise
707 one molecule of STIL for every SAS-6 dimer (Bauer *et al*, 2016). Other important regulators of centriole
708 duplication, such as CEP192, CEP152, CEP63, RTTN, CEP110/CCP110, CEP97 and CEP76 were also
709 detected, and are either constant or accumulate during meiotic divisions (Table 1). Interestingly, our
710 phosphoproteome reveals that several of these proteins are phosphorylated during meiotic maturation.
711 STIL is phosphorylated at S554, which is located in a Cdk1 phosphorylation consensus (Appendix Figure
712 S5A), an interesting observation since phosphorylation of STIL by Cdk1-Cyclin reduces the efficiency of
713 daughter centriole assembly. This phosphorylation provides an explanation why centrioles cannot
714 duplicate during M-phase (Zitouni *et al*, 2016; Steinacker *et al*, 2022). A massive CEP97 phosphorylation
715 occurs at MI at 8 distinct sites, only 3 of them lying within a Cdk1 consensus motif (Appendix Figure S5B).
716 Remarkably, one of the phosphosites of CEP97, S633, has been recently shown to be phosphorylated by
717 the kinase Dyrk1a in multiciliated cells of *Xenopus* embryos (Lee *et al*, 2022); it is required for centriole
718 duplication. Therefore, although centrioles are not assembled, all centriolar proteins are expressed in the
719 full-grown oocyte and these components serve as a stock for the biogenesis of the centrioles of the
720 embryo. Our results suggest that specific phosphorylations of proteins regulating centriole assembly could
721 prevent the *de novo* establishment of centrioles in the oocyte.

722 ***PCM proteins.*** The core element of the PCM is the γ-tubulin ring complex (γ-TuRC) which is the
723 basic element for nucleation of microtubules from microtubule-organizing centers (MTOCs) (Oakley &
724 Oakley, 1989). It includes γ-tubulin that is combined with other proteins known as GCP2/tubgcp2 to

725 GCP6/tubgcp6. Some PCM proteins or regulators of PCM assembly have been described in functional
726 studies to be present in the oocyte and then recruited to the zygotic centrosome as maternal components.
727 These include γ-tubulin (Stearns & Kirschner, 1994; Gard, 1994; Félix *et al*, 1994), pericentrin (Dictenberg
728 *et al*, 1998), Nek2B (Fry *et al*, 2000; Uto, 2000), SSX2IP (Bärenz *et al*, 2013),TPX2, PRC1, Kif4A, Eg5/Kif11,
729 CLASP1/Xorbit and Kif22/Xkid, CEP152 (Hatch *et al*, 2010), NEDD1 (Liu & Wiese, 2008), Maskin/TACC3
730 (Stebbins-Boaz *et al*, 1999; Peset *et al*, 2005), XMAP215/CKAP5 (Popov *et al*, 2002; Kinoshita *et al*, 2002)
731 and Nercc1/NEK9 (Roig *et al*, 2005).

732 Most of the PCM proteins were detected in our proteomic dataset and either accumulate or stay
733 constant during meiotic divisions (Table 1). Our dataset highlights that γ-tubulin accumulates during
734 meiotic divisions at the time the oocytes enter MII (Table 1-table supplement 1C). GCP2 and 4 are
735 expressed at a lower level than γ-tubulin (Table 1), in agreement with the expected stoichiometry of GCPs-
736 γ-tubulin in the γ-TuRC (Sulimenko *et al*, 2022). The phosphorylation of γ-TuRC components is known to
737 affect the stability and the activation of the complex (Sulimenko *et al*, 2022). We detected the
738 phosphorylation of GCP3 at S814 (Class IV) and GCP6 at S1173 (Class III) (Table 1-table supplement 1D).
739 This second phosphosite is well conserved in the human protein and targeted by Plk4, which regulates
740 centriole duplication (Bahtz *et al*, 2012). These results indicate that the oocyte, despite the absence of
741 centrioles, prepares a functional centrosomal machinery by accumulating and/or phosphorylating some
742 of the PCM proteins. Apart of the γ-TuRC complex, we found that 10 other PCM proteins are
743 phosphorylated during meiotic maturation (CEP192, SSX2IP, CEP41, TACC3/Maskin, Nucleophosmin,
744 Katanin, Kif11, Kif15/Eg5, Numa and Dynein). CEP192 is a coiled-coil scaffolding protein that recruits γ-
745 TuRC, Aurora-A and Plk1 to the centrosome for its maturation. Our phosphoproteome reveals that
746 CEP192, a Class II protein, is phosphorylated at 7 sites between prophase and MI, 5 of them corresponding
747 to Cdk1 phosphorylation sites (Table 1-table supplement 1E). Plk1 is recruited to its many different
748 locations in the cell through its Polo-Box-Domain (PBD), which binds to phosphorylated S-S/T(p) motifs
749 (Elia *et al*, 2003a, 2003b; Lee *et al*, 1998; Reynolds & Ohkura, 2003). Two of the CEP192 sites identified in
750 our phosphoproteome, S991 and S1227, correspond to such motifs. Therefore, by attracting Plk1, CEP192
751 phosphorylation could prepare the reconstitution of a functional centrosome at fertilization.
752

753 **Assembly of microtubule spindles and microtubule dynamics**

754 *Xenopus* prophase oocytes are inefficient in their ability to support microtubule polymerization (Jessus *et*
755 *al*, 1984; Gard & Kirschner, 1987; Heidemann & Kirschner, 1975), although microtubules are formed at
756 the cortical and nuclear envelope level, where γ-tubulin foci are also localized (Gard, 1994; Jessus *et al*,

757 1988). The ability to assemble microtubule asters is acquired at the time of NEBD, when a giant disk-
758 shaped MTOC generates a large microtubular monoaster at the basal region of the disintegrating nucleus
759 (Huchon *et al*, 1981; Gard, 1994). Therefore, MTOC and microtubule-associated proteins (MAPs) must be
760 finely regulated by post-translational modifications at time of NEBD. The transient microtubule monoaster
761 transports the meiotic chromosomes to the animal cortex, where the first meiotic spindle is assembled
762 (Huchon *et al*, 1981; Gard, 1992). Due to the absence of centrioles, meiotic spindles are barrel-shaped
763 and are formed by centrosome-independent microtubule nucleation originating from the chromosomes
764 and involving chromatin and the Ran GTPase (Gruss & Vernos, 2004), much like spindles of vascular plant
765 cells. Moreover, the two successive spindles are differentially regulated. The MI spindle is a transient and
766 dynamic structure while the MII spindle is stable for hours, anchored to the plasma membrane until
767 fertilization (Gard, 1992). Therefore, it is possible that MAPs are specifically and differentially regulated
768 at MI and MII (Classes III and V). Finally, a major change in microtubule assembly occurs during the
769 transition from meiosis to embryonic mitosis. The assembly of the first embryonic spindle integrates the
770 meiotic chromosome-dependent pathway with the newly formed centrosomes (Cavazza *et al*, 2016).
771 Thereafter, subsequent embryonic spindles depend solely on the microtubule nucleating activity of the
772 centrosomes (Kirschner, 1986). All these critical transitions in the way of assembling a microtubular
773 spindle depend on the proteins stored in the oocyte.

774 Many regulators of the microtubular spindle are highly regulated during meiotic divisions, both at
775 level of their accumulation (Figure 2B-C) and by post-translation modifications (Figure 8). At least 5
776 microtubule regulatory proteins undergo specific patterns of phosphorylation that deserve attention
777 (Figure 8). Katanin (KATNB1), which is responsible for the majority of M-phase severing activity in *Xenopus*
778 eggs and is activated by Cdk1 (McNally & Thomas, 1998), displays a bi-modal pattern of phosphorylation,
779 increasing at the time of formation of the monoaster-MTOC and MI spindle, decreasing during MI-MII
780 transition and increasing again at MII (Figure 8). Kif11/Eg5 phosphorylation occurs at T936 and T937
781 starting NEBD (Figure 8). Both phosphosites were reported in a broad range of models, and the second
782 site was shown to be phosphorylated by Cdk1 (Blangy *et al*, 1995; Cahu *et al*, 2008; Giet *et al*, 1999) (Figure
783 8). Kif11/Eg5 controls the relative stability of bipolar versus monopolar organization of spindles in *Xenopus*
784 egg extracts (Mitchison *et al*, 2005) but also centrosome disjunction and/or separation. Hence, Kif11 is a
785 good candidate to be an important player regulating the original changes in microtubule dynamics and
786 organization of the two successive spindles. Kif15, also known as XKlp2, a plus end-directed kinesin protein
787 required for centrosome separation and maintenance of spindle bipolarity in *Xenopus* egg extracts (Boleti
788 *et al*, 1996), is phosphorylated at S681 and S692 during meiotic maturation. S681 is rather phosphorylated

789 at MI while S692 is specific of MII (Figure 8), suggesting a potential distinct regulation of Kif15 on
790 microtubule dynamics at MI and MII. In contrast to Kif11/Eg5 and Kif15, some kinesins from the kinesin-
791 14 family, such as Kifc1 whose protein level increases during meiotic divisions (Figure 2C), as well as
792 dyneins, are motor proteins that move to microtubules in the opposite direction to kinesins. Among the
793 dynein family, the two paralog genes dynein light intermediate chain (DynC1LI1 and DynC1LI2) play
794 important roles in mitosis, including positioning the spindle and focusing the MTs into poles. Our
795 phosphoproteome reveals multiple phosphorylations of these proteins, starting in MI and remaining
796 constant or progressively increasing until MII, as for S197 of DynC1LI1 (S207 in human) (Figure 8). This
797 agrees with previous data showing that S197 is phosphorylated by Cdk1 (Dell *et al*, 2000; Addinall *et al*,
798 2001) and that DynC1LI becomes hyperphosphorylated at the time of NEBD and remains
799 hyperphosphorylated throughout the rest of meiosis (Huang *et al*, 1999). Additionally, our
800 phosphoproteome reveals that 3 sites (495, 498 and 501) are phosphorylated around NEBD and get
801 dephosphorylated after MI (Class III), hence being correlated with the 1st meiotic division and not the 2nd
802 one, while 6 other sites (197,396, 409,446, 452, and 467) are phosphorylated both in MI and MII (Class II)
803 (Figure 8). Dynein is required for organization of the original microtubule/MTOC array that is organized at
804 NEBD, together with XMAP215, XKCM1 and Numa (Becker *et al*, 2003). The formation of this oocyte
805 original monoaster/MTOC could involve the dynein phosphorylations that transiently take place precisely
806 at this period.

807 Strikingly, MI and MII spindles segregate chromosomes and chromatids in a very different way. In
808 MI, the homologous chromosomes are segregated, whereas in MII the sister chromatids are displaced in
809 the daughter cells, due to a specific organization of kinetochores and regulation of cohesins. In MI, arm
810 cohesins are phosphorylated and degraded whereas centromeric cohesins are protected from cleavage
811 by Sugoshin (Sgo1)-PP2A. This allows the separation of chromosomes, but chromatids are still attached
812 together. In MII, centromeric cohesins are fully degraded, allowing the segregation of sister chromatids,
813 as during mitosis (Wassmann, 2022). How a fraction of cohesins is protected from cleavage in MI but not
814 in MII is still not entirely clear since the phosphorylation of cohesins and their partners, which are not very
815 abundant proteins, is difficult to be detected with conventional shotgun phosphoproteomics. Notably,
816 our phosphoproteomic studies highlight new sites differentially phosphorylated between MI and MII
817 within these proteins. Sgo1 and two components of the cohesin complex, Pds5b and Wapl, are
818 increasingly phosphorylated during meiotic divisions (Class IV) (Table 1-table supplement 1E).
819 Noteworthy, S1069 of Wapl is a putative Plk1 site (Grosstessner-Hain *et al*, 2011; Kettenbach *et al*, 2011).
820 By highlighting new sites differentially phosphorylated between MI and MII, our phosphoproteomic

821 studies provide clues to elucidate the still unknown mechanisms of the meiotic mechanism of cohesion
822 protection-deprotection.
823

824 **Evolutional conservation of the phospho-proteome between *Xenopus* and mouse**

825 We compared our phosphoproteome to a dataset obtained during meiotic divisions in mouse oocytes
826 (Sun *et al*, 2024). We identified 408 phosphorylation sites present in both datasets (see Methods)
827 (Appendix 7). These sites correspond to 320 *Xenopus* proteins and 277 mouse proteins. Note that when
828 multiple mouse proteins share the same phospho-peptide sequence, they are grouped together in the
829 mouse dataset. However, alignment with *Xenopus* data allows us to resolve which specific mouse protein
830 is phosphorylated, thereby enriching the mouse dataset by leveraging information from *Xenopus*
831 measurements. We then assessed whether the changes in phosphorylation between prophase and
832 metaphase II were consistent between *Xenopus* and mouse meiotic maturation (Figure 9A). Interestingly,
833 the phosphorylation dynamics were significantly correlated between the two datasets (Pearson
834 coefficient: 0.39, $p < 0.0001$) (Figure 9A). Furthermore, the changes in phosphorylation observed in
835 *Xenopus* oocytes (range of the Log_2 Fold Change (MII/Pro): -4.27 and 7.03) were substantially greater than
836 those measured in the mouse dataset (range of the Log_2Fold Change(MII/Pro): -2.55 and 3.72), likely
837 reflecting the higher dynamic range achieved by our workflow. Among the key phosphorylation events
838 detected in both datasets are those involved in the activation of Cdk1 and the Mos/MAPK pathway.
839 Notably, phosphorylation of Plk1 at T210 (mouse numbering, T201 in *Xenopus*), which is catalyzed by
840 Aurora A and is critical for Plk1 activation (Macůrek *et al*, 2008), as well as phosphorylation of Gwl at S442
841 (mouse numbering, 467 in *Xenopus*), increased in both datasets (Figures 6B and 9A-B). Similarly, both
842 datasets consistently detected phosphorylation of Erk2 at T183 (mouse numbering, T188 in *Xenopus*),
843 which reflects MEK-dependent activation of this kinase (Payne *et al*, 1991)(Figures 6B and 9A-B). Among
844 the conserved sites whose phosphorylation increases during meiosis, several are known targets of Cdk1
845 and Erk/MAPK (Figure 9B), consistent with the activation of these kinases during meiotic maturation. We
846 experimentally confirmed the phosphorylation of Fak1 at S910, Erk2 at T188, and Plk1 at T201 by western
847 blot (Figure 9C). Moreover, by microinjecting the Cdk1-specific inhibitor Cip1 in oocytes in order to
848 prevent Cdk1 activation, we demonstrated that Cdk1 is required for phosphorylation of all these
849 substrates, whether they are direct targets of Cdk1 or Erk/MAPK (Figure 9C). This aligns with previous
850 reports indicating that MAPK pathway activation in oocytes occurs downstream of the initial activation of
851 Cdk1 (Santoni *et al*, 2024). Interestingly, AKTS1/PRAS40 phosphorylation decreases during meiotic
852 maturation in both species (Figure 9A-B). We experimentally validated the dephosphorylation of

853 AKTS1/PRAS40 at S208 and showed that this event occurs at NEBD and depends on Cdk1 activity (Figure
854 9C). AKTS1/PRAS40 is a direct inhibitor of mTORC1 by competing with 4E-BP1 and S6K1 for binding to
855 raptor (Wang *et al*, 2007; Oshiro *et al*, 2007). AKTS1/PRAS40 is phosphorylated on S184 (mouse
856 numbering, S208 in *Xenopus*) by mTORC1, which leads to its dissociation from mTOR and enhances its
857 ability to phosphorylate its substrates (Oshiro *et al*, 2007). Interestingly, previous studies suggest that
858 translation of ribosomal proteins, which are targets of mTOR signaling via the TOP motif located in their
859 5'-UTR, decreases during meiotic maturation (Luong *et al*, 2020). Our findings support these observations
860 and provide additional evidence for the downregulation of mTOR activity upon meiotic resumption.
861

862 **DISCUSSION**

863 The amphibian oocyte and egg have long been a source of inspiration and a source of
864 experimental opportunity for important areas of biology, such as nuclear organization, spindle formation,
865 cell polarity, fertilization, mitosis and meiosis, endocrine signaling and intracellular signal transduction. As
866 experimental embryology gave way to genetic approaches in the late 20th century to study embryonic
867 development, the attractiveness of amphibian oocytes declined.

868 The original advantages of the amphibian oocyte are now becoming more obvious, as it becomes
869 important to link complex cellular processes, like cell division, to signal transduction. These processes are
870 difficult to study because they occur at a single cell or even at subcellular level. Indeed, many important
871 cell-division related processes involve transient changes occurring in specific compartments of the cell,
872 like the endoplasmic reticulum, the mitotic apparatus, the nuclear and plasma membranes, or the
873 cytoskeleton. Additionally, meiotic and mitotic divisions occupy a very short fraction of the life span of
874 germ and somatic cells, making it hard to study them in cultured cells. Frog oocytes and eggs show
875 exquisite synchrony of cell division, allowing to have large cohort of cells at the same stage of the cell
876 cycle. Therefore, we and others have returned to the awesome power of the amphibian oocyte and egg
877 to study the signal transduction, intracellular posttranslational changes surrounding the onset of meiotic
878 and mitotic divisions and fertilization at a single cell level.

879 Importantly, the ingenious and sensitive tools developed to study the transcriptional regulation
880 are of little use in the study of a cell type that does not transcribe RNA and of events that are regulated
881 post-translationally, as meiotic and early embryonic divisions. For a long time, we lacked general tools for
882 identification and measurement of the activity of the regulators of these processes, impairing our ability
883 to connect the morphological changes previously described by histology to the respective molecular
884 events. One manner to investigate these pathways is using pharmacological inhibitors, but their non-
885 specificity and the complexity of pathways pose serious limitations. For years, phosphorylation events
886 have been extensively studied using candidate-based approaches, as site-specific mutagenesis and
887 phosphospecific antibodies. These targeted-approaches have several caveats. The selection of the
888 putative sites of phosphorylation is based on *in silico* evidence, limiting the analysis to proteins bearing
889 canonical consensus sequences and hence our knowledge of novel phosphorylation motifs. When
890 multiple putative phosphorylation sites are present in the same protein, mutagenesis of individual sites
891 or combinations of sites becomes too complex, impairing identification of the phosphorylation sites used
892 *in vivo* and their interdependency or redundancy. Moreover, the time-consuming production of phospho-
893 specific antibodies is not scalable to high throughput applications. Mass spectrometry has the potential

894 of shedding light on these intricated networks. However, the current tools are unable to accurately
895 quantify the level of proteins and phosphorylated proteins at the single cell level -except for the frog
896 oocytes and eggs, thanks to their exceptional size and high protein content.

897 Oocyte meiotic maturation is a key biological process. First, it transforms the oocyte into a
898 fertilizable cell at the origin of life of any animal. Second, since meiosis derives from mitosis, thanks to
899 cellular adaptations that were necessary to produce a haploid gamete (preventing an S-phase between
900 the two divisions, modifying the functioning of the spindle during meiosis I, establishing division arrests
901 needed for the oocyte to grow or to wait for sperm, performing asymmetrical divisions to save nutrient
902 reserves, etc.), its study provides the opportunity to understand how cell division can adapt and diversify
903 in living systems, depending on specific cellular organization and specialized functions.

904 In this paper, we have applied the current state of the art of quantitative mass spectrometry to
905 oocyte maturation and meiotic divisions using quantitative proteomics and quantitative
906 phosphoproteomics. We have temporally correlated events with oocyte maturation induced naturally by
907 progesterone to *Xenopus* full-grown oocytes and watched the progression through meiosis I to the natural
908 arrest at the second meiotic metaphase. We have been able to correlate the proteomic measurements
909 with the physiological changes as the oocyte, as it goes from an early prophase I state through to a second
910 meiotic metaphase state. We find dramatic changes in the oocyte nucleus and the meiotic spindles and
911 drastic modifications to the standard cell cycle. These dramatic changes are choreographed principally by
912 signaling pathways employing kinases and phosphatases. In all animals, meiotic maturation relies on the
913 dynamics of phosphorylation events, either during the signaling pathway that leads to Cdk1 activation or
914 during the Cdk1 downstream period that orchestrates the structural events of the two meiotic divisions.
915 The candidate-based approaches have provided a global scheme of this process based on the knowledge
916 of a few kinases that have been extensively studied for years. However, this scheme still does not provide
917 a very comprehensive picture of the meiotic process, since it does not take into account hundreds of
918 unknown critical kinases, substrates and phosphosites. Our quantitative proteomics and
919 phosphoproteomics approach allowed to obtain a much deeper and comprehensive dynamic picture of
920 the phosphorylated sites during meiotic maturation. This has enabled us to describe and support with
921 biochemical precision the various processes in the oocyte, determine the relative timing of various site
922 phosphorylations and molecular processes, thereby challenging or suggesting the epistatic sequences of
923 specific molecular pathways. Furthermore, we confirmed the importance of certain previously known
924 phosphosites, identified the likely kinases or in some cases the kinase families responsible for substrate

phosphorylation, and established connections between phosphorylation events and intracellular remodeling, as well as regulatory mechanisms such as translation and protein degradation.

In addition to explaining the order of diverse events of chromatin remodeling, nuclear organization, plasma membrane transformations, cytoskeletal changes of meiosis, our proteomic and phospho-proteomic datasets should provide a large number of experimental avenues for exploring similar events in both mitotic and meiotic stages of diverse organisms. This molecular data will enable us to better understand regulatory pathways involving chromosome behavior, spindle formation, nuclear and plasma membrane regulation, and signal transduction and derive insights far beyond the scope of meiosis and oocyte maturation. One such insight might come from a closer analysis of the quality control mechanisms in the oocyte. Both nucleopore remodeling (King *et al*, 2019) and E2/E3 ubiquitin ligases are involved in housekeeping and quality control, specifically in the removal of aggregated and orphan complex proteins, as the germ cell of an organism prepares to become the next generation

938 **METHODS**

939 **Oocytes collection and *in vitro* maturation**

940 The research with *Xenopus laevis* was performed under the oversight of the Harvard Medical Area
941 Institutional Animal Care and Use Committee. Mature *Xenopus laevis* females were used after priming
942 with pregnant mare serum gonadotropin (PMSG, 50 IU per frog). A sample of ovary tissue was surgically
943 removed, rinsed in 1× Marc's modified Ringer's (MMR) and placed in OR2 buffer (83 mM NaCl, 2.5 mM
944 KCl, 1 mM $CaCl_2$, 1 mM $MgCl_2$, 1 mM Na_2HPO_4, 5 mM HEPES, pH 7.8) and oocytes were manually
945 defolliculated. Prophase oocytes were selected and kept in dishes with agar beds to avoid sticking to the
946 dish. For the Cip1 experiment, prophase oocytes were microinjected with 60 ng of GST-XenCip1, as
947 previously described (Santoni *et al*, 2024). Maturation was induced by incubation at 18 °C with 10 µg/mL
948 progesterone in OR2 buffer.

949 Oocytes were flash frozen with liquid nitrogen in bunches of ten or fifty for protein and phospho-
950 proteomics measurements respectively. All samples were taken in triplicates, each biological replicate
951 was performed with different frogs. The first sample was taken from untreated oocytes at the time of
952 progesterone treatment, the second timepoint 2 hours after progesterone treatment, with hourly
953 timepoints past that, up to 9 hours post treatment.

954

955 **Oocyte lysis and digestion into peptides**

956 For each condition the oocytes were lysed at a ratio of 6 µL buffer/embryo in the same buffer as (Presler
957 *et al*, 2017) (0.25 M sucrose, 1% replacement NP-40, 10 mM EDTA, 25 mM HEPES, 1 mM TCEP, 10 µM
958 Combretastatin, 10 µM Cytochalasin D, Roche Protease Inhibitor Mini EDTA free, and Phosstop inhibitor
959 (Roche) at pH 7.2). The yolk was removed by spinning the samples at 4,000 g for 4 minutes at 4°C. Both
960 the supernatant and all lipids were transferred for a new tube. The concentration of HEPES was raised to
961 0.1 M and SDS was added to 20%. After addition of DTT to 5 mM, the samples were denatured in a 60°C
962 water bath for 20 minutes. After the samples temperatures return to room temperature, N-
963 Ethylmaleimide (NEM) was added to 15 mM, tubes were mixed thoroughly, and the reaction proceeded
964 for 1 hour. Then additional DTT was added to 5 mM to quench the excess NEM. The samples were flash
965 frozen and stored at -80°C until the methanol chloroform precipitation (Wessel & Flügge, 1984). Protein
966 was precipitated by methanol-chloroform precipitation. Due to the large volume of lysate (~ 1 mL), the
967 precipitation was performed in glass 15 mL Corex tubes (No. 8441). The tubes were cleaned for a two-
968 hour chromic acid incubation and rinsed extensively in filtered water. Then they were autoclaved and
969 before use for the precipitation, they were rinsed with HPLC H_20. The centrifugations were done in a JA

970 50 30 Ti rotor in a Beckman Avanti J-30I centrifuge at 21,000 g for either 6 minutes or 15 minutes. After
971 the last supernatant was removed, the pellets were air dried for 15 minutes and resuspended in 0.6 mL
972 of 6 M guanidine, 50 M EPPS pH 8.5 and transferred to a 2 mL Eppendorf tube. The samples were
973 incubated for 5 minutes at 65°C and the protein amount was determined by a BCA Assay. The solution
974 was diluted to 2 M guanidine with 10 mM EPPS pH 8.5. Lysyl endopeptidase (FUJIFILM WAKO (129-02541)
975 resuspended with HPLC H_20 to ~2 mg/mL) was added to a concentration of 20 ng/mL and the initial
976 digestion proceeded for 12 hours at room temperature with gentle shaking. The samples were further
977 diluted to 0.5 M guanidine with 10 mM EPPS pH 8.5 and Trypsin protease (Sequencing Grade Modified
978 Trypsin, Promega) was added to a final concentration of 10 ng/mL along with an additional 20 ng/mL of
979 LysC. The samples were incubated in a 37°C room for 8 hours on a nutator.
980
981 **Phospho-peptide enrichment**
982 To carry out the phosphoproteomic analysis, we made the conventional steps of digesting the proteins
983 from each time sample with trypsin and specifically labeling them with isobaric tags (TMT-10 reagents).
984 Tagged samples and the phosphor-peptides were enriched on an IMAC column. Importantly, we chose to
985 multiplex peptides before the phosphor-peptide enrichment to improve data quality. There is a tradeoff
986 of decreased yield and therefore depth, as it is not economical to label more than a few milligrams of
987 material. We used 2.5-4 mgs of TMT-labeled peptides per replicate, enriched with 5 µm Titanium Dioxide
988 microspheres (GL Sciences 5020-75000) and fractioned as previously described (Presler *et al*, 2017). A
989 typical yield of 50-80 µg of peptides eluted from the column, with a median phosphor-peptide enrichment
990 of ~80%.
991
992 **Phosphatase treatment of *Xenopus* samples prepared for parallel phospho-enrichment**
993 We adapted the method that we used to phosphatase-treat digested peptides (Presler *et al*, 2017) for the
994 larger samples used here for the parallel phospho-enrichment. We chose to phosphatase treat when
995 proteases were present in the samples (but after the protease digestion sequence described above) to
996 enable the de-phosphorylated peptides to have the cleavage pattern expected if they were present
997 initially in the de-phosphorylated state. We used the heat-labile Alkaline Shrimp Phosphatase (Affymetrix
998 Inc, USA). We used a 3k Amicon Centrifugal Filter to exchange the enzyme storage buffer to 10 mM EPPS
999 pH 8.5 instead of Tris-HCl pH 7.5. We also concentrated the phosphatase to between 3-4 U/µL (confirmed
1000 by p-nitrophenyl phosphate assay). We added an estimated 833 units of phosphatase to two of the
1001 samples built to contain representative mixture of peptides (TMT 131N, channel 10: 100 oocytes collected

at the latest timepoint, and TMT 131C, channel 11: 50 oocytes collected at the first timepoint combined with 50 oocytes collected at the last timepoint). To samples that were not phosphatase-treated, we added the same volume of blank phosphatase buffer: 5 mM EPPS pH 8, 50% glycerol. To all samples, we added $MgCl_2$ to 10 mM and EDTA to 0.1 mM (to chelate metals that might compete with the magnesium necessary for enzymatic activity). All the samples were incubated with gentle shaking at room temperature for 12 hours. The phosphatase was then inactivated by incubation with gentle shaking in an air-incubator at 65°C for 15 minutes. Peptide fractionation and TMT-MS3 LC/MS were carried out as done previously (Presler *et al*, 2017).

Computing phospho-occupancy systematically

To compute phospho-occupancy, we used the phospho_occupancy_matlab package, available as part of our code repository (https://github.com/elizabeth-van-itallie) implementing the methods previously described (Van Itallie *et al*, 2025). We grouped phospho-peptides by unique phosphosite identifiers. In order to rigorously reflect the measurement accuracy and to take advantage of many measurements of the same phosphosite (including on peptides with different missed-cleavages or oxidized methionines), we used BACIQ (Peshkin *et al*, 2019) to compute the estimated trend with confidence intervals. Then, we created phosphosite sets to connect phosphosites on residues that could be on the same peptide. We made these assignments based on whether the individual phosphosites were ever measured with another phosphosite as a composite phosphosite. In order to determine occupancy, we needed to measure the phosphosite as a different form (usually not-phosphorylated). To do this, we identified non-phosphorylated peptides measured from the same experimental conditions that include the residue(s) of the phosphosite. Again, multiple non-phosphorylated peptides can include the residues of interest and the same peptide sequences can be measured multiple times. Therefore, we again use BACIQ (Peshkin *et al*, 2019) to aggregate these measurements in a trend with confidence intervals.

Comparison of mouse and *Xenopus* phosphosites

To compare the dynamics of mouse and *Xenopus* phosphosites between two species, we used the *phospho_matching* package, available as part of our code repository (https://github.com/elizabeth-van-itallie) implementing the methods previously described (Van Itallie *et al*, 2025). We first matched the phosphosites using the protein sequence and phosphorylated residues, then filtered the list to only keep matched phosphosites measured in both datasets. For cross-species phosphomatching, we used the

default parameters that are defined in the methods section in (Van Itallie *et al*, 2025): BLOSUM90 substitution penalty matrix and blastp alignment results with E-value less than 1e-20.

Mass spectrometry data mapping and analysis

Peptide-Spectra matches were performed as previously described (Sonnett *et al*, 2018). Assignment of MS2 spectra was performed using the SEQUEST (Eng *et al*, 1994) algorithm by searching the data against the appropriate proteome reference set acquired from Xenbase (*Xenopus laevis* assembly 9.1) along with common contaminants: human keratins and trypsin. The target-decoy strategy was used to construct a second database of reversed sequences that were used to estimate the false discovery rate on the peptide level. SEQUEST searches were performed using a 20 ppm precursor ion tolerance with the requirement that both N- and C-terminal peptide ends are consistent with the protease specificities of LysC and Trypsin. TMT (+229.162932 Da) was set as a static modification on N-termini and lysines peptides, and N-ethyl maleimide (+125.047679 Da) was set as a static modification on cysteine residues. Oxidation of methionine (+15.99492 Da) was set as a variable modification. A peptide level MS2 spectral assignment false discovery rate of 1% was obtained by applying the target-decoy strategy with linear discriminant analysis. Peptides of 7 amino acids length or longer were ranked by linear discriminant analysis score and were filtered to a ratio of 1% reverses/forwards + reverses. Peptides were assigned to proteins and a second filtering step to obtain a 1% FDR on the protein level was applied. Peptides that matched multiple proteins were assigned to the proteins with the most unique peptides. We only used Isolation Specificity > 0.75 spectra.

Estimation of the absolute abundance of proteins

The absolute protein concentration was estimated according previously published methods (Wühr *et al*, 2014; Peshkin *et al*, 2019), based here on ion current prorated to the isobarically labeled fractions. The respective sample fractions were estimated using our previously published Bayesian approach (Peshkin *et al*, 2019), which integrates peptide signal and peptide-level measurement agreement into a maximum likelihood estimate of the true protein ratio and the associated confidence interval (Peshkin *et al*, 2019). See Appendix Supplementary Methods.

Western blot and Antibodies

Oocyte homogenization and SDS-page was performed as previously described in (Santoni *et al*, 2024). The following antibodies were used: Karyopherin (1:2000, goat, Santa Cruz sc-1863), pT188-pY190-Erk2

(1:2000, mouse, Cell Signaling 9106), pT201-Plk1 (1:1000, Abcam Ab39068), pS910-FAK (1:5000, rabbit, Invitrogen 4459G) and pS183-Akts1/PRAS40 (1:5000, rabbit, Cell Signaling 5936). The appropriate secondary HRP-coupled antibodies were used at 1:10000 dilution (Jackson Immunoresearch).

Data availability

The mass spectrometry proteomics raw data and reference set of sequences have been deposited to the ProteomeXchange consortium via the PRIDE partner repository with the dataset identifier MassIVE MSV000094498. In addition, we developed a multi-functional Web portal to release the data and enable interactive interrogation (https://xenopus.hms.harvard.edu/index_oocyte.html). All of the aspects from overall protein trends to individual clusters to specific phosphosites and stoichiometry information are easily available. The portal provides per-protein link to external information about each human protein by symbol from GeneCards (https://www.genecards.org/) and respective *Xenopus* protein at Xenbase (https://www.xenbase.org/xenbase/).

ACKNOWLEDGMENTS

This work was supported by the National Center for Scientific Research (CNRS) and Sorbonne University, the National Research Agency (ANR) grants 18-CE13-0013-01 (CJ) and ANR-23-CE12-0045-01 (EMD), Sorbonne University Emergence grant (EMD), the ARC foundation grant ARCPJA2023080006901 (EMD), Amaranth Foundation (LP) and the NIH OD award R24 OD031956 (LP and MWK).

AUTHOR CONTRIBUTIONS

Leonid Peshkin: Conceptualization; Methodology; Experiments; Software; Formal Analysis; Data Curation; Writing; Supervision. **Enrico M Daldello**: Formal Analysis; Experiments; Writing; Supervision. **Elizabeth Van Itallie**: Software; Formal Analysis; Data Curation; Writing. **Matthew Sonnett**: Methodology; Formal Analysis. **Johannes Kreuzer**: Formal Analysis; Data Curation. **Wilhelm Haas**: Methodology; Formal Analysis. **Marc W Kirschner**: Conceptualization; Methodology; Experiments; Writing; Supervision. **Catherine Jessus**: Writing; Formal Analysis; Supervision. **Marc W Kirschner** and **Catherine Jessus** contributed equally to this work.

DISCLOSURE AND COMPETING INTERESTS STATEMENT

The authors declare no competing interests.

1101 **REFERENCES**
1102

1103 Addinall SG, Mayr PS, Doyle S, Sheehan JK, Woodman PG & Allan VJ (2001) Phosphorylation by cdc2-
1104 CyclinB1 Kinase Releases Cytoplasmic Dynein from Membranes. *Journal of Biological Chemistry*
1105 276: 15939–15944

1106 Angres B, Müller AHJ, Kellermann J & Hausen P (1991) Differential expression of two cadherins in
1107 *Xenopus laevis*. *Development* 111: 829–844

1108 Araki K, Naito K, Haraguchi S, Suzuki R, Yokoyama M, Inoue M, Aizawa S, Toyoda Y & Sato E (1996)
1109 Meiotic Abnormalities of c-mos Knockout Mouse Oocytes: Activation after First Meiosis or
1110 Entrance into Third Meiotic Metaphase1. *Biol Reprod* 55: 1315–1324

1111 Babiano R, Gamalinda M, Woolford JL & de la Cruz J (2012) Saccharomyces cerevisiae ribosomal protein
1112 L26 is not essential for ribosome assembly and function. *Mol Cell Biol* 32: 3228–3241

1113 Bahtz R, Seidler J, Arnold M, Haselmann-Weiss U, Antony C, Lehmann WD & Hoffmann I (2012) GCP6 is a
1114 substrate of Plk4 and required for centriole duplication. *Journal of Cell Science* 125: 486–496

1115 Bansal S & Tiwari S (2019) Mechanisms for the temporal regulation of substrate ubiquitination by the
1116 anaphase-promoting complex/cyclosome. *Cell Div* 14: 14

1117 Bärenz F, Inoue D, Yokoyama H, Tegha-Dunghu J, Freiss S, Draeger S, Mayilo D, Cado I, Merker S, Klinger
1118 M, *et al* (2013) The centriolar satellite protein SSX2IP promotes centrosome maturation. *Journal*
1119 *of Cell Biology* 202: 81–95

1120 Barnard DC, Cao Q & Richter JD (2005) Differential Phosphorylation Controls Maskin Association with
1121 Eukaryotic Translation Initiation Factor 4E and Localization on the Mitotic Apparatus. *Molecular*
1122 *and Cellular Biology* 25: 7605–7615

1123 Bauer M, Cubizolles F, Schmidt A & Nigg EA (2016) Quantitative analysis of human centrosome
1124 architecture by targeted proteomics and fluorescence imaging. *The EMBO Journal* 35: 2152–
1125 2166

1126 Becker BE, Romney SJ & Gard DL (2003) XMAP215, XKCM1, NuMA, and cytoplasmic dynein are required
1127 for the assembly and organization of the transient microtubule array during the maturation of
1128 Xenopus oocytes. *Developmental Biology* 261: 488–505

1129 Bement WM & Capco DG (1990) Transformation of the amphibian oocyte into the egg: Structural and
1130 biochemical events. *J Elec Microsc Tech* 16: 202–234

1131 Bhatt RR & Ferrell JE (2000) Cloning and Characterization of Xenopus Rsk2, the Predominant p90 Rsk
1132 Isozyme in Oocytes and Eggs. *Journal of Biological Chemistry* 275: 32983–32990

1133 Blangy A, Lane HA, d'Hérin P, Harper M, Kress M & Niggt EA (1995) Phosphorylation by p34cdc2
1134 regulates spindle association of human Eg5, a kinesin-related motor essential for bipolar spindle
1135 formation in vivo. *Cell* 83: 1159–1169

1136 Blitz IL & Cho KWY (2021) Control of zygotic genome activation in Xenopus. *Curr Top Dev Biol* 145: 167–
1137 204

1138 Blomen VA, Májek P, Jae LT, Bigenzahn JW, Nieuwenhuis J, Staring J, Sacco R, Van Diemen FR, Olk N,
1139 Stukalov A, *et al* (2015) Gene essentiality and synthetic lethality in haploid human cells. *Science*
1140 350: 1092–1096

1141 Bluemink JG, Hage WJ, van den Hoef MH & Dictus WJ (1983) Freeze-fracture electron microscopy of
1142 membrane changes in progesterone-induced maturing oocytes and eggs of Xenopus laevis. *Eur J*
1143 *Cell Biol* 31: 85–93

1144 Bodart J-FL, Baert FY, Sellier C, Duesbery NS, Flament S & Vilain J-P (2005) Differential roles of p39Mos–
1145 Xp42Mpk1 cascade proteins on Raf1 phosphorylation and spindle morphogenesis in Xenopus
1146 oocytes. *Developmental Biology* 283: 373–383

1147 Boke E, Ruer M, Wühr M, Coughlin M, Lemaitre R, Gygi SP, Alberti S, Drechsel D, Hyman AA & Mitchison
1148 TJ (2016) Amyloid-like Self-Assembly of a Cellular Compartment. *Cell* 166: 637–650

1149 Boleti H, Karsenti E & Vernos I (1996) Xklp2, a Novel Xenopus Centrosomal Kinesin-like Protein Required
1150 for Centrosome Separation during Mitosis. *Cell* 84: 49–59

1151 Bouftas N, Schneider L, Halder M, Demmig R, Baack M, Cladière D, Walter M, Al Abdallah H, Kleinhempel
1152 C, Messaritaki R, *et al* (2022) Cyclin B3 implements timely vertebrate oocyte arrest for
1153 fertilization. *Developmental Cell* 57: 2305-2320.e6

1154 Brunet S, Dumont J, Lee KW, Kinoshita K, Hikal P, Gruss OJ, Maro B & Verlhac M-H (2008) Meiotic
1155 Regulation of TPX2 Protein Levels Governs Cell Cycle Progression in Mouse Oocytes. *PLoS ONE* 3:
1156 e3338

1157 Cahu J, Olichon A, Hentrich C, Schek H, Drinjakovic J, Zhang C, Doherty-Kirby A, Lajoie G & Surrey T
1158 (2008) Phosphorylation by Cdk1 Increases the Binding of Eg5 to Microtubules In Vitro and in
1159 Xenopus Egg Extract Spindles. *PLoS ONE* 3: e3936

1160 Campanella C, Andreuccetti P, Taddei C & Talevi R (1984) The modifications of cortical endoplasmic
1161 reticulum during in vitro maturation of *Xenopus laevis* oocytes and its involvement in cortical
1162 granule exocytosis. *J Exp Zool* 229: 283–293

1163 Cao Q, Zhao C, Wang C, Cai L, Xia M, Zhang X, Han J, Xu Y, Zhang J, Ling X, *et al* (2021) The Recurrent
1164 Mutation in PATL2 Inhibits Its Degradation Thus Causing Female Infertility Characterized by
1165 Oocyte Maturation Defect Through Regulation of the Mos-MAPK Pathway. *Front Cell Dev Biol* 9:
1166 628649

1167 Castro A, Mandart E, Lorca T & Galas S (2003) Involvement of Aurora A Kinase during Meiosis I-II
1168 Transition in Xenopus Oocytes. *J Biol Chem* 278: 2236–2241

1169 Cavazza T, Peset I & Vernos I (2016) From meiosis to mitosis: the sperm centrosome defines the kinetics
1170 of spindle assembly after fertilization. *Journal of Cell Science*: jcs.183624

1171 Celebic D, Polat I, Legros V, Chevreux G, Wassmann K & Touati SA (2024) Qualitative rather than
1172 quantitative phosphoregulation shapes the end of meiosis I in budding yeast. *EMBO J*

1173 Charbonneau M & Grey RD (1984) The onset of activation responsiveness during maturation coincides
1174 with the formation of the cortical endoplasmic reticulum in oocytes of Xenopus laevis.
1175 *Developmental Biology* 102: 90–97

1176 Charlesworth A, Yamamoto TM, Cook JM, Silva KD, Kotter CV, Carter GS, Holt JW, Lavender HF, MacNicol
1177 AM, Ying Wang Y, *et al* (2012) Xenopus laevis zygote arrest 2 (zar2) encodes a zinc finger RNA-
1178 binding protein that binds to the translational control sequence in the maternal Wee1 mRNA
1179 and regulates translation. *Dev Biol* 369: 177–190

1180 Chen J, Melton C, Suh N, Oh JS, Horner K, Xie F, Sette C, Blelloch R & Conti M (2011) Genome-wide
1181 analysis of translation reveals a critical role for deleted in azoospermia-like (Dazl) at the oocyte-
1182 to-zygote transition. *Genes Dev* 25: 755–766

1183 Cheng K-Y (2003) The crystal structure of the human polo-like kinase-1 polo box domain and its
1184 phospho-peptide complex. *The EMBO Journal* 22: 5757–5768

1185 Chew TG, Peaston A, Lim AK, Lorthongpanich C, Knowles BB & Solter D (2013) A Tudor Domain Protein
1186 SPINDLIN1 Interacts with the mRNA-Binding Protein SERBP1 and Is Involved in Mouse Oocyte
1187 Meiotic Resumption. *PLoS ONE* 8: e69764

1188 Choi T, Fukasawa K, Zhou R, Tessarollo L, Borror K, Resau J & Vande Woude GF (1996) The Mos/mitogen-
1189 activated protein kinase (MAPK) pathway regulates the size and degradation of the first polar
1190 body in maturing mouse oocytes. *Proc Natl Acad Sci USA* 93: 7032–7035

1191 Christou-Kent M, Kherraf Z, Amiri-Yekta A, Le Blévec E, Karaouzène T, Conne B, Escoffier J, Assou S,
1192 Guttin A, Lambert E, *et al* (2018) PATL 2 is a key actor of oocyte maturation whose invalidation
1193 causes infertility in women and mice. *EMBO Mol Med* 10

1194 Cohen-Fix O, Peters JM, Kirschner MW & Koshland D (1996) Anaphase initiation in Saccharomyces
1195 cerevisiae is controlled by the APC-dependent degradation of the anaphase inhibitor Pds1p.
1196 *Genes Dev* 10: 3081–3093

1197 Colman A, Jones EA & Heasman J (1985) Meiotic maturation in Xenopus oocytes: a link between the
1198 cessation of protein secretion and the polarized disappearance of Golgi apparati. *The Journal of*
1199 *cell biology* 101: 313–318

1200 Cordes VC, Reidenbach S & Franke WW (1995) High content of a nuclear pore complex protein in
1201 cytoplasmic annulate lamellae of Xenopus oocytes. *Eur J Cell Biol* 68: 240–255

1202 Daldello EM, Le T, Poulhe R, Jessus C, Haccard O & Dupré A (2015) Control of Cdc6 accumulation by Cdk1
1203 and MAPK is essential for completion of oocyte meiotic divisions in *Xenopus*. *J Cell Sci* 128:
1204 2482–2496

1205 De Magistris P & Antonin W (2018) The Dynamic Nature of the Nuclear Envelope. *Current Biology* 28:
1206 R487–R497

1207 De Matteis MA, Wilson C & D'Angelo G (2013) Phosphatidylinositol-4-phosphate: The Golgi and beyond.
1208 *BioEssays* 35: 612–622

1209 Deák P, Donaldson M & Glover DM (2003) Mutations in *mákos* , a *Drosophila* gene encoding the Cdc27
1210 subunit of the anaphase promoting complex, enhance centrosomal defects in *polo* and are
1211 suppressed by mutations in *twins/aar* , which encodes a regulatory subunit of PP2A. *Journal of*
1212 *Cell Science* 116: 4147–4158

1213 Delattre M & Gönczy P (2004) The arithmetic of centrosome biogenesis. *Journal of Cell Science* 117:
1214 1619–1630

1215 Dell KR, Turck CW & Vale RD (2000) Mitotic Phosphorylation of the Dynein Light Intermediate Chain is
1216 Mediated by cdc2 Kinase. *Traffic* 1: 38–44

1217 Deng J, Lang S, Wylie C & Hammes SR (2008) The Xenopus laevis Isoform of G Protein-Coupled Receptor
1218 3 (GPR3) Is a Constitutively Active Cell Surface Receptor that Participates in Maintaining Meiotic
1219 Arrest in X. laevis Oocytes. *Molecular Endocrinology* 22: 1853–1865

1220 Dictenberg JB, Zimmerman W, Sparks CA, Young A, Vidair C, Zheng Y, Carrington W, Fay FS & Doxsey SJ
1221 (1998) Pericentrin and γ-Tubulin Form a Protein Complex and Are Organized into a Novel Lattice
1222 at the Centrosome. *The Journal of Cell Biology* 141: 163–174

1223 Drysdale TA & Elinson RP (1992) Cell Migration and Induction in the Development of the Surface
1224 Ectodermal Pattern of the *Xenopus laevis* Tadpole: (*Xenopus* /ciliated cell/hatching
1225 gland/cement gland/ectodermal differentiation). *Dev Growth Differ* 34: 51–59

1226 Dumont JN (1972) Oogenesis inXenopus laevis (Daudin). I. Stages of oocyte development in laboratory
1227 maintained animals. *J Morphol* 136: 153–179

1228 Dupré A, Daldello EM, Nairn AC, Jessus C & Haccard O (2014) Phosphorylation of ARPP19 by protein
1229 kinase A prevents meiosis resumption in Xenopus oocytes. *Nat Commun* 5: 3318

1230 Dupre A, Jessus C, Ozon R & Haccard O (2002) Mos is not required for the initiation of meiotic
1231 maturation in Xenopus oocytes. *EMBO J* 21: 4026–4036

1232 Duran-Arqué B, Cañete M, Castellazzi CL, Bartomeu A, Ferrer-Caelles A, Reina O, Caballé A, Gay M,
1233 Arauz-Garofalo G, Belloc E, *et al* (2022) Comparative analyses of vertebrate CPEB proteins define
1234 two subfamilies with coordinated yet distinct functions in post-transcriptional gene regulation.
1235 *Genome Biol* 23: 192

1236 Elia AEH, Cantley LC & Yaffe MB (2003a) Proteomic Screen Finds pSer/pThr-Binding Domain Localizing
1237 Plk1 to Mitotic Substrates. *Science* 299: 1228–1231

1238 Elia AEH, Rellos P, Haire LF, Chao JW, Ivins FJ, Hoepker K, Mohammad D, Cantley LC, Smerdon SJ & Yaffe
1239 MB (2003b) The Molecular Basis for Phosphodependent Substrate Targeting and Regulation of
1240 Plks by the Polo-Box Domain. *Cell* 115: 83–95

1241 El-Jouni W, Haun S, Hodeify R, Hosein Walker A & Machaca K (2007) Vesicular traffic at the cell
1242 membrane regulates oocyte meiotic arrest. *Development* 134: 3307–3315

1243 Ems-McClung SC, Emch M, Zhang S, Mahnoor S, Weaver LN & Walczak CE (2020) RanGTP induces an
1244 effector gradient of XCTK2 and importin α/β for spindle microtubule cross-linking. *Journal of Cell*
1245 *Biology* 219: e201906045

1246 Eng JK, McCormack AL & Yates JR (1994) An approach to correlate tandem mass spectral data of
1247 peptides with amino acid sequences in a protein database. *J Am Soc Mass Spectrom* 5: 976–989

1248 Feldherr CM (1974) The binding characteristics of the nuclear annuli. *Experimental Cell Research* 85:
1249 271–277

1250 Félix M, Antony C, Wright M & Maro B (1994) Centrosome assembly in vitro: role of gamma-tubulin
1251 recruitment in Xenopus sperm aster formation. *The Journal of cell biology* 124: 19–31

1252 Ferby I, Blazquez M, Palmer A, Eritja R & Nebreda AR (1999) A novel p34(cdc2)-binding and activating
1253 protein that is necessary and sufficient to trigger G(2)/M progression in Xenopus oocytes. *Genes*
1254 *Dev* 13: 2177–2189

1255 Fisher DL, Brassac T, Galas S & Dorée M (1999) Dissociation of MAP kinase activation and MPF activation
1256 in hormone-stimulated maturation of Xenopus oocytes. *Development* 126: 4537–4546

1257 Frank-Vaillant M, Jessus C, Ozon R, Maller JL & Haccard O (1999) Two Distinct Mechanisms Control the
1258 Accumulation of Cyclin B1 and Mos in *Xenopus* Oocytes in Response to Progesterone. *MBoC* 10:
1259 3279–3288

1260 Fry AM, Descombes P, Twomey C, Bacchieri R & Nigg EA (2000) The NIMA-related kinase X-Nek2B is
1261 required for efficient assembly of the zygotic centrosome in Xenopus laevis. *Journal of Cell*
1262 *Science* 113: 1973–1984

1263 Furuno N, Nishizawa M, Okazaki K, Tanaka H, Iwashita J, Nakajo N, Ogawa Y & Sagata N (1994)
1264 Suppression of DNA replication via Mos function during meiotic divisions in Xenopus oocytes.
1265 *EMBO J* 13: 2399–2410

1266 Gaffré M, Martoriati A, Belhachemi N, Chambon J-P, Houliston E, Jessus C & Karaiskou A (2011) A critical
1267 balance between Cyclin B synthesis and Myt1 activity controls meiosis entry in *Xenopus* oocytes.
1268 *Development* 138: 3735–3744

1269 Gard DL (1992) Microtubule organization during maturation of Xenopus oocytes: Assembly and rotation
1270 of the meiotic spindles. *Developmental Biology* 151: 516–530

1271 Gard DL (1994) γ-Tubulin Is Asymmetrically Distributed in the Cortex of Xenopus Oocytes.
1272 *Developmental Biology* 161: 131–140

1273 Gard DL (1999) Confocal microscopy and 3-D reconstruction of the cytoskeleton ofXenopus oocytes.
1274 *Microsc Res Tech* 44: 388–414

1275 Gard DL, Affleck D & Error BM (1995) Microtubule Organization, Acetylation, and Nucleation in Xenopus
1276 laevis Oocytes: II. A Developmental Transition in Microtubule Organization during Early
1277 Diplotene. *Developmental Biology* 168: 189–201

1278 Gard DL, Hafezi S, Zhang T & Doxsey SJ (1990) Centrosome duplication continues in cycloheximide-
1279 treated Xenopus blastulae in the absence of a detectable cell cycle. *The Journal of cell biology*
1280 110: 2033–2042

1281 Gard DL & Kirschner MW (1987) Microtubule assembly in cytoplasmic extracts of Xenopus oocytes and
1282 eggs. *The Journal of cell biology* 105: 2191–2201

1283 Gavin A-C, Ainle AN, Chierici E, Jones M & Nebreda AR (1999) A p90 ^{rsk} Mutant Constitutively Interacting
1284 with MAP Kinase Uncouples MAP Kinase from p34 ^{cdc2} /Cyclin B Activation in *Xenopus* Oocytes.
1285 *MBoC* 10: 2971–2986

1286 Gawantka V, Ellinger-Ziegelbauer H & Hausen P (1992) β-integrin is a maternal protein that is inserted
1287 into all newly formed plasma membranes during early *Xenopus* embryogenesis. *Development*
1288 115: 595–605

1289 Gerhart J, Wu M & Kirschner M (1984) Cell cycle dynamics of an M-phase-specific cytoplasmic factor in
1290 Xenopus laevis oocytes and eggs. *The Journal of cell biology* 98: 1247–1255

1291 Giet R, Uzbekov R, Cubizolles F, Le Guellec K & Prigent C (1999) The Xenopus laevis Aurora-related
1292 Protein Kinase pEg2 Associates with and Phosphorylates the Kinesin-related Protein XlEg5.
1293 *Journal of Biological Chemistry* 274: 15005–15013

1294 Glotzer M, Murray AW & Kirschner MW (1991) Cyclin is degraded by the ubiquitin pathway. *Nature* 349:
1295 132–138

1296 Groisman I, Jung M-Y, Sarkissian M, Cao Q & Richter JD (2002) Translational Control of the Embryonic
1297 Cell Cycle. *Cell* 109: 473–483

1298 Gromley A, Yeaman C, Rosa J, Redick S, Chen C-T, Mirabelle S, Guha M, Sillibourne J & Doxsey SJ (2005)
1299 Centriolin Anchoring of Exocyst and SNARE Complexes at the Midbody Is Required for Secretory-
1300 Vesicle-Mediated Abscission. *Cell* 123: 75–87

1301 Grosstessner-Hain K, Hegemann B, Novatchkova M, Rameseder J, Joughin BA, Hudecz O, Roitinger E,
1302 Pichler P, Kraut N, Yaffe MB, *et al* (2011) Quantitative Phospho-proteomics to Investigate the
1303 Polo-like Kinase 1-Dependent Phospho-proteome. *Molecular & Cellular Proteomics* 10:
1304 M111.008540

1305 Gruss O (2018) Animal Female Meiosis: The Challenges of Eliminating Centrosomes. *Cells* 7: 73

1306 Gruss OJ & Vernos I (2004) The mechanism of spindle assembly. *The Journal of Cell Biology* 166: 949–955

1307 Gwon Y, Maxwell BA, Kolaitis R-M, Zhang P, Kim HJ & Taylor JP (2021) Ubiquitination of G3BP1 mediates
1308 stress granule disassembly in a context-specific manner. *Science* 372: eabf6548

1309 Haccard O & Jessus C (2006) Oocyte Maturation, Mos and Cyclins—A Matter of Synthesis: Two
1310 Functionally Redundant Ways to Induce Meiotic Maturation. *Cell Cycle* 5: 1152–1159

Hansen DV, Tung JJ & Jackson PK (2006) CaMKII and Polo-like kinase 1 sequentially phosphorylate the cytostatic factor Emi2/XErp1 to trigger its destruction and meiotic exit. *Proceedings of the National Academy of Sciences* 103: 608–613

Hatch EM, Kulukian A, Holland AJ, Cleveland DW & Stearns T (2010) Cep152 interacts with Plk4 and is required for centriole duplication. *Journal of Cell Biology* 191: 721–729

Heidemann SR & Kirschner MW (1975) Aster formation in eggs of Xenopus laevis. Induction by isolated basal bodies. *The Journal of cell biology* 67: 105–117

Heim A, Niedermeier ML, Stengel F & Mayer TU (2022) The translation regulator Zar1l controls timing of meiosis in *Xenopus* oocytes. *Development* 149: dev200900

Hochegger H, Klotzbücher A, Kirk J, Howell M, le Guellec K, Fletcher K, Duncan T, Sohail M & Hunt T (2001) New B-type cyclin synthesis is required between meiosis I and II during Xenopus oocyte maturation. *Development* 128: 3795–3807

Houliston E, Le Guellec R, Kress M, Philippe M & Le Guellec K (1994) The kinesin-related protein Eg5 associates with both interphase and spindle microtubules during Xenopus early development. *Dev Biol* 164: 147–159

Huang C-YF, Chang C-PB, Huang C-L & Ferrell JE (1999) M Phase Phosphorylation of Cytoplasmic Dynein Intermediate Chain and p150Glued. *Journal of Biological Chemistry* 274: 14262–14269

Huchon D, Crozet N, Cantenot N & Ozon R (1981) Germinal vesicle breakdown in the Xenopus laevis oocyte : description of a transient microtubular structure. *Reprod Nutr Dévelop* 21: 135–148

Huchon D, Rime H, Jessus C & Ozon R (1993) Control of metaphase I formation in *Xenopus* oocyte: Effects of an indestructible cyclin B and of protein synthesis. *Biology of the Cell* 77: 133–141

Hyman LE & Wormington WM (1988) Translational inactivation of ribosomal protein mRNAs during Xenopus oocyte maturation. *Genes Dev* 2: 598–605

Isobe K, Jung HJ, Yang C-R, Claxton J, Sandoval P, Burg MB, Raghuram V & Knepper MA (2017) Systems-level identification of PKA-dependent signaling in epithelial cells. *Proc Natl Acad Sci USA* 114

Jackson RJ, Hellen CUT & Pestova TV (2010) The mechanism of eukaryotic translation initiation and principles of its regulation. *Nat Rev Mol Cell Biol* 11: 113–127

Jamieson-Lucy A & Mullins MC (2019) The vertebrate Balbiani body, germ plasm, and oocyte polarity. In *Current Topics in Developmental Biology* pp 1–34. Elsevier

Jessus C (2010) MPF and the Control of Meiotic Divisions: Old Problems, New Concepts. In *Oogenesis*, Verlhac M & Villeneuve A (eds) pp 227–265. Wiley

Jessus C, Friederich E, Francon J & Ozon R (1984) In vitro inhibition of tubulin assembly by a ribonucleoprotein complex associated with the free ribosome fraction isolated from Xenopus laevis oocytes: effect at the level of microtubule-associated proteins. *Cell Differentiation* 14: 179–187

1346 Jessus C, Thibier C, Huchon D & Ozon R (1988) Taxol reveals cortical sites of microtubule assembly in
1347 Xenopus oocytes. Role of the nucleus. *Cell Differentiation and Development* 25: 57–63

1348 Jia J, Tang S, Yue X, Jing S, Zhu L, Tan C, Gao J, Du Y, Lee I & Qian Y (2023) An A-kinase anchoring protein
1349 (ACBD3) coordinates traffic-induced PKA activation at the Golgi. *Journal of Biological Chemistry*
1350 299: 104696

1351 Johnson JL, Yaron TM, Huntsman EM, Kerelsky A, Song J, Regev A, Lin T-Y, Liberatore K, Cizin DM, Cohen
1352 BM, *et al* (2023) An atlas of substrate specificities for the human serine/threonine kinome.
1353 *Nature*

1354 Josefsberg Ben-Yehoshua L, Lewellyn AL, Thomas P & Maller JL (2007) The Role of Xenopus Membrane
1355 Progesterone Receptor β in Mediating the Effect of Progesterone on Oocyte Maturation.
1356 *Molecular Endocrinology* 21: 664–673

1357 Kado RT, Marcher K & Ozon R (1981) Electrical membrane properties of the Xenopus laevis oocyte
1358 during progesterone-induced meiotic maturation. *Developmental Biology* 84: 471–476

1359 Kaufman OH, Lee K, Martin M, Rothhämel S & Marlow FL (2018) rbpms2 functions in Balbiani body
1360 architecture and ovary fate. *PLoS Genet* 14: e1007489

1361 Kessel RG, Tung HN, Beams HW & Lin JJ-C (1986) Is the nuclear envelope a 'generator' of membrane?:
1362 Developmental sequences in cytomembrane elaboration. *Cell Tissue Res* 245

1363 Kettenbach AN, Schweppe DK, Faherty BK, Pechenick D, Pletnev AA & Gerber SA (2011) Quantitative
1364 Phosphoproteomics Identifies Substrates and Functional Modules of Aurora and Polo-Like
1365 Kinase Activities in Mitotic Cells. *Sci Signal* 4

1366 Keuss MJ, Thomas Y, Mcarthur R, Wood NT, Knebel A & Kurz T (2016) Characterisation of the
1367 mammalian family of DCN-type NEDD8 E3 ligases. *Journal of Cell Science*: jcs.181784

1368 King GA, Goodman JS, Schick JG, Chetlapalli K, Jorgens DM, McDonald KL & Ünal E (2019) Meiotic cellular
1369 rejuvenation is coupled to nuclear remodeling in budding yeast. *Elife* 8: e47156

1370 Kinoshita K, Habermann B & Hyman AA (2002) XMAP215: a key component of the dynamic microtubule
1371 cytoskeleton. *Trends in Cell Biology* 12: 267–273

1372 Kinterová V, Kaňka J, Bartková A & Toralová T (2022) SCF Ligases and Their Functions in Oogenesis and
1373 Embryogenesis—Summary of the Most Important Findings throughout the Animal Kingdom.
1374 *Cells* 11: 234

1375 Kirschner M (1986) Beyond self-assembly: From microtubules to morphogenesis. *Cell* 45: 329–342

1376 Kishimoto T (2003) Cell-cycle control during meiotic maturation. *Current Opinion in Cell Biology* 15: 654–
1377 663

1378 Klima M, Tóth DJ, Hexnerova R, Baumlova A, Chalupska D, Tykvart J, Rezabkova L, Sengupta N, Man P,
1379 Dubankova A, *et al* (2016) Structural insights and in vitro reconstitution of membrane targeting
1380 and activation of human PI4KB by the ACBD3 protein. *Sci Rep* 6: 23641

1381 Kobayashi H, Minshull J, Ford C, Golsteyn R, Poon R & Hunt T (1991) On the synthesis and destruction of
1382 A- and B-type cyclins during oogenesis and meiotic maturation in Xenopus laevis. *J Cell Biol* 114:
1383 755–765

1384 Koch LB, Spanos C, Kelly V, Ly T & Marston AL (2024) Rewiring of the phosphoproteome executes two
1385 meiotic divisions in budding yeast. *EMBO J* 43: 1351–1383

1386 Kraft C (2003) Mitotic regulation of the human anaphase-promoting complex by phosphorylation. *The*
1387 *EMBO Journal* 22: 6598–6609

1388 Kufer TA, Silljé HHW, Körner R, Gruss OJ, Meraldi P & Nigg EA (2002) Human TPX2 is required for
1389 targeting Aurora-A kinase to the spindle. *The Journal of Cell Biology* 158: 617–623

1390 Kumar H, Pushpa K, Kumari A, Verma K, Pergu R & Mylavarapu SVS (2019) The exocyst complex and
1391 Rab5 are required for abscission by localizing ESCRT III subunits to the cytokinetic bridge. *Journal*
1392 *of Cell Science* 132: jcs226001

1393 Kutay U, Jühlen R & Antonin W (2021) Mitotic disassembly and reassembly of nuclear pore complexes.
1394 *Trends in Cell Biology* 31: 1019–1033

1395 Labbé JC, Vigneron S, Méchali F, Robert P, Roque S, Genoud C, Goguet-Rubio P, Barthe P, Labesse G,
1396 Cohen-Gonsaud M, *et al* (2021) The study of the determinants controlling Arpp19 phosphatase-
1397 inhibitory activity reveals an Arpp19/PP2A-B55 feedback loop. *Nat Commun* 12: 3565

1398 Larabell CA & Chandler DE (1989) The coelomic envelope of Xenopus laevis eggs: A quick-freeze, deep-
1399 etch analysis. *Developmental Biology* 131: 126–135

1400 Leaf DS, Roberts SJ, Gerhart JC & Moore H-P (1990) The secretory pathway is blocked between the
1401 trans-Golgi and the plasma membrane during meiotic maturation in Xenopus oocytes.
1402 *Developmental Biology* 141: 1–12

1403 Lee KS, Grenfell TZ, Yarm FR & Erikson RL (1998) Mutation of the polo-box disrupts localization and
1404 mitotic functions of the mammalian polo kinase Plk. *Proc Natl Acad Sci USA* 95: 9301–9306

1405 Lee M, Nagashima K, Yoon J, Sun J, Wang Z, Carpenter C, Lee H-K, Hwang Y-S, Westlake CJ & Daar IO
1406 (2022) CEP97 phosphorylation by Dyrk1a is critical for centriole separation during
1407 multiciliogenesis. *Journal of Cell Biology* 221: e202102110

1408 Leesch F, Lorenzo-Orts L, Pribitzer C, Grishkovskaya I, Roehsner J, Chugunova A, Matzinger M, Roitinger
1409 E, Belačić K, Kandolf S, *et al* (2023) A molecular network of conserved factors keeps ribosomes
1410 dormant in the egg. *Nature* 613: 712–720

1411 LeGuennec M, Klena N, Aeschlimann G, Hamel V & Guichard P (2021) Overview of the centriole
1412 architecture. *Current Opinion in Structural Biology* 66: 58–65

1413 Lemaître J-M, Bocquet S & Méchali M (2002) Competence to replicate in the unfertilized egg is
1414 conferred by Cdc6 during meiotic maturation. *Nature* 419: 718–722

1415 Lemonnier T, Daldello EM, Poulhe R, Le T, Miot M, Lignières L, Jessus C & Dupré A (2021) The M-phase
1416 regulatory phosphatase PP2A-B55δ opposes protein kinase A on Arpp19 to initiate meiotic
1417 division. *Nat Commun* 12: 1837

1418 Lemonnier T, Dupré A & Jessus C (2020) The G2-to-M transition from a phosphatase perspective: a new
1419 vision of the meiotic division. *Cell Div* 15: 9

1420 Lenormand J-L (1999) Speedy: a novel cell cycle regulator of the G2/M transition. *EMBO J* 18: 1869–1877

1421 Li X, Ju J, Pan Z, Wang H, Wan X, Pan M, Xu Y, Sun M & Sun S (2021) PRC1 is a critical regulator for
1422 anaphase spindle midzone assembly and cytokinesis in mouse oocyte meiosis. *FEBS J* 288: 3055–
1423 3067

1424 Linder MI, Köhler M, Boersema P, Weberruss M, Wandke C, Marino J, Ashiono C, Picotti P, Antonin W &
1425 Kutay U (2017) Mitotic Disassembly of Nuclear Pore Complexes Involves CDK1- and PLK1-
1426 Mediated Phosphorylation of Key Interconnecting Nucleoporins. *Developmental Cell* 43: 141-
1427 156.e7

1428 Liu L & Wiese C (2008) *Xenopus* NEDD1 is required for microtubule organization in *Xenopus* egg extracts.
1429 *Journal of Cell Science* 121: 578–589

1430 Lorenzo-Orts L, Strobl M, Steinmetz B, Leesch F, Pribitzer C, Roehsner J, Schutzbier M, Dürnberger G &
1431 Pauli A (2023) eIF4E1b is a non-canonical eIF4E protecting maternal dormant mRNAs. *EMBO Rep*

1432 Luong XG, Daldello EM, Rajkovic G, Yang C-R & Conti M (2020) Genome-wide analysis reveals a switch in
1433 the translational program upon oocyte meiotic resumption. *Nucleic Acids Research* 48: 3257–
1434 3276

1435 Macůrek L, Lindqvist A, Lim D, Lampson MA, Klompmaker R, Freire R, Clouin C, Taylor SS, Yaffe MB &
1436 Medema RH (2008) Polo-like kinase-1 is activated by aurora A to promote checkpoint recovery.
1437 *Nature* 455: 119–123

1438 Maller J, Wu M & Gerhart JC (1977) Changes in protein phosphorylation accompanying maturation of
1439 Xenopus laevis oocytes. *Developmental Biology* 58: 295–312

1440 Marnef A, Maldonado M, Bugaut A, Balasubramanian S, Kress M, Weil D & Standart N (2010) Distinct
1441 functions of maternal and somatic Pat1 protein paralogs. *RNA* 16: 2094–2107

1442 Maton G, Lorca T, Girault J-A, Ozon R & Jessus C (2005) Differential regulation of Cdc2 and Aurora-A in
1443 *Xenopus* oocytes: a crucial role of phosphatase 2A. *Journal of Cell Science* 118: 2485–2494

1444 Maton G, Thibier C, Castro A, Lorca T, Prigent C & Jessus C (2003) Cdc2-Cyclin B Triggers H3 Kinase
1445 Activation of Aurora-A in Xenopus Oocytes. *J Biol Chem* 278: 21439–21449

1446 McNally FJ & Thomas S (1998) Katanin Is Responsible for the M-Phase Microtubule-severing Activity in
1447 *Xenopus* Eggs. *MBoC* 9: 1847–1861

1448 McPhail JA, Lyoo H, Pemberton JG, Hoffmann RM, Van Elst W, Strating JR, Jenkins ML, Stariha JT, Powell
1449 CJ, Boulanger MJ, *et al* (2020) Characterization of the c10orf76-PI4KB complex and its necessity
1450 for Golgi PI4P levels and enterovirus replication. *EMBO Reports* 21: e48441

1451 Mendez R, Barnard D & Richter JD (2002) Differential mRNA translation and meiotic progression require
1452 Cdc2-mediated CPEB destruction. *EMBO J* 21: 1833–1844

1453 Meneau F, Dupré A, Jessus C & Daldello EM (2020) Translational Control of Xenopus Oocyte Meiosis:
1454 Toward the Genomic Era. *Cells* 9: 1502

1455 Miller BR & Forbes DJ (2000) Purification of the Vertebrate Nuclear Pore Complex by Biochemical
1456 Criteria. *Traffic* 1: 941–951

1457 Miller KE, Session AM & Heald R (2019) Kif2a Scales Meiotic Spindle Size in Hymenochirus boettgeri.
1458 *Current Biology* 29: 3720-3727.e5

1459 Minshall N, Reiter MH, Weil D & Standart N (2007) CPEB Interacts with an Ovary-specific eIF4E and 4E-T
1460 in Early *Xenopus* Oocytes. *J Biol Chem* 282: 37389–37401

1461 Mitchison TJ, Maddox P, Gaetz J, Groen A, Shirasu M, Desai A, Salmon ED & Kapoor TM (2005) Roles of
1462 Polymerization Dynamics, Opposed Motors, and a Tensile Element in Governing the Length of
1463 *Xenopus* Extract Meiotic Spindles. *MBoC* 16: 3064–3076

1464 Mueller PR, Coleman TR & Dunphy WG (1995) Cell cycle regulation of a Xenopus Wee1-like kinase.
1465 *MBoC* 6: 119–134

1466 Müller H -Arno J (2001) Of mice, frogs and flies: Generation of membrane asymmetries in early
1467 development. *Dev Growth Differ* 43: 327–342

1468 Mulner-Lorillon O, Bellé R, Cormier P, Drewing S, Minella O, Poulhe R & Schmalzing G (1995) Brefeldin A
1469 Provokes Indirect Activation of cdc2 Kinase (MPF) in Xenopus Oocytes, Resulting in Meiotic Cell
1470 Division. *Developmental Biology* 170: 223–229

1471 Nader N, Dib M, Courjaret R, Hodeify R, Machaca R, Graumann J & Machaca K (2018) VLDL receptor
1472 regulates membrane progesterone receptor trafficking and non-genomic signaling. *Journal of*
1473 *Cell Science*: jcs.212522

1474 Nader N, Dib M, Daalis A, Kulkarni RP & Machaca K (2014) Role for endocytosis of a constitutively active
1475 GPCR (GPR185) in releasing vertebrate oocyte meiotic arrest. *Developmental Biology* 395: 355–
1476 366

1477 Nader N, Dib M, Hodeify R, Courjaret R, Elmi A, Hammad AS, Dey R, Huang X-Y & Machaca K (2020)
1478 Membrane progesterone receptor induces meiosis in Xenopus oocytes through endocytosis into
1479 signaling endosomes and interaction with APPL1 and Akt2. *PLoS Biol* 18: e3000901

1480 Nakahata S, Kotani T, Mita K, Kawasaki T, Katsu Y, Nagahama Y & Yamashita M (2003) Involvement of
1481 Xenopus Pumilio in the translational regulation that is specific to cyclin B1 mRNA during oocyte
1482 maturation. *Mechanisms of Development* 120: 865–880

1483 Nakajo N, Yoshitome S, Iwashita J, Iida M, Uto K, Ueno S, Okamoto K & Sagata N (2000) Absence of
1484 Wee1 ensures the meiotic cell cycle in Xenopus oocytes. *Genes Dev* 14: 328–338

1485 Nakamura Y, Tanaka KJ, Miyauchi M, Huang L, Tsujimoto M & Matsumoto K (2010) Translational
1486 repression by the oocyte-specific protein P100 in Xenopus. *Dev Biol* 344: 272–283

1487 Nguyen AT, Prado MA, Schmidt PJ, Sendamarai AK, Wilson-Grady JT, Min M, Campagna DR, Tian G, Shi Y,
1488 Dederer V, *et al* (2017) UBE2O remodels the proteome during terminal erythroid differentiation.
1489 *Science* 357: eaan0218

1490 Oakley CE & Oakley BR (1989) Identification of γ-tubulin, a new member of the tubulin superfamily
1491 encoded by mipA gene of Aspergillus nidulans. *Nature* 338: 662–664

1492 Okano-Uchida T, Sekiai T, Lee K, Okumura E, Tachibana K & Kishimoto T (1998) In VivoRegulation of
1493 Cyclin A/Cdc2 and Cyclin B/Cdc2 through Meiotic and Early Cleavage Cycles in Starfish.
1494 *Developmental Biology* 197: 39–53

1495 Oshiro N, Takahashi R, Yoshino K, Tanimura K, Nakashima A, Eguchi S, Miyamoto T, Hara K, Takehana K,
1496 Avruch J, *et al* (2007) The Proline-rich Akt Substrate of 40 kDa (PRAS40) Is a Physiological
1497 Substrate of Mammalian Target of Rapamycin Complex 1. *Journal of Biological Chemistry* 282:
1498 20329–20339

1499 Ota R, Kotani T & Yamashita M (2011) Biochemical Characterization of Pumilio1 and Pumilio2 in Xenopus
1500 Oocytes. *Journal of Biological Chemistry* 286: 2853–2863

1501 Padmanabhan K (2006) Regulated Pumilio-2 binding controls RINGO/Spy mRNA translation and CPEB
1502 activation. *Genes Dev* 20: 199–209

1503 Pascreau G, Delcros J-G, Cremet J-Y, Prigent C & Arlot-Bonnemains Y (2005) Phosphorylation of Maskin
1504 by Aurora-A Participates in the Control of Sequential Protein Synthesis during Xenopus laevis
1505 Oocyte Maturation. *Journal of Biological Chemistry* 280: 13415–13423

1506 Patra D & Dunphy WG (1998) Xe-p9, a *Xenopus* Suc1/Cks protein, is essential for the Cdc2-dependent
1507 phosphorylation of the anaphase- promoting complex at mitosis. *Genes Dev* 12: 2549–2559

1508 Payne DM, Rossomando AJ, Martino P, Erickson AK, Her JH, Shabanowitz J, Hunt DF, Weber MJ & Sturgill
1509 TW (1991) Identification of the regulatory phosphorylation sites in pp42/mitogen-activated
1510 protein kinase (MAP kinase). *The EMBO Journal* 10: 885–892

1511 Peset I, Seiler J, Sardon T, Bejarano LA, Rybina S & Vernos I (2005) Function and regulation of Maskin, a
1512 TACC family protein, in microtubule growth during mitosis. *The Journal of Cell Biology* 170:
1513 1057–1066

1514 Peshkin L, Gupta M, Ryazanova L & Wühr M (2019) Bayesian Confidence Intervals for Multiplexed
1515 Proteomics Integrate Ion-statistics with Peptide Quantification Concordance*[S]. *Molecular &*
1516 *Cellular Proteomics* 18: 2108–2120

1517 Peshkin L, Wühr M, Pearl E, Haas W, Freeman RM, Gerhart JC, Klein AM, Horb M, Gygi SP & Kirschner
1518 MW (2015) On the Relationship of Protein and mRNA Dynamics in Vertebrate Embryonic
1519 Development. *Developmental Cell* 35: 383–394

1520 Peuchen EH, Cox OF, Sun L, Hebert AS, Coon JJ, Champion MM, Dovichi NJ & Huber PW (2017)
1521 Phosphorylation Dynamics Dominate the Regulated Proteome during Early Xenopus
1522 Development. *Sci Rep* 7: 15647

1523 Piqué M, López JM, Foissac S, Guigó R & Méndez R (2008) A Combinatorial Code for CPE-Mediated
1524 Translational Control. *Cell* 132: 434–448

1525 Popov AV, Severin F & Karsenti E (2002) XMAP215 Is Required for the Microtubule-Nucleating Activity of
1526 Centrosomes. *Current Biology* 12: 1326–1330

1527 Presler M, Van Itallie E, Klein AM, Kunz R, Coughlin ML, Peshkin L, Gygi SP, Wühr M & Kirschner MW
1528 (2017) Proteomics of phosphorylation and protein dynamics during fertilization and meiotic exit
1529 in the *Xenopus* egg. *Proc Natl Acad Sci USA* 114: E10838–E10847

1530 Reimann JDR, Freed E, Hsu JY, Kramer ER, Peters J-M & Jackson PK (2001) Emi1 Is a Mitotic Regulator
1531 that Interacts with Cdc20 and Inhibits the Anaphase Promoting Complex. *Cell* 105: 645–655

1532 Rempel RE, Sleight SB & Maller JL (1995) Maternal Xenopus Cdk2-Cyclin E Complexes Function during
1533 Meiotic and Early Embryonic Cell Cycles That Lack a G1 Phase. *Journal of Biological Chemistry*
1534 270: 6843–6855

1535 Reverte CG, Ahearn MD & Hake LE (2001) CPEB Degradation during Xenopus Oocyte Maturation
1536 Requires a PEST Domain and the 26S Proteasome. *Dev Biol* 231: 447–458

1537 Reynolds N & Ohkura H (2003) Polo boxes form a single functional domain that mediates interactions
1538 with multiple proteins in fission yeast polo kinase. *Journal of Cell Science* 116: 1377–1387

1539 Ríos-Cardona D, Ricardo-González RR, Chawla A & Ferrell JE (2008) A role for GPRx, a novel GPR3/6/12-
1540 related G-protein coupled receptor, in the maintenance of meiotic arrest in Xenopus laevis
1541 oocytes. *Dev Biol* 317: 380–388

1542 Roig J, Groen A, Caldwell J & Avruch J (2005) Active Nercc1 Protein Kinase Concentrates at Centrosomes
1543 Early in Mitosis and Is Necessary for Proper Spindle Assembly. *MBoC* 16: 4827–4840

1544 Rong Y, Ji S-Y, Zhu Y-Z, Wu Y-W, Shen L & Fan H-Y (2019) ZAR1 and ZAR2 are required for oocyte meiotic
1545 maturation by regulating the maternal transcriptome and mRNA translational activation. *Nucleic*
1546 *Acids Research* 47: 11387–11402

1547 Ross J (1997) A hypothesis to explain why translation inhibitors stabilize mRNAs in mammalian cells:
1548 mRNA Stability and mitosis. *BioEssays* 19: 527–529

1549 Sadler SE & Maller JL (1985) Inhibition of Xenopus oocyte adenylate cyclase by progesterone: a novel
1550 mechanism of action. *Adv Cyclic Nucleotide Protein Phosphorylation Res* 19: 179–194

1551 Sagata N, Daar I, Oskarsson M, Showalter S & Vande Woude G (1989a) The product of the mos proto-
1552 oncogene as a candidate 'initiator' for oocyte maturation. *Science* 245: 643–646

1553 Sagata N, Oskarsson M, Copeland T, Brumbaugh J & Woude GFV (1988) Function of c-mos proto-
1554 oncogene product in meiotic maturation in Xenopus oocytes. *Nature* 335: 519–525

1555 Sagata N, Watanabe N, Vande Woude GF & Ikawa Y (1989b) The c-mos proto-oncogene product is a
1556 cytostatic factor responsible for meiotic arrest in vertebrate eggs. *Nature* 342: 512–518

1557 Santoni M, Meneau F, Sekhsoukh N, Castella S, Le T, Miot M & Daldello EM (2024) Unraveling the
1558 interplay between PKA inhibition and Cdk1 activation during oocyte meiotic maturation. *Cell*
1559 *Reports* 43: 113782

1560 Sasaki J, Ishikawa K, Arita M & Taniguchi K (2012) ACBD3-mediated recruitment of PI4KB to picornavirus
1561 RNA replication sites: Picornaviral protein/ACBD3/PI4KB complex. *The EMBO Journal* 31: 754–
1562 766

1563 Session AM, Uno Y, Kwon T, Chapman JA, Toyoda A, Takahashi S, Fukui A, Hikosaka A, Suzuki A, Kondo
1564 M, *et al* (2016) Genome evolution in the allotetraploid frog Xenopus laevis. *Nature* 538: 336–343

1565 Setoyama D, Yamashita M & Sagata N (2007) Mechanism of degradation of CPEB during Xenopus oocyte
1566 maturation. *Proc Natl Acad Sci USA* 104: 18001–18006

1567 Sharma K, D'Souza RCJ, Tyanova S, Schaab C, Wiśniewski JR, Cox J & Mann M (2014) Ultradeep Human
1568 Phosphoproteome Reveals a Distinct Regulatory Nature of Tyr and Ser/Thr-Based Signaling. *Cell*
1569 *Reports* 8: 1583–1594

1570 Solc P, Kitajima TS, Yoshida S, Brzakova A, Kaido M, Baran V, Mayer A, Samalova P, Motlik J & Ellenberg J
1571 (2015) Multiple Requirements of PLK1 during Mouse Oocyte Maturation. *PLoS ONE* 10:
1572 e0116783

1573 Sonnett M, Gupta M, Nguyen T & Wühr M (2018) Quantitative Proteomics for Xenopus Embryos II, Data
1574 Analysis. In *Xenopus*, Vleminckx K (ed) pp 195–215. New York, NY: Springer New York

1575 Stearns T & Kirschner M (1994) In vitro reconstitution of centrosome assembly and function: The central
1576 role of γ-tubulin. *Cell* 76: 623–637

1577 Stebbins-Boaz B, Cao Q, de Moor CH, Mendez R & Richter JD (1999) Maskin Is a CPEB-Associated Factor
1578 that Transiently Interacts with eIF-4E. *Molecular Cell* 4: 1017–1027

1579 Steinacker TL, Wong S-S, Novak ZA, Saurya S, Gartenmann L, Van Houtum EJH, Sayers JR, Lagerholm BC
1580 & Raff JW (2022) Centriole growth is limited by the Cdk/Cyclin-dependent phosphorylation of
1581 Ana2/STIL. *Journal of Cell Biology* 221: e202205058

1582 Sulimenko V, Dráberová E & Dráber P (2022) γ-Tubulin in microtubule nucleation and beyond. *Front Cell*
1583 *Dev Biol* 10: 880761

1584 Sun H, Han L, Guo Y, An H, Wang B, Zhang X, Li J, Jiang Y, Wang Y, Sun G, *et al* (2024) The global
1585 phosphorylation landscape of mouse oocytes during meiotic maturation. *EMBO J* 43: 4752–4785

1586 Swartz SZ, Nguyen HT, McEwan BC, Adamo ME, Cheeseman IM & Kettenbach AN (2021) Selective
1587 dephosphorylation by PP2A-B55 directs the meiosis I-meiosis II transition in oocytes. *eLife* 10:
1588 e70588

1589 Taieb FE, Gross SD, Lewellyn AL & Maller JL (2001) Activation of the anaphase-promoting complex and
1590 degradation of cyclin B is not required for progression from Meiosis I to II in Xenopus oocytes.
1591 *Current Biology* 11: 508–513

1592 Takagi M, Absalon MJ, McLure KG & Kastan MB (2005) Regulation of p53 Translation and Induction after
1593 DNA Damage by Ribosomal Protein L26 and Nucleolin. *Cell* 123: 49–63

1594 Tanos BE, Yang H-J, Soni R, Wang W-J, Macaluso FP, Asara JM & Tsou M-FB (2013) Centriole distal
1595 appendages promote membrane docking, leading to cilia initiation. *Genes Dev* 27: 163–168

1596 Tavernier N, Noatynska A, Panbianco C, Martino L, Van Hove L, Schwager F, Léger T, Gotta M & Pintard L
1597 (2015) Cdk1 phosphorylates SPAT-1/Bora to trigger PLK-1 activation and drive mitotic entry in *C.*
1598 *elegans* embryos. *Journal of Cell Biology* 208: 661–669

1599 Tavernier N, Sicheri F & Pintard L (2021) Aurora A kinase activation: Different means to different ends.
1600 *Journal of Cell Biology* 220: e202106128

1601 Terasaki M, Runft LL & Hand AR (2001) Changes in Organization of the Endoplasmic Reticulum during
1602 *Xenopus* Oocyte Maturation and Activation. *MBoC* 12: 1103–1116

1603 Thibier C, De Smedt V, Poulhe R, Huchon D, Jessus C & Ozon R (1997) In Vivo Regulation of Cytostatic
1604 Activity inXenopusMetaphase II-Arrested Oocytes. *Developmental Biology* 185: 55–66

1605 Thillaiappan NB, Smith HA, Atakpa-Adaji P & Taylor CW (2021) KRAP tethers IP3 receptors to actin and
1606 licenses them to evoke cytosolic Ca2+ signals. *Nat Commun* 12: 4514

1607 Thomas Y, Cirillo L, Panbianco C, Martino L, Tavernier N, Schwager F, Van Hove L, Joly N, Santamaria A,
1608 Pintard L, *et al* (2016) Cdk1 Phosphorylates SPAT-1/Bora to Promote Plk1 Activation in C.
1609 elegans and Human Cells. *Cell Reports* 15: 510–518

1610 Torres JZ, Ban KH & Jackson PK (2010) A Specific Form of Phospho Protein Phosphatase 2 Regulates
1611 Anaphase-promoting Complex/Cyclosome Association with Spindle Poles. *MBoC* 21: 897–904

1612 Tzeng Y-W, Li D-Y, Chen Y, Yang C-H, Chang C-Y & Juang Y-L (2018) LMO7 exerts an effect on mitosis
1613 progression and the spindle assembly checkpoint. *The International Journal of Biochemistry &*
1614 *Cell Biology* 94: 22–30

1615 Uto K (2000) Nek2B, a novel maternal form of Nek2 kinase, is essential for the assembly or maintenance
1616 of centrosomes in early Xenopus embryos. *The EMBO Journal* 19: 1816–1826

1617 Van Itallie E, Sonnett M, Kalocsay M, Wuhr M, Peshkin L & Kirschner MW (2025) Transitions in the
1618 proteome and phospho-proteome during Xenopus laevis development. *bioRxiv preprint*

1619 Vigneron S, Sundermann L, Labbé J-C, Pintard L, Radulescu O, Castro A & Lorca T (2018) Cyclin A-cdk1-
1620 Dependent Phosphorylation of Bora Is the Triggering Factor Promoting Mitotic Entry.
1621 *Developmental Cell* 45: 637-650.e7

1622 Vik TA & Ryder JW (1997) Identification of Serine 380 as the Major Site of Autophosphorylation of
1623 Xenopus pp90rsk. *Biochemical and Biophysical Research Communications* 235: 398–402

1624 Virant-Klun I, Leicht S, Hughes C & Krijgsveld J (2016) Identification of Maturation-Specific Proteins by
1625 Single-Cell Proteomics of Human Oocytes. *Molecular & Cellular Proteomics* 15: 2616–2627

1626 Walczak CP, Leto DE, Zhang L, Riepe C, Muller RY, DaRosa PA, Ingolia NT, Elias JE & Kopito RR (2019)
1627 Ribosomal protein RPL26 is the principal target of UFMylation. *Proc Natl Acad Sci USA* 116:
1628 1299–1308

1629 Wang L, Harris TE, Roth RA & Lawrence JC (2007) PRAS40 Regulates mTORC1 Kinase Activity by
1630 Functioning as a Direct Inhibitor of Substrate Binding. *Journal of Biological Chemistry* 282:
1631 20036–20044

1632 Warner JR & McIntosh KB (2009) How Common Are Extraribosomal Functions of Ribosomal Proteins?
1633 *Molecular Cell* 34: 3–11

1634 Wassmann K (2022) Separase Control and Cohesin Cleavage in Oocytes: Should I Stay or Should I Go?
1635 *Cells* 11: 3399

1636 Wessel D & Flügge UI (1984) A method for the quantitative recovery of protein in dilute solution in the
1637 presence of detergents and lipids. *Anal Biochem* 138: 141–143

1638 Whitmire E, Khan B & Coué M (2002) Cdc6 synthesis regulates replication competence in Xenopus
1639 oocytes. *Nature* 419: 722–725

1640 Wilk K, Bilinski S, Dougherty MT & Kloc M (2005) Delivery of germinal granules and localized RNAs via
1641 the messenger transport organizer pathway to the vegetal cortex of Xenopus oocytes occurs
1642 through directional expansion of the mitochondrial cloud. *Int J Dev Biol* 49: 17–21

1643 Wind M, Kelm O, Nigg EA & Lehmann WD (2002) Identification of phosphorylation sites in the polo-like
1644 kinases Plx1 and Plk1 by a novel strategy based on element and electrospray high resolution
1645 mass spectrometry. *Proteomics* 2: 1516–1523

1646 Woodland HR (1974) Changes in the polysome content of developing Xenopus laevis embryos. *Dev Biol*
1647 40: 90–101

1648 Wu X-J, Thomas P & Zhu Y (2018) Pgrmc1 Knockout Impairs Oocyte Maturation in Zebrafish. *Front*
1649 *Endocrinol* 9: 560

1650 Wühr M, Freeman RM, Presler M, Horb ME, Peshkin L, Gygi SP & Kirschner MW (2014) Deep Proteomics
1651 of the Xenopus laevis Egg using an mRNA-Derived Reference Database. *Current Biology* 24:
1652 1467–1475

Yamamoto TM, Cook JM, Kotter CV, Khat T, Silva KD, Ferreyros M, Holt JW, Knight JD & Charlesworth A (2013) Zar1 represses translation in Xenopus oocytes and binds to the TCS in maternal mRNAs with different characteristics than Zar2. *Biochimica et Biophysica Acta (BBA) - Gene Regulatory Mechanisms* 1829: 1034–1046

Yanagitani K, Juszkiewicz S & Hegde RS (2017) UBE2O is a quality control factor for orphans of multiprotein complexes. *Science* 357: 472–475

Yang C, Dominique GM, Champion MM & Huber PW (2022) Remnants of the Balbiani body are required for formation of RNA transport granules in Xenopus oocytes. *iScience* 25: 103878

Yang M, Jin Y, Fan S, Liang X, Jia J, Tan Z, Huang T, Li Y, Ma T & Li M (2019) Inhibition of neddylation causes meiotic arrest in mouse oocyte. *Cell Cycle* 18: 1254–1267

Yew N, Mellini ML, Martinez CK & Woude GFV (1992) Meiotic initiation by the mos protein in Xenopus. *Nature* 355: 649–652

Zhang M, Zhang J, Yan W & Chen X (2016) p73 expression is regulated by ribosomal protein RPL26 through mRNA translation and protein stability. *Oncotarget* 7: 78255–78268

Zhang Z, Liu R, Zhou H, Li Q, Qu R, Wang W, Zhou Z, Yu R, Zeng Y, Mu J, *et al* (2023) PATL2 regulates mRNA homeostasis in oocytes by interacting with EIF4E and CPEB1. *Development* 150: dev201572

Zitouni S, Francia ME, Leal F, Montenegro Gouveia S, Nabais C, Duarte P, Gilberto S, Brito D, Moyer T, Kandels-Lewis S, *et al* (2016) CDK1 Prevents Unscheduled PLK4-STIL Complex Assembly in Centriole Biogenesis. *Current Biology* 26: 1127–1137

Figure 1

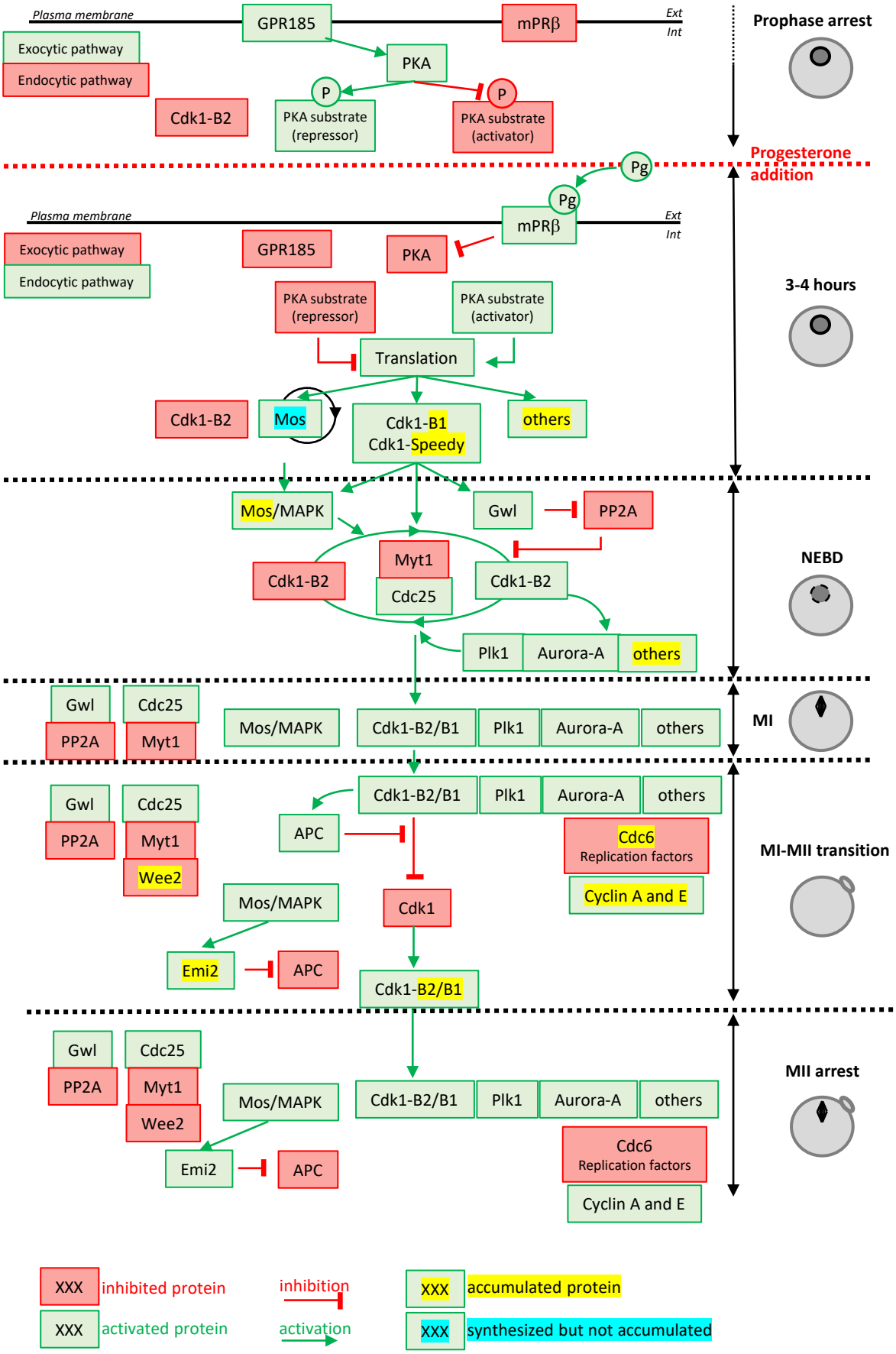
Plasma membrane
GPR185
mPRβ
Ext
Int
Prophase arrest
Exocytic pathway
Endocytic pathway
PKA
P
P
Cdk1-B2
PKA substrate (repressor)
PKA substrate (activator)
Progesterone addition
Pg
Pg
Plasma membrane
mPRβ
Ext
Int
Exocytic pathway
Endocytic pathway
GPR185
PKA
3-4 hours
PKA substrate (repressor)
PKA substrate (activator)
Translation
Cdk1-B2
Mos
Cdk1-B1
Cdk1-Speedy
others
Mos/MAPK
Gwl
PP2A
NEBD
Myt1
Cdk1-B2
Cdc25
Cdk1-B2
Plk1
Aurora-A
others
Gwl
Cdc25
PP2A
Myt1
Mos/MAPK
Cdk1-B2/B1
Plk1
Aurora-A
others
MI
Gwl
Cdc25
PP2A
Myt1
Wee2
Cdk1-B2/B1
Plk1
Aurora-A
others
APC
Cdc6
Replication factors
Cyclin A and E
MI-MII transition
Mos/MAPK
Cdk1
Emi2
APC
Cdk1-B2/B1
Gwl
Cdc25
PP2A
Myt1
Wee2
Mos/MAPK
Cdk1-B2/B1
Plk1
Aurora-A
others
MII arrest
Emi2
APC
Cdc6
Replication factors
Cyclin A and E
XXX inhibited protein
XXX activated protein
inhibition
activation
XXX accumulated protein
XXX synthesized but not accumulated

Figure 1 continued

Figure 1. Molecular events coordinating *Xenopus laevis* oocyte meiotic divisions. From top to bottom: The prophase arrest is maintained by high PKA activity due to the constitutively expressed GPR185 receptor. The exocytic pathway is active while the endocytic pathway is downregulated. Cdk1-Cyclin B2 complexes are present under an inactive state due to Cdk1 phosphorylation. Progesterone activates the mPRβ receptor, GPR185 is inactivated, the exocytosis and endocytosis pathways are inverted. PKA is inactivated and promotes translation and/or accumulation of new proteins, among them Mos (that does not accumulate due to its instability) and Cyclin B1 (due to its stabilization). New Cyclin B1 proteins associate with Cdk1 and form a starter amount of Cdk1 activity. This Cdk1 starter stabilizes Mos and promotes Cdk1-Cyclin B2 activation through the regulation of Myt1, Cdc25, Gwl and PP2A. The autoamplification loop is launched, whereby more Cdk1 is activated, more it activates kinases as Mos-MAPK, Aurora-A and Plk1, all of them contributing with Cdk1 to regulate Myt1 and Cdc25, hence accelerating Cdk1 activation. Phosphorylated substrates trigger NEBD and the MI spindle assembly as well as protein translation. APC is activated under the control of Cdk1 and leads to Cyclin B degradation. The Cdk1 activity decreases and allows anaphase I and expulsion of the 1st polar body. Under the Mos/MAPK control, Emi2/Erp1 inactivates APC, halting Cyclin B degradation. The re-accumulation of Cyclin B increases Cdk1 activity that triggers the formation of the MII spindle, avoiding the assembly of a nucleus and DNA replication. APC remains inhibited by Emi2/Erp1, what ensures the oocyte arrest in MII. Color code: red: inactivated proteins; green: activated proteins; red arrow: inhibition; green arrow: activation; yellow highlight: accumulated protein; blue highlight: protein synthesized but not accumulated.

Figure 2

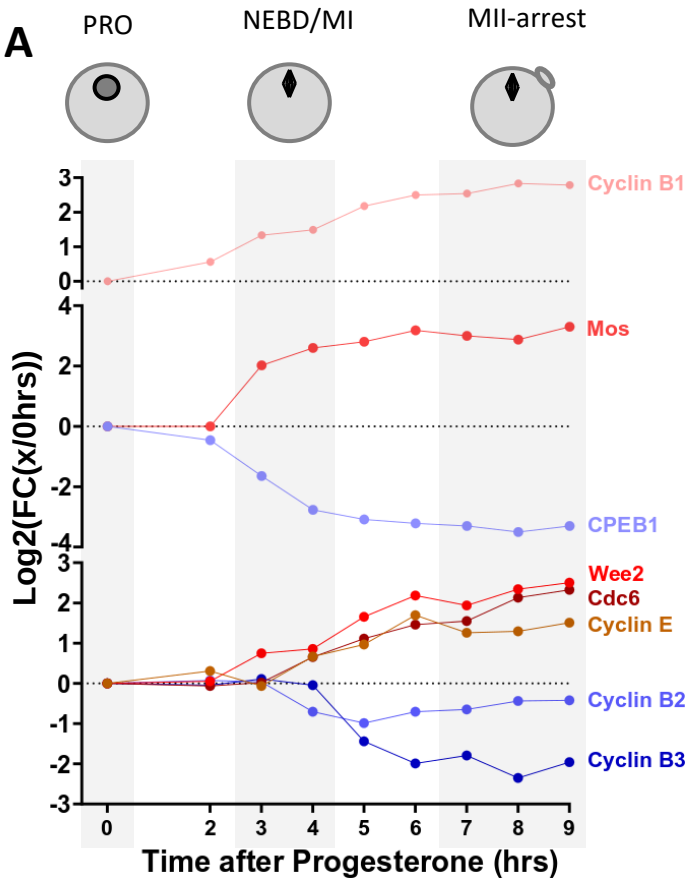
A
PRO
NEBD/MI
MII-arrest
Cyclin B1
Mos
CPEB1
Wee2
Cdc6
Cyclin E
Cyclin B2
Cyclin B3
Log2(FC(x/0hrs))
Time after Progesterone (hrs)

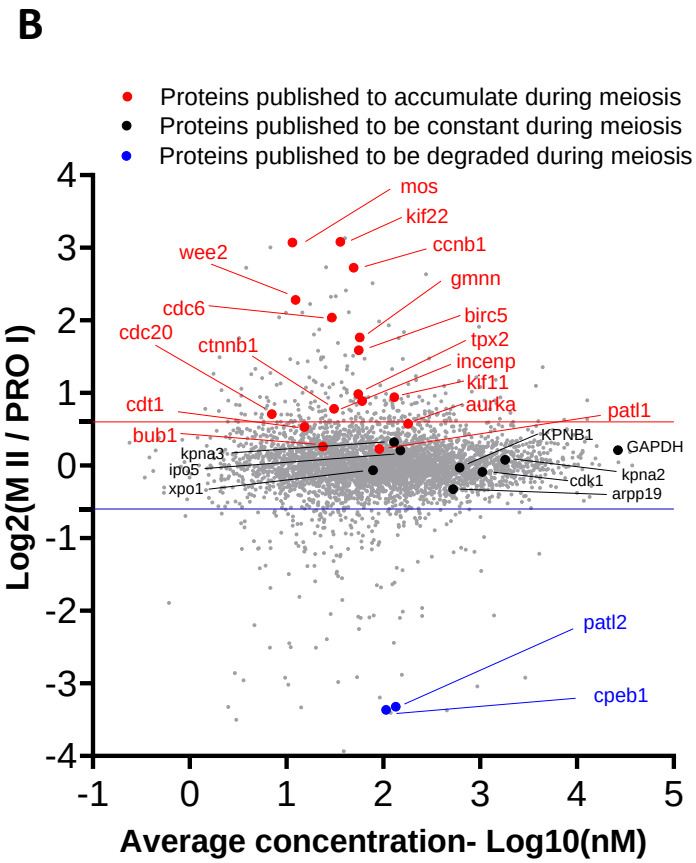
B
Proteins published to accumulate during meiosis
Proteins published to be constant during meiosis
Proteins published to be degraded during meiosis
mos
kif22
ccnb1
wee2
gmnn
cdc6
birc5
cdc20
tpx2
ctnnb1
incenp
kif11
cdt1
aurka
patl1
bub1
KPNB1
GAPDH
kpna3
ipo5
xpo1
cdk1
kpna2
arpp19
patl2
cpeb1
Log2(M II / PRO I)
Average concentration- Log10(nM)

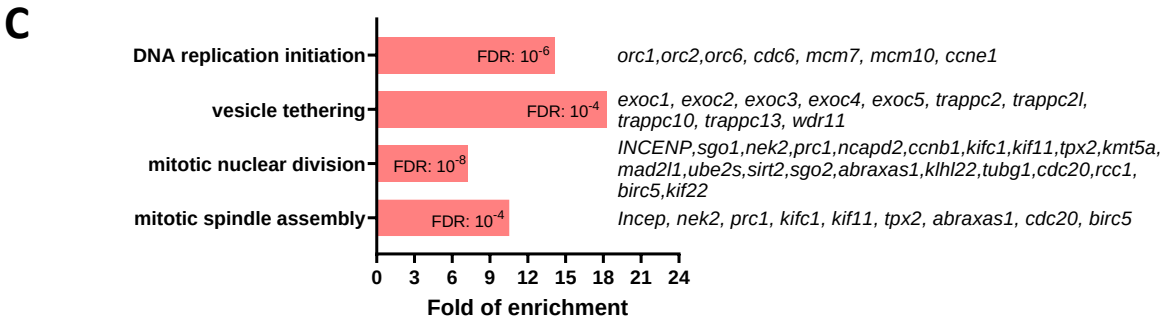
C
DNA replication initiation
FDR: 10-6
orc1,orc2,orc6, cdc6, mcm7, mcm10, ccne1
vesicle tethering
FDR: 10-4
exoc1, exoc2, exoc3, exoc4, exoc5, trappc2, trappc2l, trappc10, trappc13, wdr11
mitotic nuclear division
FDR: 10-8
INCENP,sgo1,nek2,prc1,ncapd2,ccnb1,kifc1,kif11,tpx2,kmt5a, mad2l1,ube2s,sirt2,sgo2,abraxas1,klhl22,tubg1,cdc20,rcc1, birc5,kif22
mitotic spindle assembly
FDR: 10-4
Incep, nek2, prc1, kifc1, kif11, tpx2, abraxas1, cdc20, birc5
Fold of enrichment

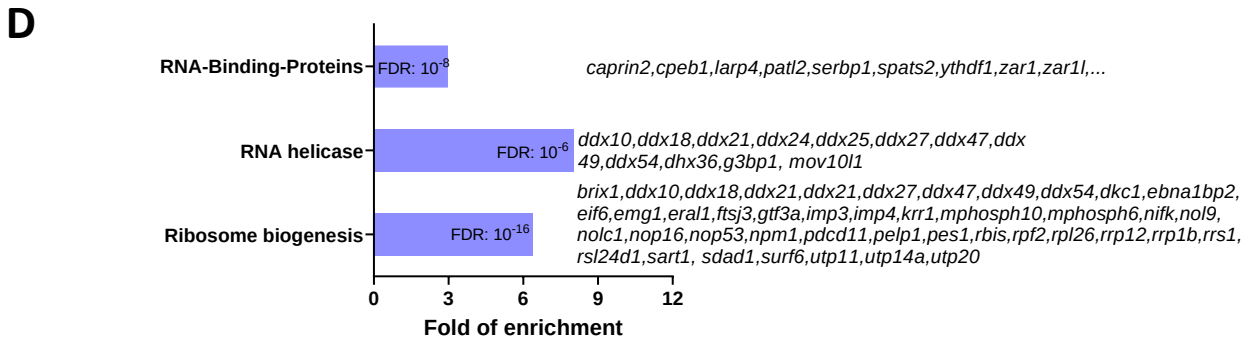
D
RNA-Binding-Proteins
FDR: 10-8
caprin2,cpeb1,larp4,patl2,serbp1,spats2,ythdf1,zar1,zar1l,...
RNA helicase
FDR: 10-6
ddx10,ddx18,ddx21,ddx24,ddx25,ddx27,ddx47,ddx 49,ddx54,dhx36,g3bp1, mov10l1
Ribosome biogenesis
FDR: 10-16
brix1,ddx10,ddx18,ddx21,ddx21,ddx27,ddx47,ddx49,ddx54,dkc1,ebna1bp2, eif6,emg1,eral1,ftsj3,gtf3a,imp3,imp4,krr1,mphosph10,mphosph6,nifk,nol9, nolc1,nop16,nop53,npm1,pdcd11,pelp1,pes1,rbis,rpf2,rpl26,rrp12,rrp1b,rrs1, rsl24d1,sart1, sdad1,surf6,utp11,utp14a,utp20
Fold of enrichment

Figure 2 continued

Figure 2. Changes in the protein levels during meiotic divisions. (**A**) The relative changes in the concentration of proteins whose accumulation/degradation has been reported to correlate with the critical stages of *Xenopus* meiotic divisions have been plotted. (**B**) Changes of protein stoichiometry during meiotic maturation. The log2 fold changes between the concentration of each protein in PRO-arrested oocytes and MII-arrested oocytes was plotted against the average concentration during meiotic divisions. The red line marks the 1.5-fold change used as a threshold to identify accumulating proteins. The blue line marks the 0.75-fold change used as threshold to distinguish proteins that are degraded during meiosis. Proteins, whose changes in homeostasis during meiotic divisions are documented in the literature, are marked with the following color code: red, for proteins accumulating; black, for proteins which are expressed at a stable level; and blue, for proteins that are degraded. (**C-D**) Gene ontology analysis of the biological processes enriched among the proteins found to accumulate (in red, panel **C**) or degraded (in blue, panel **D**) during meiosis. The statistical significance of the enrichment is expressed as false discovery rate (FDR). A representative subset of the proteins belonging to each group is displayed.

Figure 2-figure supplement 3

A

	PRO I		MI				MII - arrest							
Gene name	0	2	3	4	5	6	7	8	9	FC (MII/PRO)	Log2- FC (MII/PRO)	FC (MII/PRO) (Peuchen, 2017)	Log2- FC (MII/PRO) (Peuchen, 2017)	PMID	
kif22 (XKid)	0.018	0.019	0.036	0.053	0.074	0.094	0.120	0.138	0.187	8.5	3.1	not detected	not detected	12360284	UP
mos	0.015	0.015	0.061	0.091	0.105	0.136	0.120	0.110	0.148	8.4	3.1	0.9	-0.2	2474853	
ccnb1	0.021	0.031	0.053	0.059	0.095	0.119	0.122	0.150	0.145	6.6	2.7	not detected	not detected	10512866	
wee2	0.027	0.028	0.045	0.048	0.084	0.121	0.102	0.135	0.151	4.9	2.3	not detected	not detected	10673504	
cdc6	0.034	0.033	0.035	0.054	0.074	0.094	0.100	0.149	0.171	4.1	2.0	0.5	-1.0	12384698, 12384699,26092930	
gmnn	0.037	0.038	0.056	0.072	0.099	0.122	0.105	0.130	0.142	3.4	1.8	1.2	0.3	19656945	
birc5 (survivin)	0.044	0.047	0.053	0.056	0.085	0.101	0.113	0.145	0.139	3.0	1.6	2.2	1.1	18378691	
ccne1	0.046	0.057	0.044	0.073	0.090	0.149	0.110	0.113	0.131	2.6	1.4	not detected	not detected	11413001	
zfp36l2	0.059	0.058	0.066	0.053	0.048	0.045	0.132	0.123	0.135	2.2	1.1	not detected	not detected	18385675	
tpx2	0.057	0.061	0.071	0.085	0.098	0.107	0.109	0.115	0.115	2.0	1.0	not detected	not detected	19121998	
kif11 (Eg5)	0.058	0.061	0.073	0.077	0.091	0.100	0.103	0.110	0.119	1.9	0.9	1.7	0.8	8026619	
incenp	0.059	0.065	0.069	0.075	0.096	0.093	0.101	0.101	0.126	1.9	0.9	1.5	0.5	18378691	
ctnnb1	0.064	0.051	0.078	0.088	0.097	0.109	0.105	0.118	0.107	1.7	0.8	1.0	0.0	9876185	
cdc20	0.064	0.058	0.082	0.091	0.097	0.089	0.111	0.102	0.101	1.6	0.7	0.5	-1.1	11413001	
aurka (Eg2)	0.067	0.069	0.088	0.089	0.099	0.104	0.094	0.098	0.108	1.5	0.6	1.3	0.3	10704364	
cdt1	0.072	0.071	0.081	0.098	0.098	0.114	0.096	0.115	0.100	1.4	0.5	1.0	0.0	19656945	
bub1	0.081	0.075	0.099	0.083	0.107	0.102	0.097	0.093	0.101	1.2	0.3	not detected	not detected	11231148	
patl1	0.085	0.075	0.089	0.089	0.095	0.100	0.096	0.104	0.099	1.2	0.2	4.6	2.2	20826699	
kpna3	0.081	0.088	0.075	0.085	0.087	0.09	0.1	0.106	0.098	1.3	0.3	0.6	-0.7	26399853	CONSTANT
gapdh	0.079	0.0885	0.0815	0.083	0.0795	0.0825	0.0905	0.0925	0.0915	1.2	0.2	0.5	-1.03398944	26399853	
ipo5	0.082	0.0845	0.0835	0.0735	0.088	0.08	0.093	0.0965	0.095	1.2	0.2	0.5	-0.9	26399853	
tuba4b	0.079	0.106	0.082	0.132	0.092	0.096	0.078	0.08	0.115	1.2	0.2	0.4	-1.5	20531391	
kpna2	0.09	0.0875	0.096	0.101	0.092	0.09	0.096	0.088	0.101	1.1	0.1	1.1	0.1	26399853	
mapk1	0.092	0.095	0.093	0.098	0.091	0.099	0.092	0.099	0.086	1.0	0.0	0.6	-0.7	26092930	
kpnb1	0.1	0.088	0.08	0.086	0.077	0.093	0.087	0.092	0.115	1.0	0.0	0.5	-1.1	26399853	
xpo1	0.093	0.093	0.086	0.086	0.094	0.092	0.089	0.092	0.086	1.0	-0.1	0.6	-0.8	26399853	
acta4	0.089	0.101	0.086	0.099	0.09	0.09	0.085	0.081	0.089	1.0	-0.1	not detected	not detected	20826699	
cdk1	0.0965	0.092	0.1005	0.0975	0.098	0.095	0.0915	0.0935	0.087	0.9	-0.1	1.0	0.0	26092930	
arpp19	0.1015	0.085	0.1125	0.0885	0.1025	0.086	0.085	0.075	0.083	0.8	-0.3	0.6	-0.7	24525567	
zar1	0.211	0.096	0.109	0.083	0.088	0.086	0.076	0.062	0.064	0.3	-1.6	0.3	-1.8	23827238	
tbpl2	0.135	0.123	0.132	0.089	0.093	0.071	0.075	0.055	0.073	0.5	-1.0	not detected	not detected	19650908	DOWN
zar2	0.218	0.0985	0.0935	0.0845	0.0835	0.0795	0.065	0.0525	0.059	0.3	-1.9	not detected	not detected	23827238	
patl2	0.273	0.286	0.108	0.057	0.036	0.033	0.028	0.025	0.029	0.1	-3.3	0.4	-1.3	20826699	
cpeb1	0.306	0.223	0.098	0.045	0.036	0.033	0.031	0.027	0.031	0.1	-3.4	0.4	-1.2	11237472, 11927567	

B

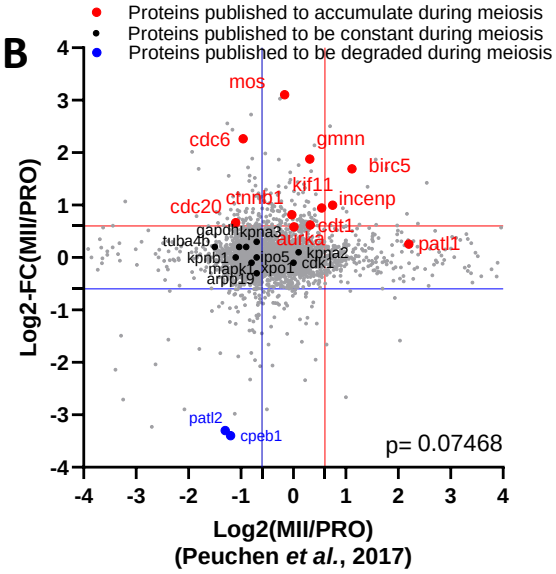

C

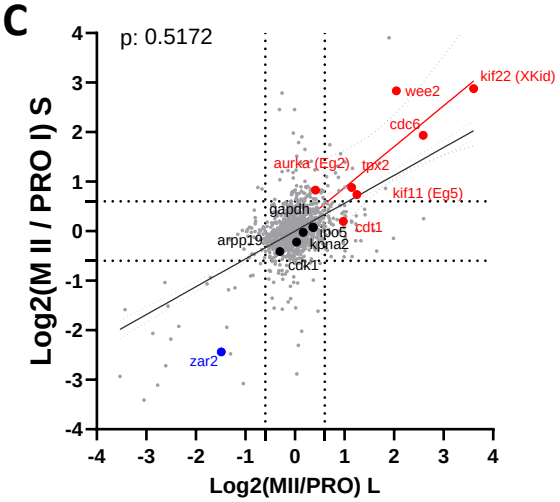

D

		S		
		UP	Constant	DOWN
L	UP	19	57	0
	Constant	62	1042	39
	DOWN	2	38	22

E

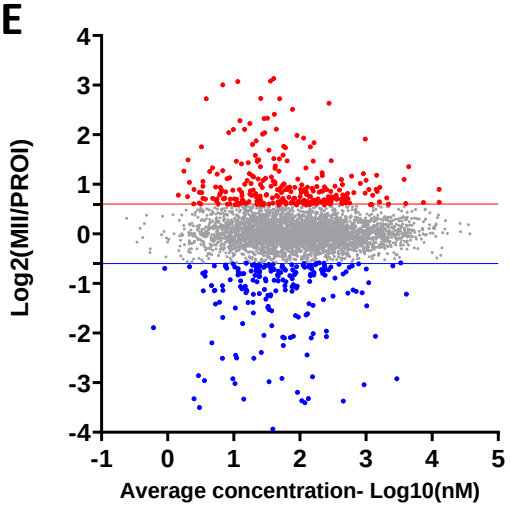

Figure 2-figure supplement 3 continued

Figure 2-figure supplement 3. Validation of the proteomic dataset. (**A**) Table summarizing proteins whose changes in protein level have been documented using Western blot. The PMID of the original publication displaying the Western blot is reported. The changes in abundance detected in our dataset are color-coded with a scale from green to red. Log2 fold changes between prophase and metaphase II from our dataset are color-coded with a scale from red to blue and compared to another previously published dataset (Peuchen *et al*, 2017). (**B**) Proteome-wide comparison of our dataset with (Peuchen *et al*, 2017). Proteins whose abundance was previously published are color-coded in red for the ones that accumulate, black for the constant, and blue for the ones that are degraded. (**C**) Changes in protein abundance between prophase and metaphase II were calculated for each protein where we could distinguish the .S and .L isoforms and plotted. The Pearson correlation between the isoforms was calculated with Prism. (**D**) Table summarizing the comparison between .S and .L isoforms presented in panel **C**. (**E**) Correlation plot between the changes in protein abundance occurring during the prophase to metaphase II transition and the average concentration of the proteins during meiotic divisions.

Figure 2-figure supplement 4

A

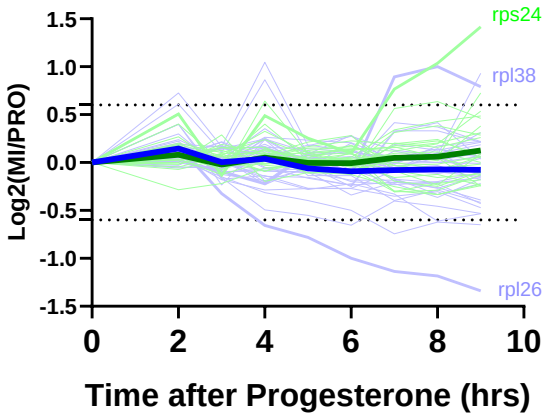

B

			n. of proteins degraded bearing the consensus	Substrates (reference)
APC	D-Box	R-x-x-L-x-x-x-x-N	56 (11%)	Ccnb 2 (PMDI: 1846030), CKAP2 (PMDI: 17339342)
	KEN	K-E-N-x-x-x-N	2 (1%)	
	ABBA	I/L/V/F-x-I/L/M/V/P-F/H/Y-x-D/E	128 (25%)	
SCF	BtrcP	D/T-SGxxS	22 (4%)	CPEB1 (PMDI: 11237472)
	FBXW7:	I/L-I/L/P-T/S-P-x-x-S/T	8 (2%)	
None of the identified degron			253 (57%)	

Figure 2-figure supplement 4. Protein degradation during meiotic maturation: ribosomal proteins, E3 ligases targets. (**A**) Changes in protein abundance of ribosomal proteins between prophase (PRO) and metaphase II (MII) are plotted. Dashed lines represent the threshold used for defining the differentially expressed proteins. (**B**) Table summarizing the different degron consensus motifs identified and the number of proteins in our dataset bearing these motifs. Examples of proteins bearing different degrons are listed along with supporting literature.

Figure 3

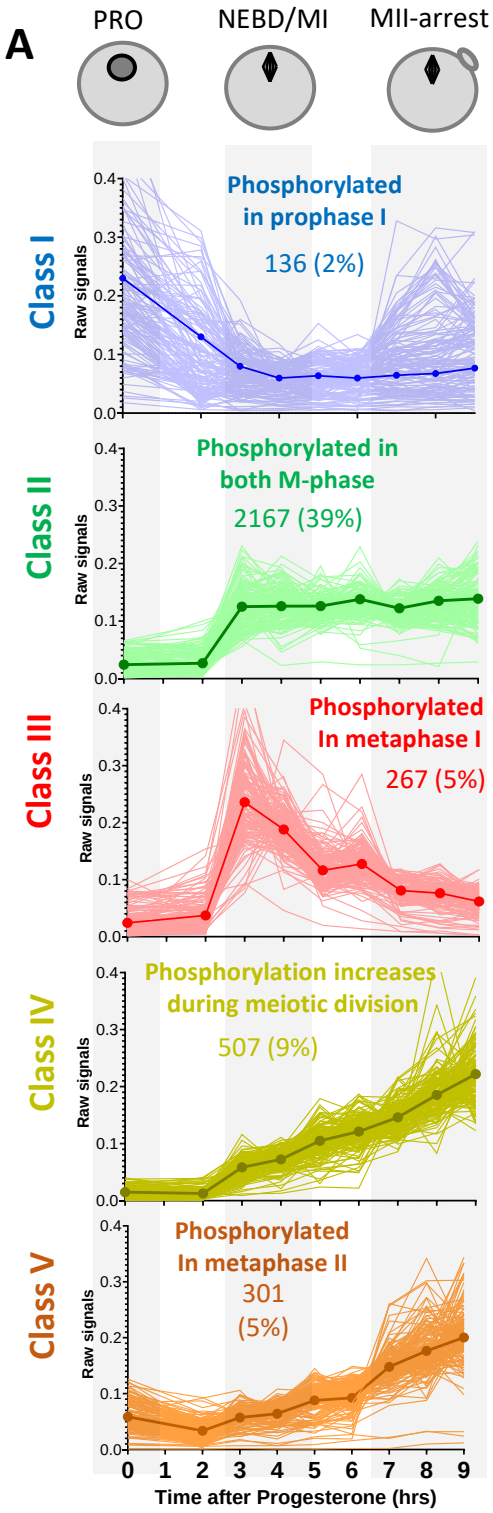

B

Class I proteins

	gene name	description	PMID
Vessicle trafficking and membrane organization	**C2CD2L**	an endoplasmic reticulum protein that functions both as membrane tether to the plasma membrane and as phospholipid transporter	32693056
	MAGI1	a scaffolding protein localized at the plasma membrane	35389514
	NKTR	a membrane-anchored protein with function in protein folding	7906541
	LDLRAP1	interacts with the cytoplasmic tail of the LDL receptor and facilitates the clathrin-mediated endocytosis of LDLR and other members of this family	15728179
	PI4KB	PKA substrate that regulates Golgi reorganization during mitosis, and is involved in Golgi-to-plasma membrane trafficking	23712958
Actin cytoskeleton	**WIPF2**	induces reorganization of the actin filament network around the plasma membrane by cooperating with WASP/WASL88	21785420
	SPTBN1	an actin crosslinking and molecular scaffold protein that is involved in Ca2+ and calmodulin-dependent exocytosis	32601107
	ITPRID2	tethers IP3 receptors to the actin under the plasma membrane to mediate Ca2+ signalling	34301929
Translation	**PATL1**	RNA binding protein involved in mRNA stabilization and translation repression	20826699
	eIF4ENIF1	binds and sequesters eIF4E inhibiting protein translation initiation.	16157702
	Maskin	component of the translation repression complex nucleated by CPEB1 that is involved in mantaining translation repression in Prophase arrested oocytes.	10635326
Ubiquitn ligases	**Ube2O**	E2/E3 ubiquitin-protein ligase with both E2 and E3 ligase activities.	30468556
	Faf2	endoplasmic reticulum–associated protein involved in the dissolution of RNA stress granules	34739333
	Ube4b	E3-ubiquitin ligase, with unknow function.	
	DCUN1D5	catalyzes the neddylation of cullins that is required for the activation of the cullin-E3 ubiquitin ligase.	26906416

Figure 3. Changes in protein phosphorylation during meiotic divisions. (**A**) Relative phosphopeptide signals were normalized for the changes in the total level of the proteins. The changes in the phosphopeptides were measured between the three biological stages of meiotic divisions (PRO = 0hr, NEBD/MI = average of 3 and 4 hours, and MII-arrest = average of 7 to 9 hours).

Figure 3 continued

Class I (n=136 - 2%, in blue) includes proteins bearing a phosphosite whose occupancy decreases during meiosis resumption (Log2FC(MI/PRO)<-1). Class II (n=2167 - 39%, in green) contains proteins that are highly phosphorylated from MI (Log2FC(MI/PRO)>1) to MII (-1<Log2FC(MII/MI)<1). Class III (n=267 - 5%, in red) consists of proteins whose phosphorylation is specific of MI (Log2FC(MI/PRO)>1, Log2FC(MII/MI)<-1). Class IV (n=507 - 9%, yellow) is composed of proteins whose phosphorylation increases from MI (Log2FC(MI/PRO)>1) to MII, picking in MII (Log2FC(MII/MI)> 1). Class V (n=301 – 5%, orange) comprises proteins whose phosphorylation does not vary in MI (-1<Log2FC(MI/PRO)<1) but are phosphorylated only in MII (Log2FC(MII/MI)>1). The average signal of each Class was plotted with a thick and dark line. (**B**) Table summarizing the proteins bearing phosphosites belonging to Class I.

Figure 3-figure supplement 1

A

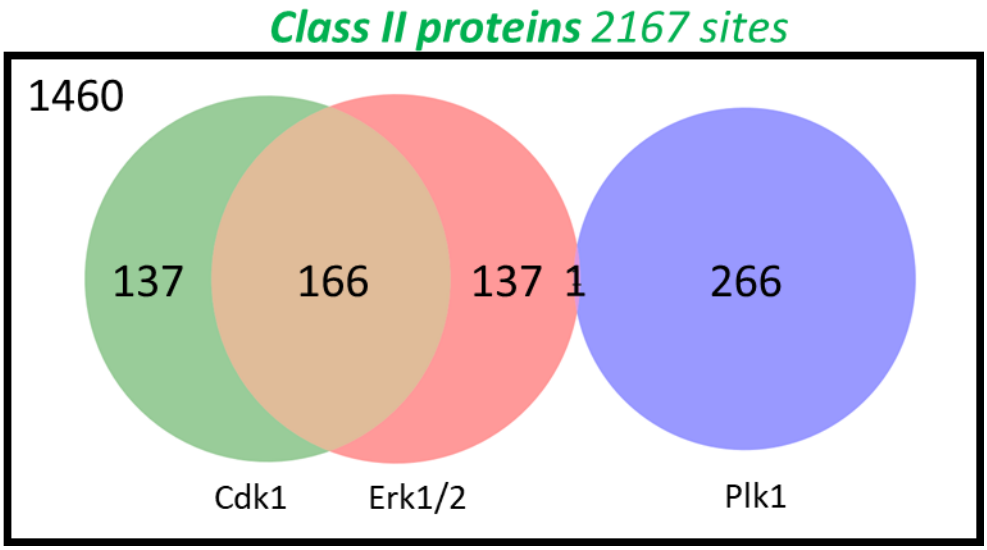

B

	Top 10 kinases									
Class I	CK2A2	CK2A1	GRK5	CAMK2G	CAMK2B	PLK2	GRK6	GRK3	TGFBR1	PLK3
Class II	CDK2	CDK3	CDK1	KIS	CDK5	CDK16	PLK1	JNK1	JNK3	ERK2
Class III	JNK1	JNK3	CDK2	P38B	CDK8	PRP4	JNK2	ERK2	CDK19	CDK17
Class IV	IKKE	CDK2	CAMK2D	BMPR2	JNK1	PLK3	TBK1	CAMK2B	PLK1	CK1G3
Class V	CK2A2	CK2A1	CAMK2G	PLK2	GRK7	GRK4	ALK7	CK1D	BMPR1A	ATM

Figure 3-figure supplement 1. (A) Venn diagram showing the number of Class II phosphosites predicted to be targeted by Cdk1, Erk1/2, and Plk1. Predictions were made using the kinase scoring tool available at https://kinase-library.phosphosite.org/kinase-library/score-site, applying a 90th percentile threshold. **(B)** Top 10 kinases whose predicted phosphorylation sites are most enriched in each class (I to V), using the kinase scoring tool available at https://kinase-library.phosphosite.org/kinase-library/score-site.

Figure 4

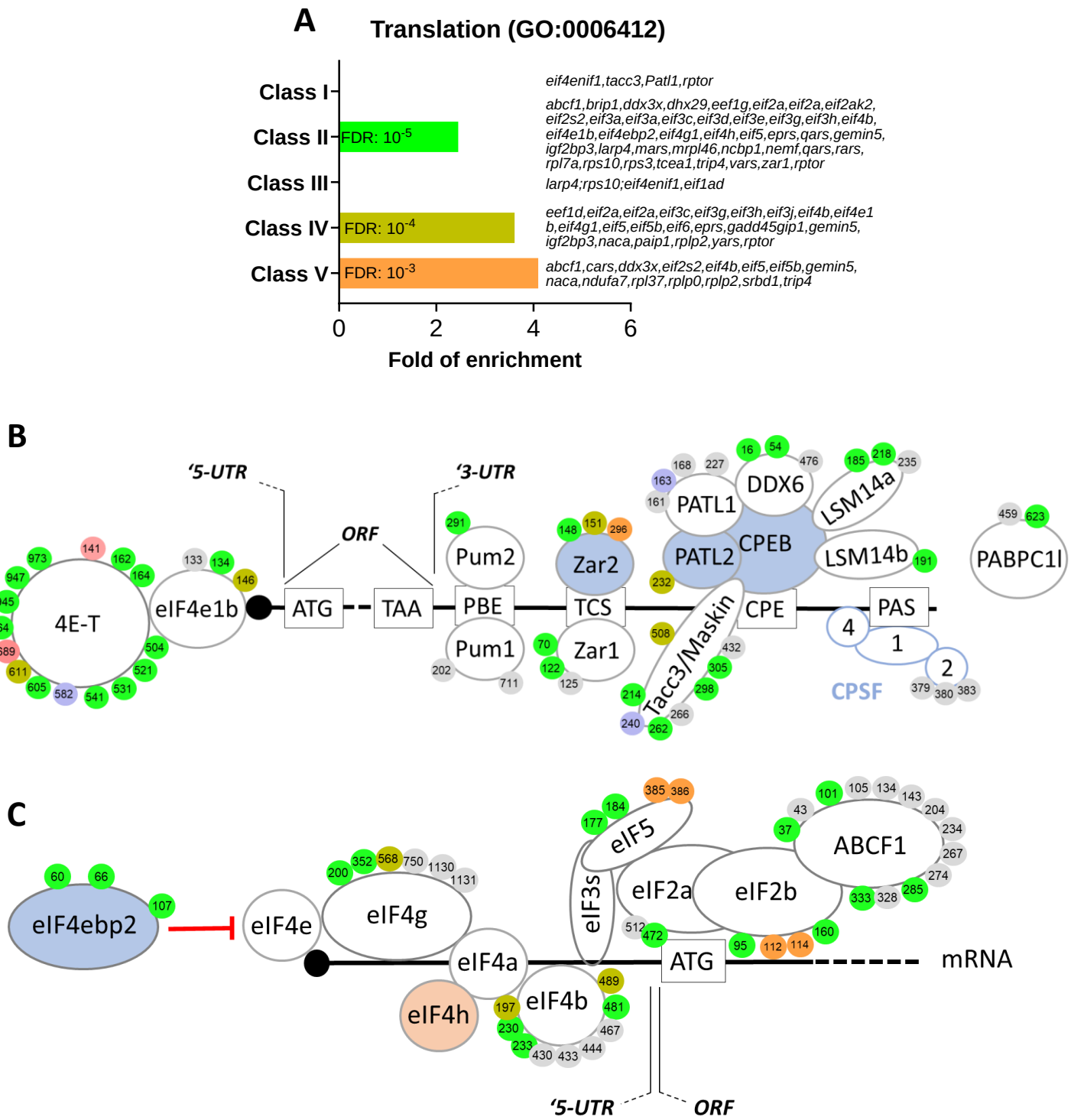

Figure 4. RNA-binding proteins and translation initiation factors are dynamically phosphorylated during meiotic divisions. (**A**) Gene ontology enrichment analysis of the biological process "translation" (GO:0006412) among the phosphopeptides found in each class defined in Fig. 3A. (**B-C**) Graphical representation of the phosphorylation dynamics of RBPs (**B**) and translation initiation factors (**C**) during meiotic divisions. Proteins are color-coded to highlight the changes in protein abundance during meiotic divisions: unchanged=white, decreased=blue, increased=light orange. The phosphorylated sites are color-coded: unchanged, grey; Class I, blue; Class II, green; Class III, red; Class IV, yellow; Class V, orange. The numbering is referred to the iso-allele which has higher number of phosphorylation sites detected.

Figure 4-figure supplement 1

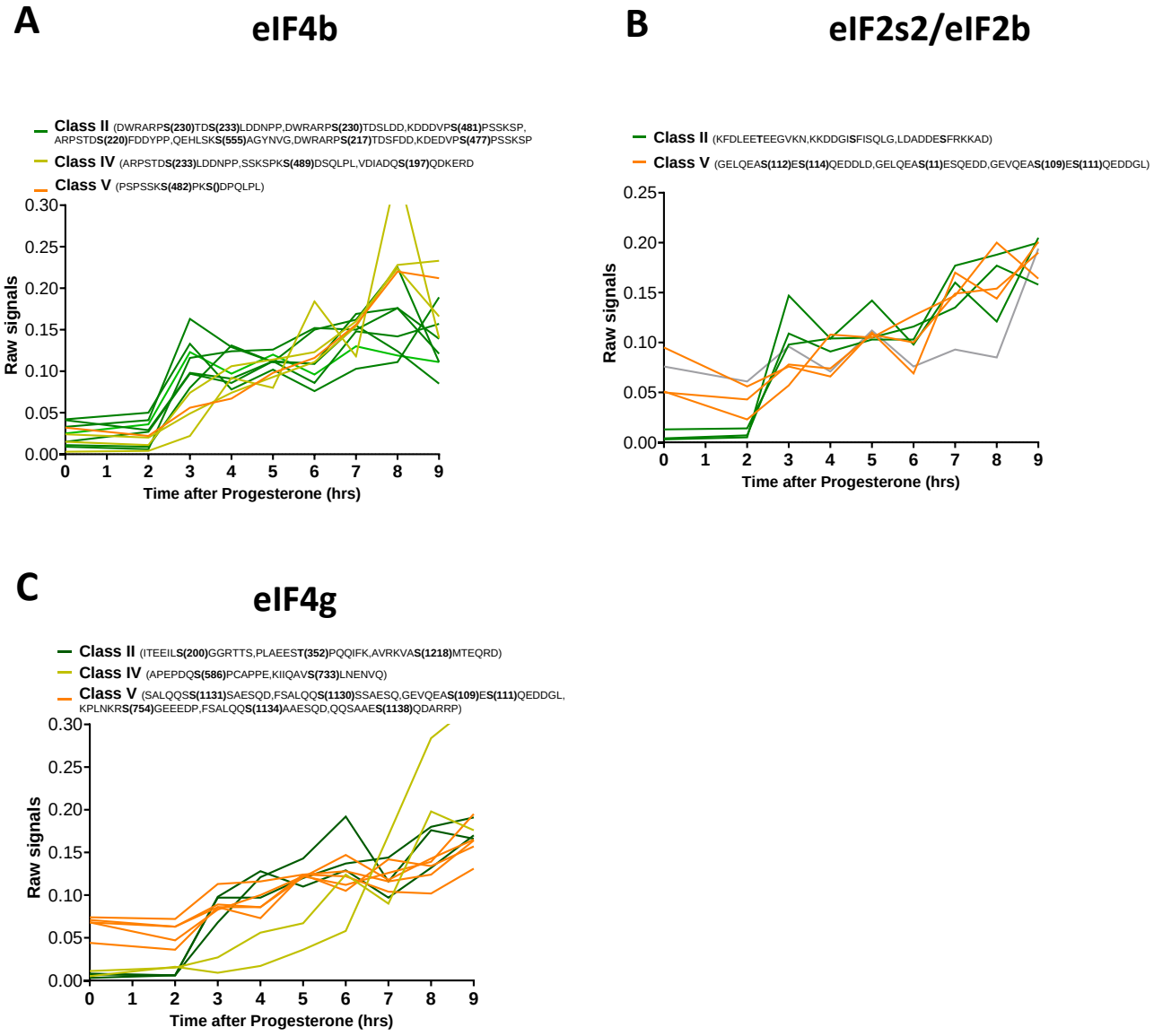

Figure 4-figure supplement 1. Phosphorylation patterns of components of the initiation translation machinery during meiotic divisions. (**A**-**C**) Levels of phosphorylation sites of eIF4b (**A**), eIF2s2/eIF2b(**B**) and eIF4g (**C**) during meiotic divisions are plotted. The phosphorylation curves are color-coded: Class II, green; Class IV, yellow, Class V, orange.

Figure 5

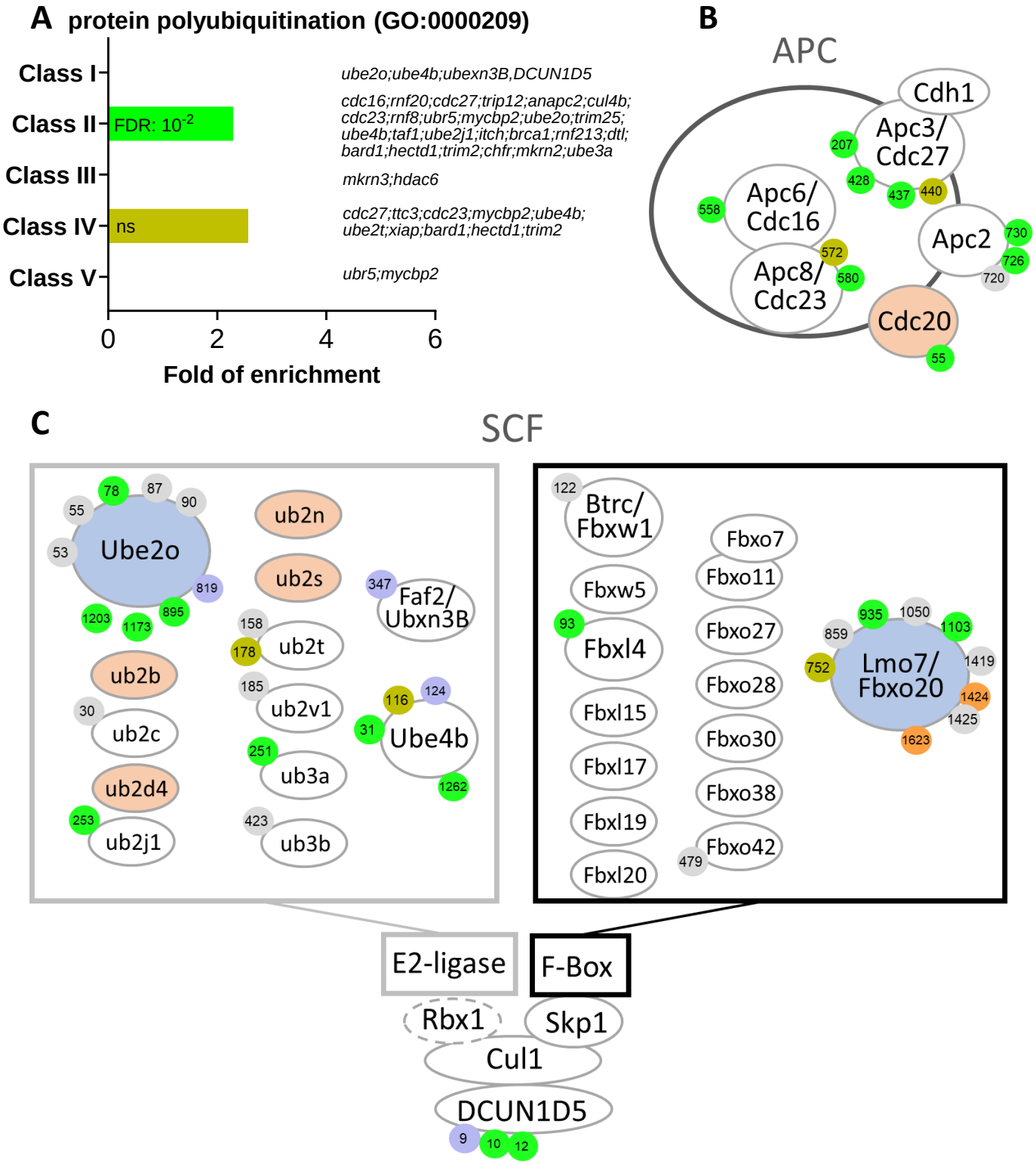

Figure 5. E2 and E3 ubiquitin ligases are highly regulated by phosphorylation. (**A**) Gene ontology enrichment analysis of the biological process "protein polyubiquitination" (GO:0000209) among the phosphopeptides found in each class defined in Fig. 3A. (**B-C**) Graphical representation of the phosphorylation dynamics of the components of two E3 ubiquitin ligases, the anaphase promoting complex (APC) (**B**) and the Skp, Cullin, F-box containing complex (SCF) (**C**) during meiotic divisions. Proteins are color-coded to highlight changes in protein abundance during meiotic divisions: unchanged=white, decreased=blue, increased=light orange. The phosphorylated sites are color-coded: unchanged, grey; Class I, blue; Class II, green; Class III, red; Class IV, yellow; Class V, orange. The numbering is referred to the iso-allele which has higher number of phosphorylation sites detected.

Figure 6

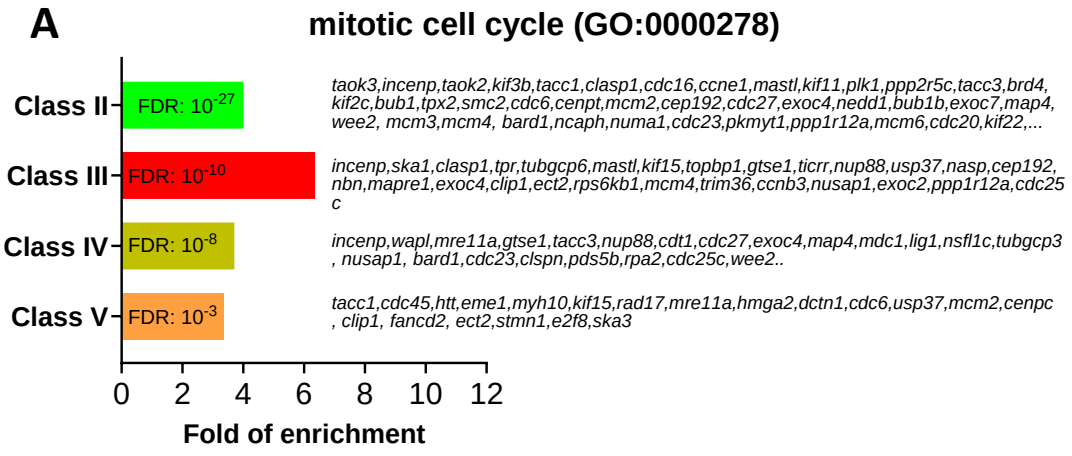
A
mitotic cell cycle (GO:0000278)
Class II
FDR: 10^-27
taok3,incenp,taok2,kif3b,tacc1,clasp1,cdc16,ccne1,mastl,kif11,plk1,ppp2r5c,tacc3,brd4, kif2c,bub1,tpx2,smc2,cdc6,cenpt,mcm2,cep192,cdc27,exoc4,nedd1,bub1b,exoc7,map4, wee2, mcm3,mcm4, bard1,ncaph,numa1,cdc23,pkmyt1,ppp1r12a,mcm6,cdc20,kif22,...
Class III
FDR: 10^-10
incenp,ska1,clasp1,tpr,tubgcp6,mastl,kif15,topbp1,gtse1,ticrr,nup88,usp37,nasp,cep192, nbn,mapre1,exoc4,clip1,ect2,rps6kb1,mcm4,trim36,ccnb3,nusap1,exoc2,ppp1r12a,cdc25 c
Class IV
FDR: 10^-8
incenp,wapl,mre11a,gtse1,tacc3,nup88,cdt1,cdc27,exoc4,map4,mdc1,lig1,nsfl1c,tubgcp3 , nusap1, bard1,cdc23,clspn,pds5b,rpa2,cdc25c,wee2..
Class V
FDR: 10^-3
tacc1,cdc45,htt,eme1,myh10,kif15,rad17,mre11a,hmga2,dctn1,cdc6,usp37,mcm2,cenpc , clip1, fancd2, ect2,stmn1,e2f8,ska3
0 2 4 6 8 10 12
Fold of enrichment

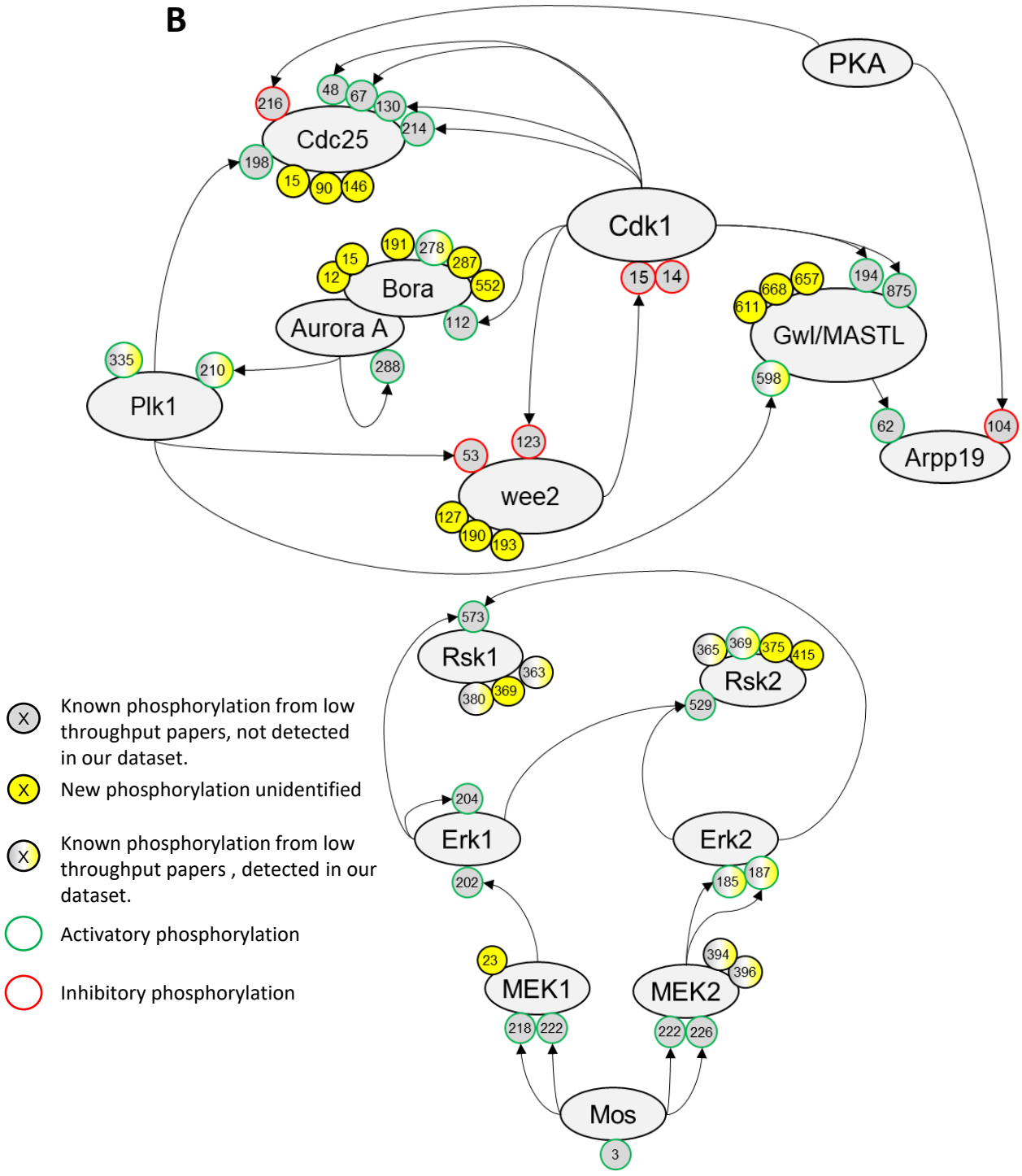
B
PKA
Cdc25
216
48
67
130
214
198
15
90
146
Cdk1
15
14
Bora
12
15
191
278
287
552
112
Aurora A
288
Plk1
335
210
Gwl/MASTL
668
657
611
194
875
598
Arpp19
62
104
wee2
53
123
127
190
193
Rsk1
573
363
380
369
Rsk2
365
369
375
415
529
Erk1
204
202
Erk2
185
187
MEK1
23
218
222
MEK2
394
396
222
226
Mos
3
Known phosphorylation from low throughput papers, not detected in our dataset.
New phosphorylation unidentified
Known phosphorylation from low throughput papers , detected in our dataset.
Activatory phosphorylation
Inhibitory phosphorylation

Figure 6 continued

Figure 6. The network of phosphorylations regulating Cdk1 and the Mos/MAPK pathway. (**A**) Gene ontology enrichment analysis of the biological process "mitotic cell cycle" (GO:0000278) among the phosphopeptides found in each class defined in Fig. 3A. (**B**) Graphical representation of the network of phosphorylations of cell cycle regulators controlling Cdk1 activation (**upper panel**) and the Mos/MAPK pathway (**lower panel**). The human nomenclature numbering has been used for the phospho-sites. The phosphosites are displayed by dots and color-coded: yellow background, new sites identified in this paper and never described elsewhere; grey background, phosphosites already documented in vertebrates by low throughput papers and not identified in this paper; grey-yellow background, phosphosites already documented in vertebrates by low throughput papers and also identified in this paper. The functional effect of the phosphorylation is indicated by the color of the dot contour line: green, activatory; red, inhibitory; black, unknown.

Figure 6-figure supplement 1

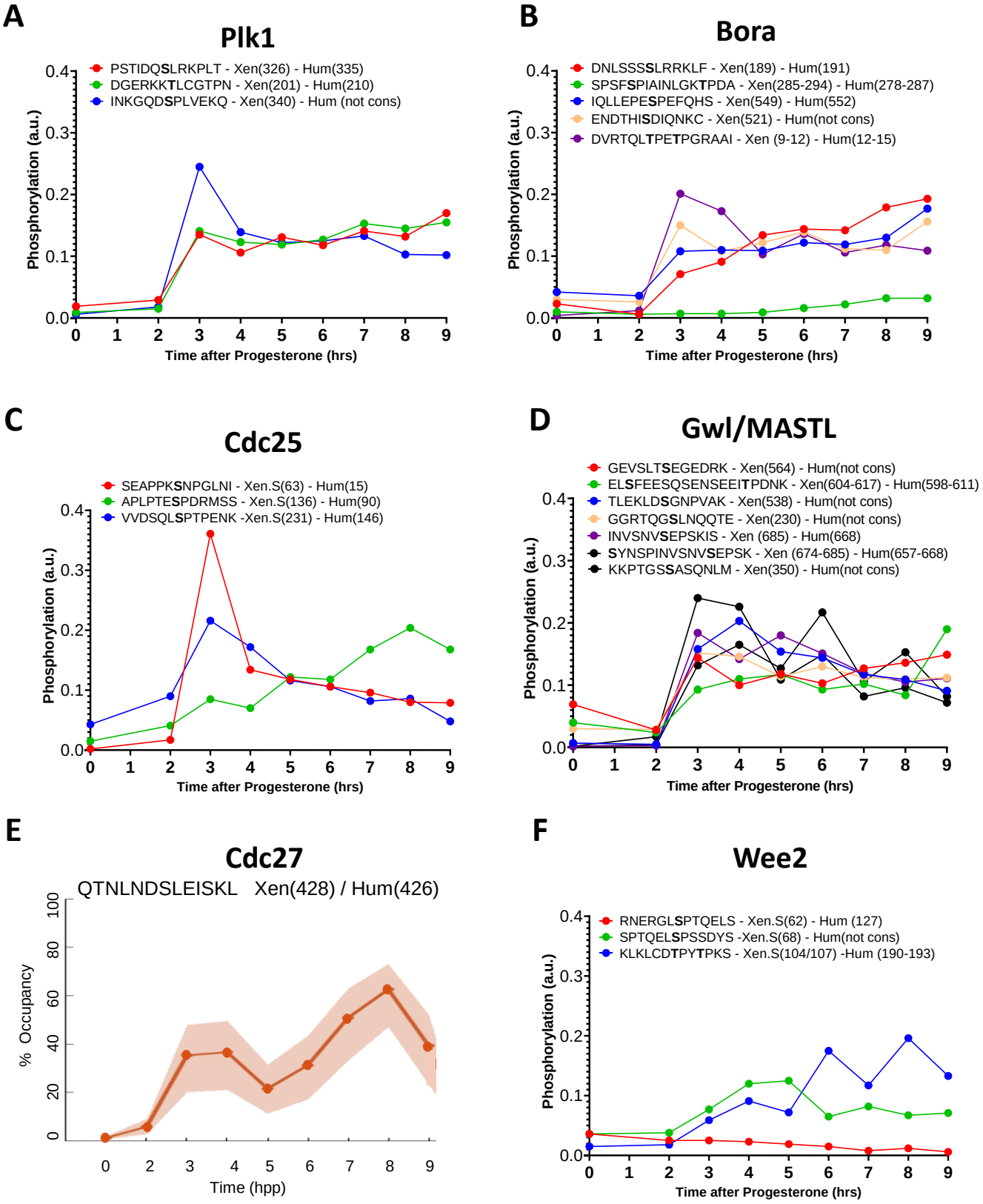

Figure 6-figure supplement 1. Phosphorylation patterns of Cdk1 regulators during meiotic divisions. (**A**-**D** and **F**) Levels of phosphorylation sites of Plk1 (**A**), Bora (**B**), Cdc25 (**C**), Gwl/MASTL (**D**) and Wee2 (**F**) during meiotic divisions are plotted. The peptide sequences are reported with the phosphorylation sites marked in bold. The number of the residue phosphorylated is reported between breakers according to the *Xenopus* and human nomenclature. (**E**) The phosphorylation occupancy for S428 of Cdc27 is plotted with its confidence intervals.

Figure 6-figure supplement 2

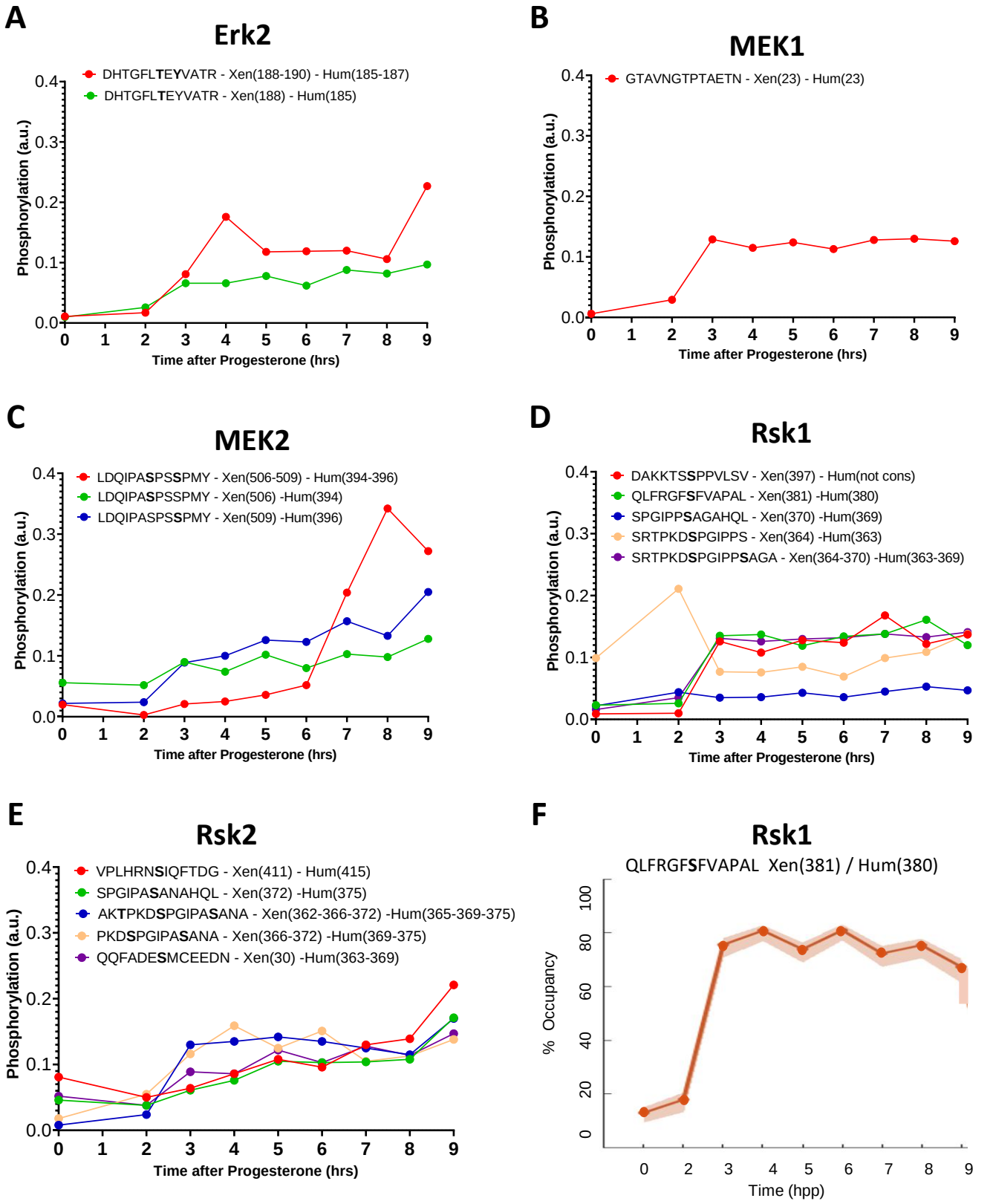

Figure 6-figure supplement 2. Phosphorylation patterns of the mos/MAPK pathway during meiotic divisions. (**A**-**E**) Levels of phosphorylation sites of Erk1 (**A**), Bora (**B**), MEK1 (**C**), MEK2 (**D**) and Rsk2 (**E**) during meiotic divisions are plotted. The peptide sequences are reported with the phosphorylation sites marked in bold. The number of the residue phosphorylated is reported between breakers according to the *Xenopus* and human nomenclature. (**F**) The phosphorylation occupancy for S381 of Rsk1 is plotted with its confidence intervals.

Figure 7

A Nucleoporins concentration (nM)

	PRO	MII
NUP107	157	161
NUP133	166	172
NUP153	117	144
NUP155	186	191
NUP160	134	140
NUP188	120	124
NUP205	360	383
NUP210	97	119
NUP214	150	131
NUP35	327	308
NUP37	309	317
NUP43	218	237
NUP50	712	725
NUP54	160	166
NUP58	385	388
NUP62	440	440
NUP85	134	145
NUP88	110	110
NUP93	665	693
NUP98	476	442

B Nuclear pore organization (GO:0006999)

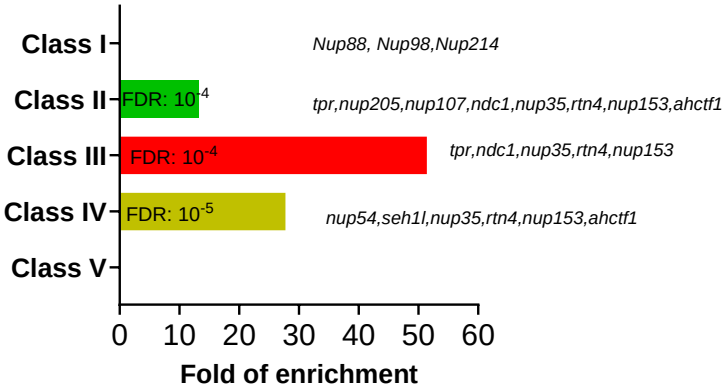

C Nup35/Nup53

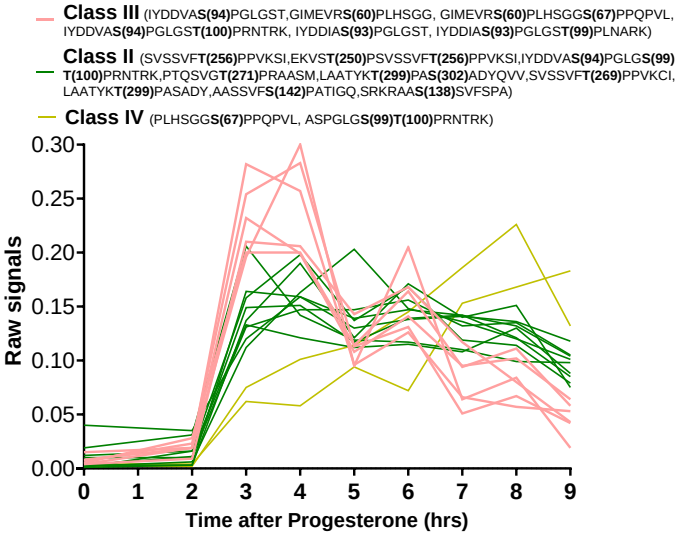

D Nup35/Nup53

GVMEMRSPLFSGG Xen(59) / Hum(59)

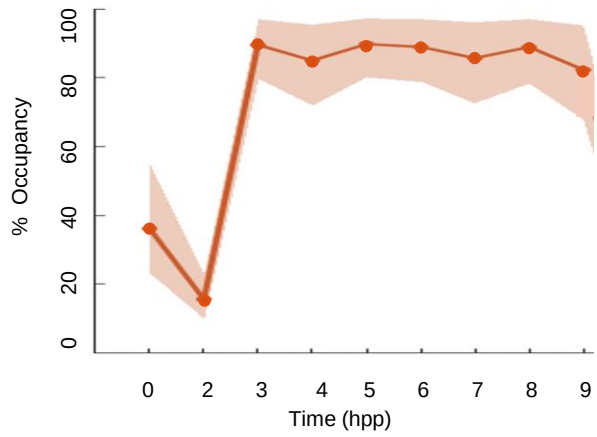

Figure 7. The phosphorylation pattern of nuclear pore components during meiotic divisions. (**A**) Absolute concentration (nM) of nucleoporins in prophase (PRO) and metaphase II (MII) oocytes. (**B**) Gene ontology enrichment analysis of the biological process "nuclear pore organization" (GO:0006999) among the phosphopeptides found in each class defined in Fig. 3A. (**C**) Phosphorylation patterns of Nup35/Nup53. The phosphorylation curves are color-coded: Class II, green; Class III, red; Class IV, yellow. (**D**) High precision phospho-occupancy calculation of S59 phosphorylation pattern of Nup35/Nup53.

Figure 8

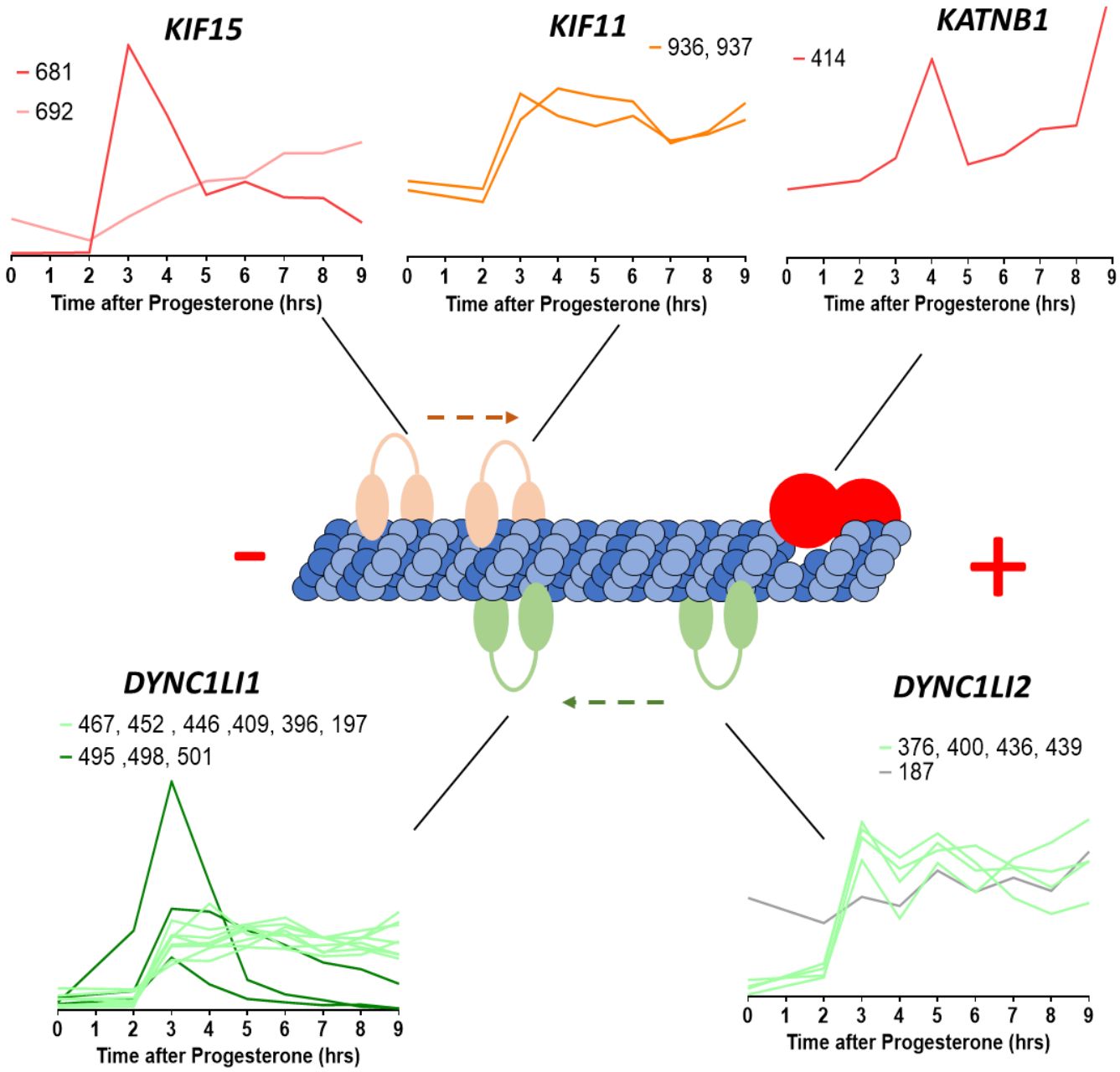

Figure 8. Microtubule-interacting proteins phosphorylation during meiotic divisions. Graphic representation of the phosphorylation dynamics of kinesins (Kif15, Kif11), dyneins (DYNC1LI1, DYNC1LI2) and katanin (KATNB1) during meiotic divisions. The sites of the phosphorylation detected are marked above each panel.

Figure 8-figure supplement 1

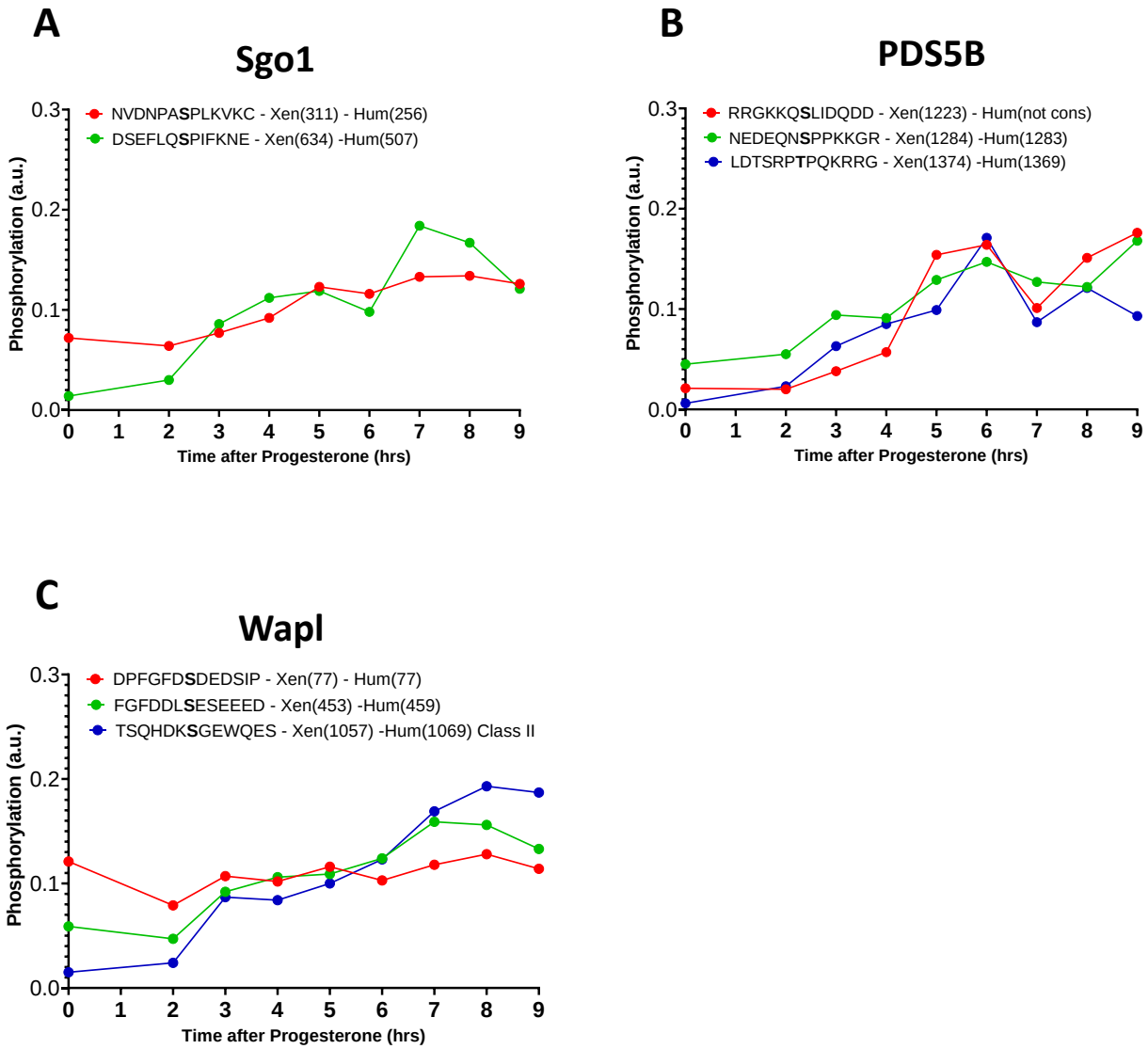

Figure 8-figure supplement 1. Phosphorylation patterns of cohesins during meiotic divisions. (**A**-**C**) The levels of phosphorylation sites of Sgo1 (**A**), PDS5B (**B**) and Wapl (**C**) during meiotic divisions are plotted. The peptide sequences are reported with the phosphorylation sites marked in bold. The position of the residue phosphorylated is reported in breakets according to the *Xenopus* and human nomenclature.

Figure 9

A

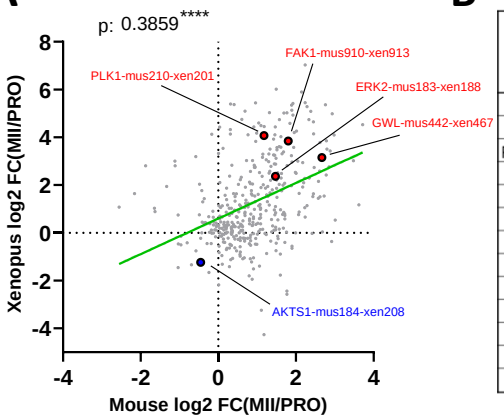

B

protein name	Mouse Sequence	Mouse Position	Xenopus Sequence	Xenopus Position	Changes during meiosis log2 FC(MII/PRO)		Kinase	PMDI
					Mouse	Xenopus		
SCFD1	STGVEN**S**PAGARP	300	APAVES**S**PSGARP	293	1.4	2.9	AMPKA1	35465820
TTK/Mps1	PKADKE**S**PPISVP	435	PGSRRV**S**PPAPSL	459	2.8	2.4	CDK	17804818
PSA5/PSMA5	RGVNTF**S**PEGRLF	16	RGVNTF**S**PEGRLF	16	2.9	3.4	CDK1	34831298
RIR2	QQQLQL**S**PLKRLT	20	ELNENV**S**PMKNLT	16	1.1	2.5	CDK1	9990288
TOP2A	CADVLP**S**PRGKRV	1211	LQEIMP**S**PHGRRV	1208	0.8	2.1	CDK1	11699638
RPS3	DEILPT**T**PISEQK	221	DEIVPT**T**PISEQK	221	2.8	3.5	CDK1 or ERK	21871177
EXOC7	SSGVPY**S**PAIPNK	250	SSGITY**S**PAVQNK	250	2.0	2.5	ERK	22595671
FAK1	LQPQEI**S**PPPTAN	910	IQPQEI**S**PPPTAN	913	1.8	3.8	ERK	15174091
TTK/Mps1	QLVGLN**S**PNSILK	820	QLIGLN**S**PNSISR	844	2.6	2.6	ERK	16950116
GEPH	STTPSE**S**PRAQAT	270	STTPSE**S**PRAQAT	412	1.9	2.0	GSK3B	21173228
MK01/ERK2	DHTGFL**T**EYVATR	183	DHTGFL**T**EYVATR	188	2.7	3.2	MEK	1849075
PLK1	EGERKK**T**LCGTPN	210	DGERKK**T**LCGTPN	201	1.2	4.1	AURKA	18615013
AKTS1	TQQYAK**S**LPVSVP	184	YQQYAR**S**LPVTVP	208	-0.5	-1.2	mTOR	18372248

C

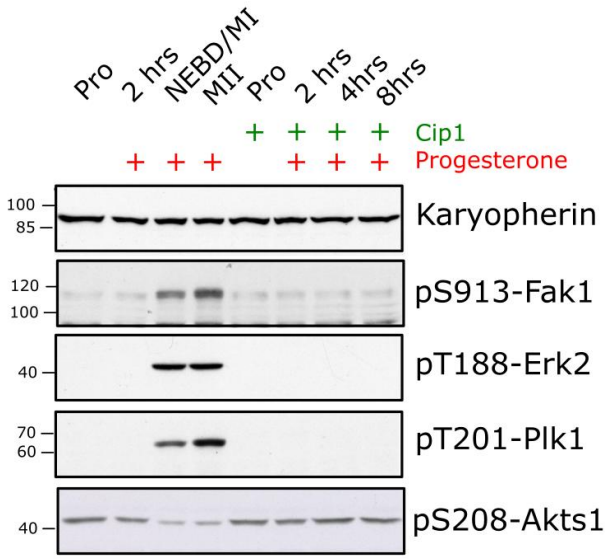

Figure 9. (A) Comparison of phosphorylation changes during meiotic divisions in *Xenopus* (our dataset) and mouse oocytes (Sun et al, 2024). Log2 fold changes in phosphorylation between prophase (PRO) and metaphase II are plotted. The Pearson correlation ($r = 0.39$, $p < 0.0001$) was calculated. **(B)** Selected examples of conserved phosphorylation sites between mouse and Xenopus. The kinase that was experimentally identified to phosphorylate the specific site is displayed together with the supporting reference. **(C)** Oocytes were microinjected with a specific inhibitor of Cdk1, Cip1. After overnight incubation, meiotic maturation was induced by progesterone. Oocytes were collected at different times after progesterone treatment. Karyopherin was used as a loading control. The phosphorylation of Fak1 at S913, Erk2 at T188, Plk1 at T201, and Akts1 at S208 was evaluated by western blot.

Table 1

		Proteome										(Wuhr,2014)	(Session,2016)
	Gene name	0	2	3	4	5	6	7	8	9	Log2 FC (MII/PRO)	Estimated concentration in MII-arrested oocytes (nM)	Count per Million (CPM) in PRO I
Proximal part	SAS-6	0.11	0.09	0.10	0.10	0.09	0.09	0.09	0.09	0.08	-0.3	36	20
	CENPJ	0.07	0.09	0.09	0.10	0.10	0.11	0.09	0.10	0.09	0.4	9	56
	Cep135	not detected										5	1
Central core	POC1B	0.05	0.05	0.07	0.08	0.09	0.14	0.11	0.10	0.11	1.2	7	96
	POC5	0.05	0.06	0.07	0.08	0.09	0.10	0.10	0.11	0.12	1.1	39	100
	CETN1	0.08	0.08	0.11	0.09	0.09	0.09	0.10	0.09	0.10	0.2	not detected	3
	SFI1	not detected										3	7
	POC1A	not detected										20	54
	CETN2	not detected										82	not detected
	WDR90	not detected										5	25
	FAM161A	not detected										not detected	34
Distal appendages	SCLT1	0.10	0.09	0.10	0.11	0.10	0.10	0.08	0.08	0.08	-0.4	13	2
	FBF1	0.11	0.12	0.11	0.12	0.11	0.11	0.08	0.07	0.06	-0.7	not detected	17
	CEP83	not detected										not detected	7
	CEP89	not detected										not detected	1
Sub-distal appendages	FBF1	0.11	0.12	0.11	0.12	0.11	0.11	0.08	0.07	0.06	-0.7	not detected	17
	CEP164	0.10	0.08	0.11	0.09	0.12	0.09	0.08	0.06	0.08	-0.4	1	not detected
	NIN	0.11	0.09	0.11	0.07	0.08	0.11	0.10	0.08	0.10	-0.2	4	27
	TUBE1	0.10	0.09	0.10	0.10	0.10	0.11	0.09	0.09	0.09	-0.1	7	8
	TUBD1	0.08	0.08	0.08	0.09	0.09	0.11	0.09	0.09	0.10	0.1	13	28
	ODF2	not detected										7	8
	CEP128	not detected										3	17
	CNTRL	not detected										6	26
	CEP170	not detected										4	3
	TCHP	not detected										2	16
	CCDC68	not detected										not detected	3
	tubz1	not detected										not detected	10
	CCDC120	not detected										not detected	not detected
Centriole duplication	CCP110	0.06	0.07	0.06	0.08	0.08	0.09	0.10	0.12	0.12	0.9	7	20
	CEP152	0.07	0.07	0.10	0.10	0.10	0.12	0.10	0.11	0.09	0.6	7	161
	CEP192	0.08	0.08	0.08	0.08	0.09	0.09	0.10	0.11	0.10	0.5	21	24
	STIL	0.08	0.08	0.07	0.08	0.10	0.11	0.10	0.11	0.12	0.5	14	100
	CEP63	0.07	0.06	0.11	0.11	0.13	0.12	0.10	0.09	0.09	0.5	4	33
	CEP76	0.07	0.07	0.07	0.08	0.09	0.14	0.10	0.07	0.12	0.5	12	57
	RTTN	0.09	0.09	0.09	0.10	0.10	0.11	0.09	0.09	0.08	0.0	18	14
	CEP97	0.10	0.10	0.10	0.10	0.09	0.10	0.10	0.09	0.09	-0.1	15	1
	SAS-6	0.11	0.09	0.10	0.10	0.09	0.09	0.09	0.09	0.08	-0.3	36	42
	Plk4	not detected										not detected	not detected
PCM	KIF22	0.02	0.02	0.04	0.05	0.07	0.09	0.12	0.14	0.19	3.1	33	464
	SSX2IP	0.03	0.03	0.05	0.07	0.09	0.11	0.11	0.13	0.16	2.1	20	10
	TUBG1	0.04	0.04	0.04	0.04	0.04	0.04	0.12	0.12	0.11	1.5	166	101
	tpx2	0.06	0.06	0.07	0.08	0.10	0.11	0.11	0.12	0.11	1.0	43	516
	kif11	0.06	0.06	0.07	0.08	0.09	0.10	0.10	0.11	0.12	0.9	44	185
	dync1li1	0.06	0.0735	0.0605	0.0675	0.062	0.0605	0.104	0.1185	0.087	0.8	169	38
	dync2h1	0.067	0.057	0.073	0.074	0.092	0.098	0.104	0.105	0.128	0.7	35	3
	prc1	0.06	0.07	0.08	0.09	0.10	0.12	0.09	0.10	0.10	0.7	32	13
	CEP152	0.07	0.07	0.10	0.10	0.10	0.12	0.10	0.11	0.09	0.6	7	33
	kif4a	0.08	0.07	0.08	0.09	0.09	0.09	0.10	0.10	0.10	0.4	100	120
	TUBGCP4	0.08	0.08	0.08	0.09	0.10	0.08	0.10	0.10	0.10	0.2	14	20
	nedd1	0.08	0.08	0.09	0.08	0.09	0.08	0.10	0.10	0.09	0.2	30	12
	dync2i1	0.0875	0.076	0.0915	0.088	0.0965	0.0975	0.0925	0.0935	0.101	0.1	not detected	11
	CKAP5	0.09	0.09	0.09	0.09	0.09	0.10	0.09	0.10	0.09	0.1	67	102
	dynll2	0.086	0.111	0.077	0.102	0.09	0.08	0.086	0.085	0.104	0.1	411	60
	dync2i2	0.089	0.081	0.1	0.099	0.106	0.098	0.09	0.087	0.095	0.0	not detected	35
	TUBGCP3	0.09	0.08	0.09	0.09	0.10	0.10	0.09	0.10	0.09	0.0	33	10
	KATNB1	0.09	0.09	0.10	0.10	0.10	0.10	0.09	0.09	0.09	0.0	20	108
	dynlt1	0.086	0.1	0.114	0.09	0.09	0.07	0.083	0.085	0.093	0.0	138	49
	dync1i2	0.091	0.104	0.104	0.073	0.081	0.106	0.091	0.089	0.092	0.0	232	48
	PCNT	0.09	0.09	0.09	0.10	0.10	0.10	0.09	0.09	0.09	0.0	16	23
	NPM2	0.08	0.10	0.08	0.12	0.08	0.08	0.07	0.07	0.09	0.0	1181	116
	dync2li1	0.086	0.074	0.084	0.086	0.089	0.091	0.082	0.081	0.091	0.0	43	4
	CLASP1	0.09	0.08	0.09	0.10	0.10	0.10	0.09	0.09	0.08	-0.1	15	48
	TUBGCP2	0.09	0.09	0.10	0.10	0.10	0.09	0.09	0.09	0.09	-0.1	59	22
	dync1li2	0.097	0.089	0.099	0.104	0.094	0.099	0.091	0.094	0.086	-0.1	26	27
	dynll1	0.099	0.101	0.094	0.096	0.092	0.105	0.089	0.093	0.089	-0.1	51	130
	NEK9	0.09	0.10	0.10	0.10	0.10	0.10	0.09	0.08	0.08	-0.2	45	27
	TACC3	0.10	0.10	0.10	0.10	0.10	0.10	0.09	0.09	0.08	-0.2	115	117
	TUBGCP6	0.10	0.09	0.11	0.10	0.10	0.10	0.08	0.08	0.08	-0.3	8	14
	NPM3	0.11	0.09	0.12	0.11	0.10	0.10	0.09	0.09	0.08	-0.3	150	70
	KATNA1	0.10	0.10	0.10	0.09	0.10	0.09	0.09	0.08	0.08	-0.3	63	30
	NPM1	0.12	0.09	0.12	0.10	0.09	0.09	0.08	0.08	0.08	-0.6	308	102
	TUBGCP5	not detected										24	not detected
	KATNAL1	not detected										5	not detected
	KATNAL2	not detected										not detected	22

Table 1 continued

Table 1. Centrosomal components during meiotic divisions. Expression patterns of the components of the centrioles and the pericentriolar material. The changes in protein abundance are color-coded: unchanged=white, decreased=blue, increased=light orange. The estimation of the protein and mRNA concentrations was derived by published datasets and color-coded on a white-green scale for protein concentrations and on a white-yellow scale for mRNA concentrations.

Table 1-table supplement 1

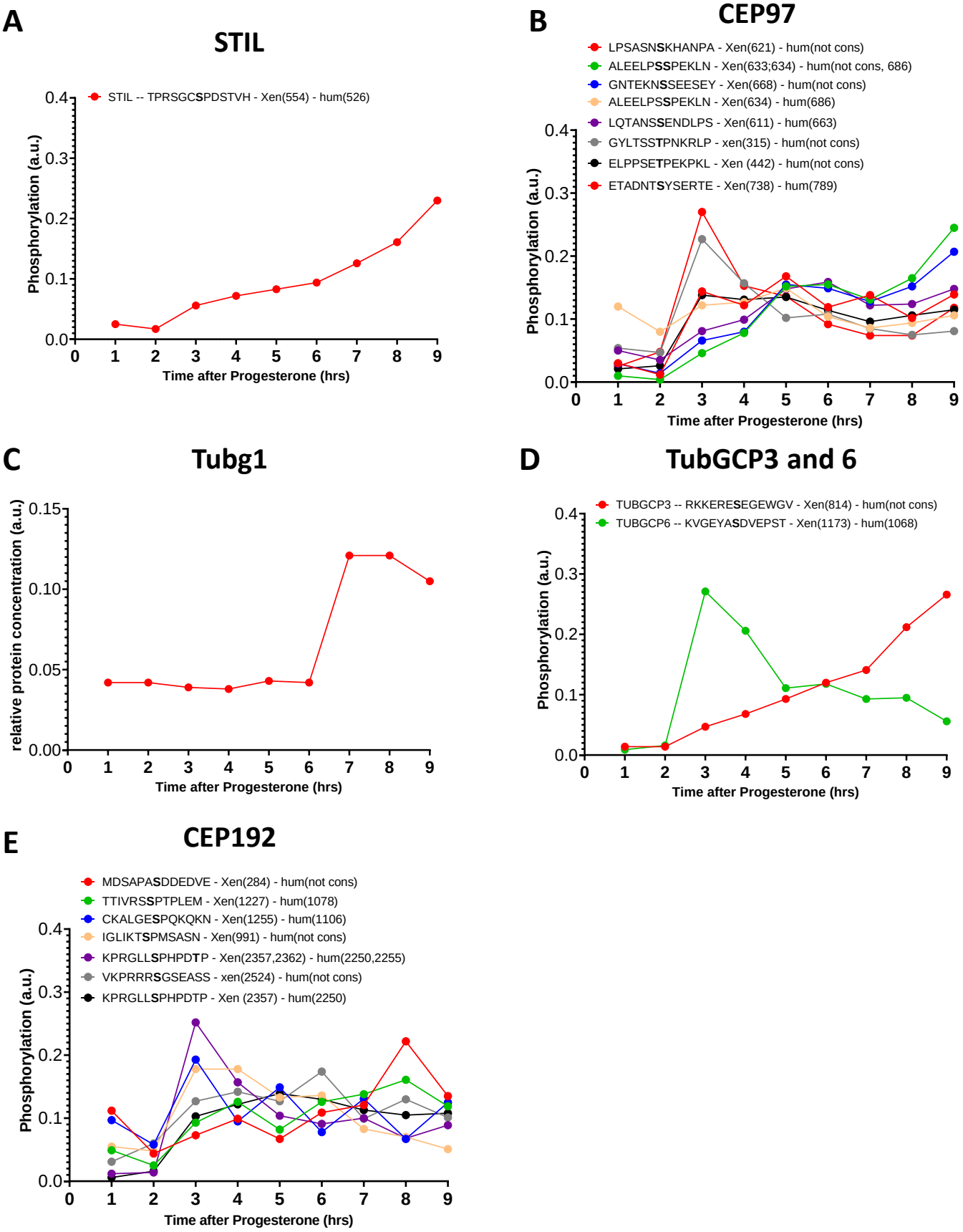

Table 1-table supplement 1. Phosphorylation patterns of centrosomal proteins during meiotic divisions. **(A-E)** The levels of phosphorylation sites of STIL (**A**), CEP97 (**B**), Tubg1 (**C**), TubGCP3 and 6 (**D**), CEP192 (**E**) during meiotic divisions are plotted. The peptide sequences are reported with the phosphorylation sites marked in bold. The number of the residue phosphorylated is reported between breakers according to the *Xenopus* and human nomenclature.